STUDY OF GAS-TUNGSTEN-ARC WELDING POWER DENSITY

FINAL REPORT
CONTRACT NAS 8-21373
12 JUNE 1969

PREPARED FOR:
NATIONAL AERONAUTICS AND SPACE ADMINISTRATION
GEORGE C. MARSHALL SPACEFLIGHT CENTER
HUNTSVILLE, ALABAMA 35812

Lockheed

PALO ALTO RESEARCH LABORATORY

LOCKHEED MISSILES & SPACE COMPANY • A GROUP DIVISION OF LOCKHEED AIRCRAFT CORPORATION
PALO ALTO, CALIFORNIA

STUDY OF GAS-TUNGSTEN-ARC WELDING POWER DENSITY

FINAL REPORT
Contract NAS 8-21373

by

R. F. Karlak
A. R. Pfluger

12 June 1969

Prepared for:
National Aeronautics and Space Administration
George C. Marshall Space Flight Center
Huntsville, Alabama 35812

Materials Sciences Laboratory
Lockheed Palo Alto Research Laboratory
LOCKHEED MISSILES & SPACE COMPANY
A Group Division of Lockheed Aircraft Corporation
Palo Alto, California 94304

FOREWORD

This final report is an account of the research performed for the NASA-Marshall Space Flight Center, on Contract No. NAS 8-21373, "Study of Welding Process Power Density," at the Lockheed Palo Alto Research Laboratory of Lockheed Missiles & Space Company, during the period 1 June 1968 to 30 May 1969. The program was managed by A. R. Pfluger under the administrative supervision of Dr. T. E. Tietz, who heads the Mechanical Metallurgy section of the Materials Sciences Laboratory (organization 52-30) managed by Dr. E. C. Burke. R. F. Karlak was responsible for the theoretical analysis and measurement of the power density of the gas tungsten arcs in this program and was assisted by J. H. Harshman. Design of the special arc apparatus was provided by R. L. Yates. C. W. Boettcher supervised the construction, modification, and operation of the experimental gas tungsten arc equipment. W. G. Jurevic was responsible for the literature survey and preparation of the annotated bibliography for the Phase I report, assisted by Mrs. H. M. Abbott. Computer programming was done by Mrs. D. J. Colvin.

ABSTRACT

One of the present major limitations of the gas-tungsten arc welding process is its limited depth capability when welding plate material. Increased power density could lead to greater penetration and higher travel speed and thus to stronger weld joints with improved weld quality. A theoretical and experimental program was conducted to analyze and characterize the normal gas-tungsten arc, particularly with regard to power density, and to perform experiments designed to increase GTA power density. The initial phase consisted of a comprehensive survey of existing information on GTA phenomena and measurement and was followed by a second phase to develop techniques for characterizing and measuring the power density of the normal DCSP gas tungsten arc. Measurements were made of the distribution of current, heat flux, and plasma-stream pressure on the anode surface as well as the distribution of continuous radiation intensity from the plasma close to the anode surface. The arcs studied were operated with argon or helium shielding at currents from 150 to 300 A and arc lengths from 1 to 3 mm (and longer in certain cases) on both water-cooled copper and molten aluminum using 3/16-in.-diameter 2% thoriated tungsten cathodes (electrodes) tapered to either a 55-mil or 94-mil-diameter tip. The third phase consisted of experiments with welding arcs modified to increase GTA power density. These modifications included use of materials with high thermionic emission such as lanthanum hexaboride or barium-calcium-aluminate impregnated tungsten as cathodes; addition of "active" gases such as hydrogen, nitrogen, chlorine, or sulfur hexafluoride to the shielding gas; and modifications to the anode composition and the use of axial magnetic fields. Significant improvement in GTA power density was obtained with the special electrode materials and with certain shielding gas additions. Power densities of the order of 10^4 W/in.^{2} were measured with the normal GTA and over 10^6 W/in.^{2} with the modified arcs. These levels still do not approach the 10^7 to 10^8 W/in.^{2} commonly obtained in electron beam welding. It was recommended that a study be made of the mechanisms of penetration in GTA and plasma-arc welding and that further work to increase welding power density concentrate on the plasma-arc process.

CONTENTS

ILLUSTRATIONS

Tables

Section 1
INTRODUCTION

1.1 BACKGROUND

The gas-tungsten-arc (GTA) and gas-metal-arc (GMA) processes are extensively used for high quality welding of aluminum and other materials. The newer electron beam welding process, because of its inherent deep penetration capability, is finding greater use in welding heavy sections with minimum degradation of material properties. However, the requirement of welding in a hard vacuum to obtain the desirable high depth-to-width ratio is a serious limitation when fabricating large structures such as the S-Ic Booster for the Saturn V vehicle.

At present, most of the welding on this vehicle and other aerospace structures is done using the gas-tungsten arc process. Refinements to the GTA process have greatly improved its capability and reliability, particularly in out-of-position welding. However, its power density (the power to the work divided by the area on which it is delivered) still is much lower than electron beam welding; as a consequence, it does not have the deep penetration capability nor the ability to weld at the very high travel speeds necessary for improved weld strength.

The effect of weld heat input on weld strength in 2219-T87 aluminum is shown in Fig. 1-1. The significantly higher strengths achieved with the electron beam process is attributed (Ref. 1) to two effects:

(1) A high pool temperature and reduced time at elevated temperature
(2) A geometrical effect wherein the extremely narrow weld zone (of reduced strength) is restricted in the amount of plastic deformation it can exhibit by the higher strength surrounding metal (thus exhibiting higher strength itself)

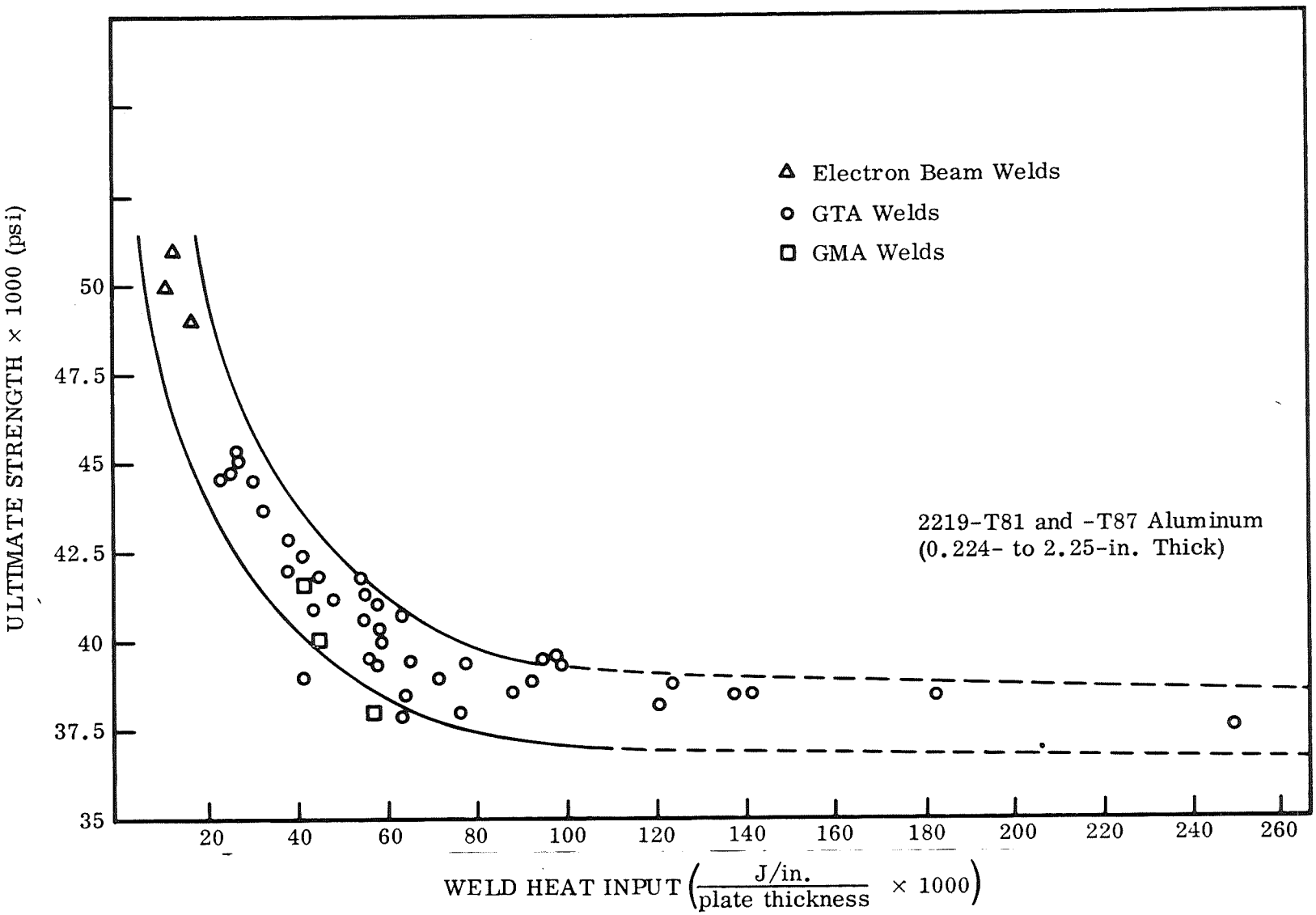

Fig. 1-1 Effect of Heat Input on Weld Strength

Efforts at MSFC and elsewhere have demonstrated improved tensile properties of GTA welds by using high travel speeds (Refs. 1 – 4). Smith et al. (Ref. 5) analyzed the temperature history of points in a 6061-T6 aluminum plate under varying conditions of travel speed and heat input. They found that increased travel speed decreased the extent of both the molten zone and the heat-affected zone, but that for a given arc heat, faster travel narrowed the HAZ faster than the weld pool. As the overaged zone narrowed down, the transverse strength of the joint increased, due to lateral constraint against plastic flow. This is the same phenomenon responsible for the usually high tensile strengths of silver-brazed butt joints. The relatively greater influence of travel speed is due to its effect being exponential whereas the effect of heat input is linear.

One of the present major limitations of the GTA process is its limited depth capability when welding plate material. Increased power density will provide greater penetration and permit higher travel speed, thus leading to higher strength welds in thick plate.

1.2 OBJECTIVES

The objectives of this study were to analyze theoretically and quantitatively the power density of gas-tungsten-arcs and to apply the knowledge obtained to the goal of increasing GTA power density.

1.3 SCOPE

The study was divided into five phases:

- Phase I – A survey and analysis of pertinent literature on GTA phenomena and measurement.
- Phase II – Definition of the normal gas-tungsten-arc by measurement and theoretical analysis. This involved the establishment of quantitative means of measuring arc power density, current density, plasma stream pressure, and other characteristics which were then used to define the arc.

- Phase III – Design and performance of experiments to increase GTA power density. Modifications were made to the normal gas-tungsten-arc, such as changing of the electrode material, making additions to the shielding gas, and superimposing magnetic fields.
- Phase IV – Analysis of results and preparation of the final report.
- Phase V – Approval and distribution of the final report.

Section 2

LITERATURE SURVEY

2.1 PROCEDURE AND SCOPE OF SURVEY

An extensive search of the literature covering gas-tungsten-arc phenomena and measurement was conducted. Abstract sources examined included the Engineering Index, Science Abstracts (A), Science Abstracts (B), NASA Scientific and Technical Aerospace Reports, and Defense Documentation Center Technical Abstracts Bulletins. Also examined in detail were the technical periodicals Welding Journal, British Welding Journal, Welding and Metal Fabrication, Welding Engineer, Welding in the World, and Journal of Applied Physics, and two Soviet periodicals, Welding Production and Automatic Welding. Copies of pertinent articles were obtained, and the references cited in these articles were examined.

A literature search was requested from the Defense Documentation Center and this yielded a listing of 59 reports, of which 19 were considered pertinent to this program. By request, the Defense Metals Information Center provided extracts of technical reports and articles from the periodical literature. Also examined in detail were the extensive holdings of LMSC's Technical Information Center, which included several literature searches previously conducted by LMSC's Information Specialists. Another important source of information was the references cited in the reports and articles examined. One of the more prolific sources was Studies of High-Current Metallic Arcs, by Wood and Beall (Ref. 6).

Particular attention was given to the literature covering the spatial aspects of the arc with regard to temperature, current density, and thermal intensity at the anode surface. Means of measuring these parameters were reviewed and the resulting information was used in selecting the measurement techniques to be used in this

program. In a like manner, information on arc phenomena which might lead to increased power density was sought and used to formulate the experiments for Phase III.

2.2 GENERAL DISCUSSION OF THE LITERATURE

Since its discovery by Sir Humphrey Davy in 1809, the electric arc has been studied by many investigators. Spraragen and Lengyel (Ref. 7) reviewed the literature on the physics of the arc and metal transfer in arc welding in 1943. A second comprehensive review of arc phenomena, metal transfer, and related engineering concepts was given by Jackson in his Adams Lecture of 1959 (Ref. 8). A third, by Wood and Beall (Ref. 6),is a review of the technical literature as an aid in understanding of electrical arcs as used in metallurgical applications. Results relevant to the distribution of electric potentials and currents, temperatures, pressures, the consumption of electrodes, the identities of particles participating in electrical conduction, and the modes and mechanisms are presented and discussed.

In undertaking this literature search, it soon became obvious that, despite the extensive research that has been conducted on electric arcs, only a small portion is germane to welding arcs. Extensive work has been done on arcs at low pressures or at very low currents, on different types of mercury vapor arcs, on arcs of metal contacts, and on various types of carbon arcs. Much of the early theory of arcs applicable to welding has come from studies of carbon arcs and therefore has been included here. More recent basic arc theories have been developed for plasma generators these apply to welding directly.

Finkelnburg (Ref. 9) has discussed general mechanisms of electric arcs as depending on the interaction of the three main parts of the discharge: the cathode drop, the anode drop, and the arc stream. The cathode drop is necessary for production of the electrons that carry the majority of the current, and the anode drop for the production of the compensating positive ions, whereas the arc stream is a column of high-temperature

plasma that enables the current to bridge the gap between the electrodes. Finkelnburg distinguishes between low-current arcs (those that operate below 80 A with low electrode current density) and high-current arcs (those that operate at currents above 100 A whose arc stream exhibits a characteristic contraction and the formation of a stiff arc column of very high temperature). Maecher (Ref. 10) showed that this contraction is the result of magnetic fields produced by the high currents which compress the plasma to the extent that appreciable radial and axial pressure gradients exist. Our interest in this study is primarily in the high-current arcs where this phenomenon dominates.

2.3 DEFINITION OF THE DCSP GAS TUNGSTEN ARC

The direct-current straight polarity gas tungsten arc (DCSP GTA) is one of the most common sources of heat used for welding metals. The work is electrically positive (SP), the electrode (cathode, here) is tungsten, and the conductive medium or arc plasma is a gas. For the sake of experimental simplicity, the "work," in research of a more fundamental nature, is generally copper internally cooled with sufficient water to prevent melting of the surface in contact with the arc.

With a given gas and flow rate as well as cathode material and size, the controllable variables are arc current, arc voltage, and arc length. Only two of these are independent. Thus, for a fixed arc length, changing the current will change the voltage to a new value which depends on the arc length. Similarly, altering the length while maintaining the current constant will cause the voltage to change. The current-length-voltage characteristics of the arc is a curved plane in V-I-l space with the voltage determined uniquely by arc length and current.

The arc characteristics are sensitive to other factors. Of particular importance is the cathode geometry and cooling. Two modes of operation can result – the "normal" mode or the "cathode-spot" mode (Ref. 11). These differ in their V-I-l characteristics, and the latter is characterized by a higher current density and heat intensity in the vicinity of the arc axis (Ref. 12). One author reports that five distinct modes exist, depending primarily on the current range (Ref. 13).

The arc can be subdivided into several regions, each characterized by specific luminous properties, temperature, and composition. Immediately about the arc axis within the arc stream is the plasma core, a very luminous region containing a high density of electrons due to the high local temperature and degree of ionization. It is in this region that most of the arc current flows. Along the entire core, except very close to the anode or cathode, the plasma exists in a state of quasi-electrical neutraility (Ref. 11); that is, the charge of electrons is exactly balanced by ions locally. Also, this region of the arc is in local thermodynamic equilibrium so that the various gaseous species present (electrons and ions) are at the same kinetic temperature (Ref. 14), assuming ideal gas behavior. It is this latter condition that permits the temperature to be calculated from spectral line intensity measurements using methods of statistical mechanics.

The region of the arc adjacent to the cathode (normally called the cathode-fall or cathode-drop region) is best described by considering four zones, each characterized by particular motion of electrons and ions (Ref. 13). Zone I contains only electrons emitted from the heated cathode. The next zone toward the anode contains electrons and ions moving away from the cathode. The third contains electrons and ions , while the fourth is the contact zone with the plasma.

At the anode surface is a nonluminous region called the anode fall or anode drop where electrons condense the anode and liberate their energy as heat.

Surrounding the arc core (or column) is a luminous sheath of heated gas that is practically un-ionized (Ref. 11). There is no sharp demarcation between these two regions; one tapers into the other. That is to say, the temperature and electron density of the arc core decreases radially from the arc axis. There is a decrease in the radial thermal gradient with distance from the cathode. Calorimetric studies (Ref. 12) have shown that the radial heat intensity distribution is very similar to the radial current density distribution, showing that much of the anode heating is caused by the arc current.

A GTA is not completely static in the sense of a metallic conductor. Self-induced magnetic forces compress the plasma and cause it to flow along the arc axis, thus producing a streaming action or jet of plasma from the cathode to the anode (Refs. 15, 16). This phenomenon not only increases the heat energy deposition on the anode but also produces a force upon it which, in a practical welding situation, could produce a depression of the weld pool. However, it also has been shown theoretically that the magnetic forces on the anode can cause a rise at the center of the pool which may cancel the opposing jet action (Ref. 17).

2.4 MEASUREMENT AND CHARACTERIZATION OF THE GTA

Welding conditions ordinarily include specific electrical and geometrical quantities which more or less determine the character of the arc. These conditions are arc length (or arc voltage), arc current, shielding gas composition, gas flow rate, and cathode geometry (i.e., composition, diameter, stick-out, and tip-shape). Generally, the specified values have been learned by experience and experimentation with practical welding. The recommended conditions have been found to produce the highest quality weld joints for the particular metal composition and dimensions on which they were determined. Although conspicuous progress has been made in welding practice using this approach, the superficial or "ad hoc" nature of the experiments has produced data that are virtually impossible to analyze in total to obtain a lucid explanation of arc phenomena from which inferences about means of further improving welding can be drawn.

A number of papers have been published describing welding-type arcs in terms of plasma physics. The arc properties reported include temperature distribution, local charged-particle concentrations, axial potential gradients, spectral characteristics, and streaming velocities. Although these studies provide a valuable basic understanding of arcs, they do not indicate how welding power density may be increased since no correlation exists between the measured quantities and the efficiency of the arc as a welding tool.

A third type of arc research has produced basic data of a more practical value; this is the experimental determination of the radial heat intensity and current density distribution at the surface of a solid, water-cooled anode simulating the workpiece. This work has shown that the current density and heat intensity distributions are very similar for the idealized experimental conditions employed (Ref. 12). For example, the cathode-spot mode of operation associated with acutely pointed thoritated tungsten cathodes produces a higher concentration of both current and heat intensity about the arc axis than does an arc operating in the normal mode. The beneficial influence of the former has been recognized and applied to common welding practice.

For the purposes of this study, the most important measurable characteristic of a DCSP-GTA is the current intensity distribution at the anode. The work of previous investigators has shown that this distribution is related to the heat intensity distribution. However, it remains to be shown that the latter is linearly related to the weld bead or heat-affected zone. Deviations could result from several factors, principally the effect of metal vapors in the plasma and the effect of the molten pool shape caused by pressure from the plasma stream.

Determination of the current density or heat intensity distribution has been made using a water-cooled anode separated into two electrically and thermally insulated segments by a thin gap (Ref. 12). The current to half of the anode is recorded as the arc is slowly traversed perpendicular to the separating line from one anode section to the other. Heat intensity measurements are made similarly but with monitoring of the cooling water flow rate and temperature rise. Clearly this procedure is not applicable when the anode is melted, so that another experimental technique is required.

The similarity between the distribution of current density and heat intensity plus the fact that the intensity of continuous radiation, in the visible range, is proportional to the electron density in the plasma (Refs. 18, 19), suggests that the continuum intensity distribution may be reasonably closely related to the current density and heat intensity distribution to permit its use as an indicator of this arc characteristic when the anode

is melted beneath the arc and the split anode cannot be employed; i.e., in a practical welding situation. Furthermore, if the distribution were found to be unaffected by melting at the anode surface, Phase III experiments could possibly be performed with greater simplicity and accuracy by using a water-cooled copper anode.

Continuum measurements may be performed by imaging the arc on a monochromator slit which has been reduced in length so that the aperture is essentially a point. The monochromator is then tuned to the desired wavelength and the arc is slowly moved at a constant rate perpendicular to the optical system so that the arc image traverses the slit. A photomultiplier at the monochromator exit slit converts the light intensity to a voltage which is fed to a recording potentiometer to produce a plot of the transverse intensity.

The radial arc-jet pressure distribution at the anode surface can be measured directly by traversing the arc across a water-cooled anode containing a small hole connected to a manometer. The pressure can be converted to practical units, e.g., dynes per centimeter squared using the density of the manometer fluid. This technique has been used successfully by Reed (Ref. 15) to measure peak pressures of 3×10^4 dynes cm^{-2} at the center of a 300-A, 5-mm-long arc in argon.

2.5 MEANS OF INCREASING ARC POWER DENSITY

From the literature survey came numerous reports relating to possible means of increasing power density of the welding arc. In the following review, the more pertinent references have been grouped into a number of categories generally related to modification of a specific portion of the arc.

2.5.1 Modification of the Shielding Gas

Among the more successful attempts to increase the power density of the gas-tungsten-arc have been studies aimed at modification of the shielding gas. The shielding gas

composition in GTA welding has a marked influence on arc voltage, power density, and thermal efficiency. Most early GTA welding was done using argon shielding. However, it was soon found that helium produced a significant increase in weld penetration and permitted higher travel speed. Thus, at present helium is widely used for DCSP-GTA welding.

The addition of hydrogen to argon to increase arc voltage and power density has been described by Helmbrecht and Oyler (Ref. 20) and successfully applied to GTA welding of stainless steel, Inconel, and Monel (Ref. 21).

Nitrogen has been found to produce significantly higher thermal efficiency in the GTA welding of copper (Refs. 22, 23).

Nestor (Ref. 12) studied the anode heat and current distribution for the following gas mixtures; argon -8.6% hydrogen, argon -17.6% nitrogen, and helium -2% argon, and found that the diatomic gas additions produced a distinct contraction of the plasma boundaries near the anode. Hydrogen addition to argon produced the most concentrated heat source, whereas the helium arcs produced the broadest heat distribution. The argon and argon-nitrogen arcs were intermediate cases. The voltages were all higher than with pure argon.

Wilkenson and Milner (Ref. 24) in discussing heat transfer from arcs pointed out the need for further investigation of dissociable gas systems and emphasized the intensified deep-penetration effect resulting from the combination of the plasma jet and liberation of the heat of reassociation at the bottom of the crater.

An increase in arc force with the addition of hydrogen to the argon shielding was reported by Uchida (Ref. 25).

Ludwig (Ref. 26) discussed the effect of the thermal conductivity of the shielding gas on the shape of the arc plasma and gave data for argon, nitrogen, and helium-shielded arc plasma.

While hydrogen, oxygen, and nitrogen in the shielding gas can lead to porosity or other weld defects, chlorine, on the other hand, has been used to overcome some of the effects of these contaminants in gas metal arc welding of aluminum (Ref. 27). Moreover, Ludwig (Ref. 28) has proposed that traces of chlorine in the gas tungsten arc form negative ions that greatly increase anode heating and result in increased penetration.

2.5.2 Modification of the Electrode (Cathode)

Modification of the electrode to achieve higher arc power density may include modification of the electrode material, the electrode shape, and electrode cooling. These three factors are closely interrelated and must be considered in the design of an improved high power density electrode.

Electrode Material. The extremely high temperatures attained in welding place severe restrictions on the materials that may be used for the electrode. Some of the desirable characteristics of electrode material for straight polarity welding are:

- High melting point
- High thermal shock resistance
- Ease of electron emission (low work function)
- Absence of chemical reactions with the shielding gas
- High electrical conductivity
- Satisfactory thermal conductivity
- Minimum of embrittlement at operating temperature
- Ability to be shaped and to hold shape

One of the most important properties of an electrode material to be used as a cathode is its thermionic emission. When the material is heated to temperatures of the order of 1200° to 3000°K, some of the outer electrons gain sufficient thermal energy to escape from the parent lattice. The energy (in electron volts) necessary to remove an electron from the material to infinity is called the work function. The work function

for a given material is normally considered to be a constant although it varies somewhat with crystallographic orientation and temperature. The Richardson equation for thermionic emission of electrons from a hot cathode is:

$$J = AT^2 \exp\left(-\frac{\phi}{kT}\right)$$

where J is the current density in A/cm^2, T the temperature (°K), ϕ the work function (eV) of the surface, k is the Boltzmann's constant, and A is a sort of emissivity coefficient which is a property of the surface and has a theoretical value of 120 $A/cm^2/deg^2$. However, it rarely ever reaches this value. It can be seen that if A is raised, T is raised, or ϕ is lowered, increased current density will result. Advantage may be taken of the increased current density by designing a cathode that limits the current flow to a very small area, thereby effectively increasing arc power density.

The literature on thermionic emission is quite extensive because of its importance in the electronic industry. Comprehensive reviews of thermionic emission have been given by Herring and Nichols (Ref. 29), and Wright (Ref. 30).

Lee et al. (Refs. 31, 32) have made a thorough theoretical analysis of the processes in an arc from the cathode to the uniform plasma and have shown the importance of the cathode work function on arc characteristics.

Thermionic electron emitters may be classified into several types:

- Pure metal emitters
- Atomic film emitters
- Activated oxide emitters
- Compound emitters

Most metals have high work functions and must be heated to temperatures above their boiling points to produce appreciable emission. The refractory metals with high melting and boiling points have been used extensively. Tungsten is most commonly used, particularly for welding electrodes.

The emission properties of a pure metal may be changed considerably if atoms or ions of other elements are adsorbed at its surface. Langmuir (Ref. 33) discovered that 1 to 2% of thorium oxide could increase the emission of pure tungsten by several orders of magnitude. The mechanism of operation of thoriated tungsten is based on the reduction of the thoria into thorium which diffuses to the surface and forms a polarized film or monolayer with a work function less than that of the thorium itself. Moreover, the rate of evaporation of the thorium is greatly reduced. Thus, the thoriated tungsten electrodes used for GTA welding can carry a higher current than pure tungsten and provide more electrons to the arc at a given temperature.

In the third type of emitter, the work function of the base metal is reduced by a monolayer of alkaline earth metal formed on the surface. This type has been extensively used in high-power electron tubes which are called dispenser cathodes. They consist of porous tungsten impregnated with a mixture of barium-calcium or barium-strontium aluminate. A monolayer of barium forms on the tungsten surface and reduces the work function. For a given current density, these emitters operate at lower temperature than pure or thoriated tungsten and they are capable of very high current density at comparable temperatures. Neurath and Gibbs (Ref. 34) evaluated this type emitter as a cathode in an arc plasma generator and reported high emission and good life at currents up to 500 A.

Very good emission properties have been reported for certain compounds, particularly the rare earth borides (Ref. 35). One of these, lanthanium hexaboride, has extremely high emission together with a low evaporation rate and high melting point. These properties are a result of the crystallographic structure which consists of a three-dimensional boron framework in whose interlattice spaces the lanthanum atoms are

embedded. The valence electrons of the metal atoms are not accepted by the B_6 complex, thus giving rise to the presence of free electrons which impart a metallic character. The strong bonds between the boron atoms impart good chemical stability and a high melting point. When this structure is heated to a sufficiently high temperature, the lanthanum atoms at the surface evaporate away. They are, however, immediately replaced by diffusion of metal atoms from the underlying cells. The boron framework does not evaporate but remains intact and provides a mechanism for constantly maintaining an active emission surface.

Electrode Configuration. The relationship of electrode geometry to DCSP-GTA weld penetration and bead width has been discussed by Gibbs (Ref. 36), Savage et al. (Ref. 37), Chihoski (Ref. 38), and Kenyon (Ref. 39). Narrower weld beads and deeper penetration generally result when the vertex angle is blunter, but arc starting is easier with the sharper tips. Savage also studied the effect of temperature distribution in the electrode and related this to electrode failure at higher current levels.

Electrode Cooling. Improved electrode cooling may be necessary to increase the welding current, maintain electrode shapes, and prevent melting of materials that provide improved electron emission. The most obvious limitation on maximum welding current, electrode shape, or the use of other electrode materials is the temperature at which the electrode operates. When excessive currents are used, the electrodes melt and contaminate the weld. Similarly, special tip configurations cannot be maintained.

Axial flow of shielding gas over the surface of the electrode is a method of cooling that has been successfully used. Wilkinson and Milner (Ref. 24) have shown that the restriction of the current to a spot at the cathode which causes an arc to act as a pump (Maecker, Ref. 19), drawing cold gas into the arc from around the cathode and causing it to form a high-temperature high-velocity jet which travels along the arc axis and impinges on the anode. The cold gas flowing over the surface of the cathode will cool it. Gases of high specific heat such as helium or hydrogen would have the greatest cooling effect.

Dissociation of a diatomic gas on the cathode surface would increase cooling still further. Noesen has described this effect where the highly endothermic (102,700 cal/mole) dissociation of hydrogen on the cathode serves to cool it (Ref. 40). A portion of this heat is recovered at the cooler anode when the hydrogen recombines. A similar effect would be obtained with hydrogen. Lee (Ref. 41) has calculated the cooling effect of electrons emitted from a cathode for various temperatures.

2.5.3 Modifications of the Anode

The majority of the investigations of arc phenomena in the literature have been made between an electrode and a water-cooled anode. These do not truly represent welding arcs which operate over a molten crater.

Goldman and White (Ref. 42) investigated six anode materials (Al, Ag, Co, Cu, W, and Zn) having a wide range of melting and boiling points and analyzed for metal vapor in the arc both at the water-cooled anode and at the tungsten cathode. Only with the aluminum anode was the presence of anode material vapors in the arc noted. Thus, the generally accepted assumption that the anode plays little or no part in the arc mechanism is true only for low-current arcs on water-cooled anodes, but not under practical welding conditions, particularly with very short arc lengths on aluminum where considerable metal vapor enters the arc.

Rykalin et al. (Ref. 43) studied the role of vapor streams of material evaporated from both the anode and cathode on the energy balance in the arc.

The influence on penetration of a GTA weld caused by trace amounts of halogens in the material being welded was reported by Ludwig (Ref. 28) in 1957. He found a four-fold difference in penetration and attributed it to the formation of negative ions which increase the anode space charge. In a more recent paper (Ref. 44), he studied the influence of impurities on penetration in stainless steel.

The effect of anode geometry was studied by Tedeschi (Ref. 45) using a two-part anode consisting of a center post and a movable outer envelope. Extension or retraction of the outer envelope permitted study of various anode configurations and thus could simulate the shape of a deep weld pool.

2.5.4 Application of Magnetic Fields

The effect of magnetic fields on the welding arc to produce the phenomenon known as "arc-blow" has been recognized for many years and much practical information has been published as to means of avoiding or minimizing its occurrence. Much less study has been made of the use of magnetic fields to modify or control the arc, and the majority of this work has been reported in the foreign literature.

The influence of an applied magnetic field is dependent upon its orientation as well as its magnitude and whether it is steady or alternating. When the magnetic force is imposed in such a manner that the field is parallel to the axis of the electrode, it is referred to as a longitudinal magnetic field. When the field direction is perpendicular to the axis of the electrode and perpendicular to the direction of electrode travel, it is referred to as a transverse field. When the field direction is parallel to the direction of travel, it is referred to as a parallel field.

The effect of unintentional magnetic fields on arc stability during production GTA welding was investigated by Ginn (Ref. 46), and the use of applied transverse fields to improve arc stability was reported.

Hicken and Jackson (Ref. 47) made a study of the effects of applied transverse magnetic fields on bead-on-plate welds in both magnetic and nonmagnetic materials. They reported that the welding arc could be deflected either forward or backward with respect to the electrode depending upon the direction in which the magnetic field was superimposed on the welding arc. The appearance of the arc also varied as a function of both the magnitude of the applied field and the type of material being welded. One effect observed was the reduction of undercutting at high travel speed. Beneficial effects were evident only when the arc was deflected forward.

Other studies of the effect of transverse magnetic fields are reported by Guile (Ref. 48) and Kovalev (Ref. 49).

The effects of longitudinal magnetic fields are quite different from those of transverse fields and appear to be more influenced by the welding current and arc length. Levakov and Lyubavskii (Ref. 50) report that under the influence of a longitudinal magnetic field, an arc will rotate, and this motion stabilizes it in space. The effect is significant only when the arc is relatively short, and longer arcs require greater current to be stable. Externally, the rotating arc looks little different from the stationary arc, but the rotation will set the molten pool spinning about its axis (at magnetic field strength in excess of 100 Oe). When the magnetic field strength is increased beyond a certain limit, a major change in arc shape takes place without loss of stability. A conical arc is formed in the shape of a uniform hollow cone with its apex on the cathode spot. The speed of rotation of the conical arc has been studied by Gvozdetskii and Mechev (Ref. 51).

Nestor (Ref. 12), in measuring the heat and current density distributions of gas tungsten arcs, used a relatively weak longitudinal magnetic field of 20 to 50 G to keep the arc axis normal to the anode plane.

2.5.5 Plasma Jet Constriction

The plasma-arc welding process may be considered as one modification to achieve higher power density. Although this process is outside the scope of the present investigation, the literature in this field was reviewed for possible application to GTA power density experiments. With the plasma arc process, a contricting orifice is used to produce a cylindrical plasma jet which allows greater arc efficiency due to increased heat transfer from the plasma jet than the less constricted plasma jet achieved with the normal gas tungsten arc. As a result, the plasma-arc process can be used to produce weldments with less heat input and higher depth-to-width ratios than in the GTA process. In addition to the constricting orifice, further control of the shape of the plasma jet is achieved by impinging a flow of cold gas in the plasma.

G. G. Graber et al. (Ref. 52) found that a transpiration-cooled porous nozzle was an effective constrictor which might permit greater concentration of the arc power than water-cooled copper.

Another characteristic of the plasma-arc process that contributes to high depth-to-width ratios is the pressure exerted on molten weld metal by the constricted plasma. This pressure provides the keyhole effect that is one of the important characteristics of the plasma arc process. With the keyhole, molten metal is forced from under the plasma, allowing it to impinge on cooler solid metal. Because heat transfer from a plasma jet increases with differential temperature, this effect may also increase the efficiency of the process.

Much literature has been published on plasma-arc welding, both here and abroad. There is great interest in this process in the Soviet Union, and a number of papers have been presented on the basic thermal characteristics (Refs. 53 – 56).

A detailed study of this process was presented by Okada and Maruo (Ref. 57) at the Symposium on the Physics of the Welding Arc held in London, 29 October – 2 November 1962. Electric characteristics, flame temperature, pressure distribution, heat efficiency, and the use of magnetic fields were discussed.

2.5.6 Use of Pulsed Current

Recent application of pulsed DCSP current for GTA welding butt joints in pipe and tubing has resulted in improved control of weld penetration and a significant improvement in weld quality. Studies of current pulsation reported by Vilkas (Refs. 58, 59) have shown an increase in weld penetration in both 2219 aluminum and 18% Ni maraging steel. Needham (Ref. 60) reported an increase in effective melting, with greater modulation (i.e., increase in severity of pulse wave shape). He attributes this to two factors: (1) The efficiency of utilization of the energy transfer into the plate is enhanced due to the high rate of heat input, which greatly exceeds the available heat

sink during the pulse, and (2) the thermal efficiency of the arc is improved, since at high current the intense plasma stream from the cathode adds further energy. Thus, characteristics of a high current arc can be reproduced in arcs of lower mean current.

Section 3

GTA MEASUREMENT AND CHARACTERIZATION (PHASE II)

3.1 BACKGROUND

Review of the literature cited in the Phase I bibliography revealed four measurable arc properties of potential value. They are: the radial distribution of current density, heat flux, continuum intensity, and pressure at the anode surface. The radial distribution of current density is important since the product of any locally measured value and the anode-material electron work function is the electrical energy-density flowing into the anode at that point and a narrowing of the distribution; that is, concentrating the current about the arc axis is tantamount to increasing the arc efficiency in terms of the electrical contribution to metal melting.

It should be understood that the current-density-work-function product gives the quantity of electrical energy deposited at the anode surface only and this in itself may not completely account for the "penetration" observed with the same arc conditions during practical welding unless ramifications are considered. If, for example, the molten pool surface peak temperature remains such that little material evaporates, the effect of concentrating the current about the arc axis (increasing the power density) will produce a weld bead of cross section more closely approaching a half-cylinder. This is the limiting case for a point heat source moving along a straight line on a surface. However, experience shows that this is not the case since depth-to-width ratios much larger than one-half are frequently encountered in practice.

Improved penetration as the result of concentrating the current about the arc axis only, that is, without modifying the arc characteristics in any other way, can produce greater penetration only if the heat source effectively extends below the work-piece surface. In the absence of all externally applied forces other than those produced by the current

at the surface, this can occur only by a phenomenon found to contribute significantly to the very high depth-to-width ratios observed in electron-beam welding, i.e., back pressure on the liquid metal by rapidly evaporating atoms. This back pressure tends to depress the surface of the molten weld pool and thus allows the source to deposit its energy at increasing depths below the surface (Ref. 61).

How the heat flux from an arc on the surface of a body may cause a crater to form by melting and evaporation can be understood by considering the case of a semi-infinite solid with the source extended uniformly over the free surface. While the conditions are not the same as for the concentrated heat source in the case of a welding arc, the resulting conclusion still applies as can be seen by considering a small region of the solid near the arc axis where the lateral heat flow in the solid is negligible.

Using the one-dimensional time-dependent heat flow equation (Ref. 62),

$$\frac{\partial U}{\partial t} = k \frac{\partial^2 U}{\partial x^2} \tag{3.1}$$

i.e., Fick's second law, where $U = U(x, t)$ is the temperature at any time (t) and distance from the surface (x), with the boundary conditions

$$U(x, o) = 0 \qquad (x > 0)$$

$$- K \frac{\partial U}{\partial x} (u, t) = \varphi_o \qquad \text{and} \qquad \lim_{x \to \infty} U(x, t) = 0 \qquad (t > 0)$$

results in an equation for the time dependence of the surface temperature of the form

$$U(u, t) = 2\varphi_o \left(\frac{t}{\pi K c \delta} \right)^{1/2} \tag{3.2}$$

where φ_o is the constant heat flux density at the surface, K is the thermal conductivity, c is the specific heat, and δ is the density, all of which are assumed to be constant.

In the case of aluminum, neglecting heat of fusion, assuming that the heat capacity is the same for the liquid phase, and that no heat is absorbed in evaporation, it can be calculated from Eq. (3.2) that the surface temperature will attain the boiling point after 0.2 sec when the thermal energy into the surface is 10 kW cm^{-2}, slightly less than the peak value reported by Nestor (Ref. 12) for the case of 1.6 mm, 200 A, cathode-spot-mode arc operating in helium with 2% argon added for stabilization.

The general equation for the time-dependent temperature distribution in the same solid, i.e.,

$$U = \frac{\varphi_o}{K} 2\left[\sqrt{\frac{kt}{\pi}}\, e^{-(x^2/4kt)} - x \operatorname{erfc} \frac{x}{2\sqrt{kt}}\right] \tag{3.3}$$

can be used to show that in the same time, under the same assumptions used previously, the temperature 0.5 cm from the surface will be 530°C, or less than the melting point.

The more precise theoretical expression for the steady state temperature distribution from a moving point source on a semi-infinite solid was first given by Rosenthal (Refs. 65, 66, 67). However, the equation presented does not define the temperature on the plate surface below the source. The predicted temperature at this point is always infinite.

Doubling the rate of heat input will cause the surface to reach a given temperature in one-fourth the time. Applying this to the previous case shows that when the surface is at the boiling point (2450°C), the temperature 0.5 cm from the surface will be only 72°C, assuming 0°C uniform temperature initially. Thus in this case, surface evaporation will occur as previously but with much steeper thermal gradients in the block.

It is apparent that in either case evaporation of metal from the surface will occur and part of the incident energy will be absorbed as heat of evaporation. No precise calculation of the evaporation rate has been made since the complexities thus introduced in the derivation have not been resolved. However, the steeper gradients and higher surface temperature produced in a shorter time interval, as the source intensity is increased, shows that more of the incident heat will be available for evaporation.

Increasing the surface evaporation rate will have two effects: the surface will recede at a faster rate from material loss, and the evaporation back pressure displacing molten metal will also increase since this pressure is proportional to the evaporation rate per unit area (Refs. 61, 68). Of course, the thickness of molten metal layer will decrease with increased power density (increased temperature gradient) so that eventually cratering will be due primarily to surface erosion essentially in the solid state since the liquid layer will be infinitesimal in thickness. When this occurs, the influence of plasma streaming on molten metal will be negligible. The stream will then act only as a source of heat to the crater.

The radial distribution of heat flux includes the contribution from the aforementioned electron condensation in addition to heat deposited from the arc by plasma streaming and/or thermal conduction across the gas-metal interface as well as radiation from the incandescent gas and loss of electron kinetic energy. The contribution from radiation is known to be negligibly small but this is not true of the others. Thus a measurement of the radial heat flux distribution in conjunction with the current distribution reveals additional information about other factors upon which penetration depends. As in the case of electron condensation, this heating can produce a surface evaporation rate sufficient to depress the weld pool and thus extend the heat source below the weldment surface. As the source of heat becomes more intense and concentrated about the arc axis, it will extend deeper into the weldment and improved penetration will result.

Measurement of the continuum-intensity radial distribution near the anode surface may be a secondary means of establishing the current density radial distribution when conditions preclude the direct measurement technique. According to Griem (Ref. 69), Finkelnburg (Ref. 19), and Maecker (Refs. 19, 70, 71), for wavelengths in the visible range of the spectrum, the theoretical equation for the continuum intensity has a weak dependence on temperature, thus permitting a determination of the electron-ion product. With local microscopic neutrality, this amounts to measuring the square of the electron density or essentially the square of the electrical conductivity if an analogy is made to a metallic conductor wherein the electrical conductivity is proportional to the electron concentration (density).

Finally, but of no lesser importance, is the radial distribution of pressure on the anode produced by the plasma jet. This streaming, partly due to Lorentz forces generated by the arc's self-magnetic field, may influence the depth-to-width ratio or penetration in two ways. First, the stream or jet carries heat in the form of extremely high temperature gases to the anode surface. The energy deposited contributes to the melting and evaporation of metal and subsequently to depression of the molten metal surface by evaporation back-pressure as in the case of electron condensation stated previously. Furthermore, the streaming pressure also contributes to depression of the molten pool surface by momentum transfer as the stream impinges on the work piece. Obviously, a narrower distribution and higher peak pressure will produce greater penetration, other arc features being unchanged.

Heat transfer to the anode by the plasma stream has been termed gas-kinetic heating and it appears to be the second most important source of energy transfer by an arc after electron condensation. Radiation plays a negligible role in heating the anode, particularly in the immediate vicinity of the weld zone. The thermal energy of electrons may be sufficient to produce significant heating of the anode surface (Ref. 12). Unless the shielding gas contains a diatomic specie or one which can become negatively ionized, the above heat transfer and penetration mechanisms are the only ones possible. If diatomic species are present, heat transfer can occur also by recombination for diatomic gases or by liberation of ionization energy in the case of gases which form negative ions such as oxygen or the halides.

The radial distribution of current density, heat flux, continuum intensity, and arc pressure on the anode have been measured in this program phase for the case of GTA's in argon. With helium shielding, only the continuum-intensity distribution and arc pressure were measured since a stable arc could not be maintained without applying an external magnetic field to "stiffen" the plasma. Details of the techniques employed including apparatus design, the experimental procedures, and data reduction are described in the following subsections.

3.2 TECHNIQUES

3.2.1 Introduction

The very nature of the arc makes determination of the distributions of current and heat flux very difficult. Physical probes, either as points or lines, have two disadvantages, (1) the intense heat of the arc rapidly destroys most useful materials and (2) such probes will distort the arc by perturbing the fields, currents, and plasma stream. There is one indirect method which causes no disturbance in the plasma. This is the spectroscopic probe described by Olsen which simply analyzes the atomic radiation from a line-of-sight in the plasma (Refs. 11, 72). Another technique, the surface probe described by Nestor (Refs. 12, 72), causes minor disturbances in the arc and is limited to moderate power densities. However, it is the only method which will produce data related to the power density distribution on the anode by actually measuring the heat deposited on it. Both techniques require the arc to have rotational symmetry about its axis and require that the axis is normal to the anode surface.

The continuum measurements provide only an indication of the current density distribution since a precise description requires knowledge of the radial temperature distribution in the plane of the measurements. However, the temperature dependence is small, therefore the error near the core is not too large (Ref. 70).

The surface probe, as its name implies, is used to determine the radial distribution indirectly by measuring the change in the flux (current or heat) received by a collecting surface as the area intercepting the flux is increased. This is accomplished by moving the surface into the source at a constant rate along a line on its surface perpendicular to the arc axis. Line probes are used by passing a line collector, e.g., the axis of an optical system, through the source perpendicular to the source axis. As in the surface probe case, this is an indirect measurement requiring mathematical treatment of the data to yield the radial distribution. Point probes measure the radial distribution directly. In this case a point sensor, such as the open end of a small-diameter tube to measure pressure, is moved radially through the source while the sensor output is recorded.

3.2.2 Current and Heat Flux Measurement

In the surface-probe measurements, use is made of an anode divided into two electrically and thermally isolated sections by a splitting plane perpendicular to the surface upon which the arc impinges. The current and thermal energy arriving on one section are recorded as a function of the perpendicular distance from the splitting plane to the arc axis on the anode surface. Radial variations of the heat flux and current densities are then calculated from these data as follows. (See Appendix A, also.)

Defining, in the plane of the anode surface, x the distance from the arc axis perpendicular to the splitting plane, r the radius from the arc axis outward, R the radius beyond which the current or heat transferred to the anode are zero, and the radial distribution functions $i(r)$ [or $\dot{q}(r)$] giving, respectively, the current density (or heat flux intensity) at any distance r from the arc axis, then the current intercepted by the monitored anode is given as a function of these quantities by:

$$I(x) = 2 \int_{x}^{R} i(r) r \cos^{-1}(x/r)\, dr \qquad (3.4)$$

and similarly for the heat flux, $I(x)$ [or $\dot{Q}(x)$] is the measured current or heat flux to the monitored anode section as a function of x. The fluxes i or $\dot{q}$ must be functions of r only. The source must have rotational symmetry.

The factor $i(r)$ [or $\dot{q}(r)$] in Eq. (3.4), the radial distribution functions sought, can be obtained by differentiation with respect to x (Liebnitz's rule) which gives the integral

$$I'(x) = 2 \int_x^R \frac{i(r) r \, dr}{(x^2 - r^2)^{1/2}} \tag{3.5}$$

where $I'(x) = d/dx \, [I(x)]$.

This is the well known Abel's integral, the solution of which can immediately be written as

$$i(r) = \frac{1}{\pi} \int_r^R \frac{I'(x) \, dx}{(x^2 - r^2)^{1/2}} \tag{3.6}$$

Since $I(x)$ is not available in functional form, but is only experimental data, the calculation of the radial distribution function must be performed numerically. Appendix A gives a derivation of the numerical procedure used for computer calculation of the required distributions.

3.2.3 Continuum Intensity Measurement

The radial continuum intensity distribution a small distance above the anode is calculated from data obtained by means of an optical arrangement which is, in effect, a line probe. This apparatus is external to the arc apparatus and operated simultaneously with the current and heat probe to ensure that the data are comparable. An

achromatic lens projects the arc image upon the foreshortened narrow slit of a grating monochrometer as the arc is moved at a constant velocity perpendicular to the optical axis and arc axis in the plane of the anode surface. A photomultiplier at the exit slit provides an output to a recording potentiometer which is proportional to the intensity of the radiation, at a particular wavelength, incident on the spectrometer entrance point (slit).

Because the plasma is transparent, the intensity measured originates from all points in the arc along the system optical axis. With the inherent axial symmetry of the plasma, this means that the measured continuum intensity originates from a chord as it moves through the plasma at a constant rate. Denoting the measured intensity by $S(x)$ where x is the perpendicular distance from the optical axis (chord) from the arc axis, the radial intensity distribution $s(r)$ is given by

$$S(x) = 2\int_{x}^{R} \frac{s(r)r\,dr}{(r^2 - x^2)^{1/2}} \tag{3.7}$$

This equation has the same form as Eq. (3.5) and thus inverts to the form

$$s(r) = -\frac{1}{\pi}\int_{r}^{R} \frac{S'(x)\,dx}{(x^2 - r^2)^{1/2}} \tag{3.8}$$

The minus sign appears in this case since $s(r)$ must be positive, but the slope $S'(x)$ of the observed function is negative.

Again, as for the case of the current density and heat flux, integral (3.8) cannot be solved in closed form but requires a similar numerical method suitable for computer use.

Comparison of Eqs. (3.6) and (3.8) reveals an interesting relationship which is helpful in understanding the similarity between the surface probe and line probe techniques. The integral of (3.6) is identical to that of (3.8) except that the former requires the second derivative of the data function and the latter the first derivative. This is because the increment to the measured current or heat flux produced by infinitesimal change in (x), the distance of the arc axis from the splitting plane, is effectively a line probe measurement at that point. In other words, the surface probe measurement is essentially a line probe measurement with all contributions accumulated as the probe moves from the arc boundary toward its center. The numerical inversion procedure used to calculate the radial distribution from both types of probe obviously will be similar. In fact, the matrix of coefficients based on the geometry of the surface probe and used for performing the numerical calculation are derived from those for the line probe as shown in Appendix A.

3.2.4 Plasma Stream Pressure

Determination of the radial pressure distribution at the anode surface differs from the previously described techniques in that it is obtained directly as an experimental measurement. The apparatus for this is simply a water-cooled copper anode with a 13.5-mil-diameter hole drilled through the surface and connected with a small tube to a water manometer.

3.3 APPARATUS

A special arc apparatus was designed and constructed for this work. The design criteria were based on similar work reported in the literature and on consideration of efficiency, speed, and accuracy in meeting the program objectives. Perpendicularity of the arc axis on the anode and rotational symmetry were to be retained throughout each test. Ancillary apparatus was selected and modified when necessary to provide suitable sensitivity ranges and reliability. Assembly of the components into a complete experimental setup required care to ensure isolation of individual electronic equipment and the absence of any ground loop which could produce distorted or spurious measurement. A description of the individual components follows.

3.3.1 Arc Assembly

Design of the arc assembly (Figs. 3-1, 3-2, and 3-3) was predicated on the experimental requirements. The welding torch was to be equivalent to one of commercial design, with the following features: (1) the length was to be adjustable while maintaining the arc axis normal to the anode surface; (2) the anode-cathode assembly had to be vertically adjustable manually to permit positioning of the arc image on the spectrograph slit; (3) the anode had to be driven at a constant slow rate relative to the cathode in a horizontal plane parallel to its surface and perpendicular to the plane defined by the arc axis and optic axis of the spectrometer assembly; (4) the anode required a manual adjustment in the direction of the optic axis to permit positioning of the arc on a fresh region of the anode surface if a position of it became degraded; and (5) it was necessary to drive the entire arc assembly in the same manner as the anode in order to scan the arc image across the spectrometer slit.

The welding torch requirement was satisfied by modifying the front end of a Linde HW 27 torch to provide a support, current connection, gas lead, and water cooling as shown in Fig. 3-2. A number 12 cup with a gas lens was used for all experiments. Also visible in the figure are: (1) the vertical arc positioning screw, (2) the longitudinal anode positioning screw, (3) the spectrometer projection lens, (4) the side-viewing lens, and (5) the direct side-viewing port.

The anode assembly shown was to improve arc symmetry by equalizing as much as possible all currents, which deflect the arc by the magnetic field they produce. However, it can be shown that magnetic interaction, or arc flow, cannot be completely eliminated in the vicinity of the splitting plane, regardless of the anode design.

Figure 3-3 is the split anode assembly. It has the leads extending vertically from each end of the sections where they are bolted to the phenolic base. This splits the arc current as it enters the anode into two equal and opposite streams which produce a null magnetic-field resultant perpendicular to the arc axis. The internal water-cooling

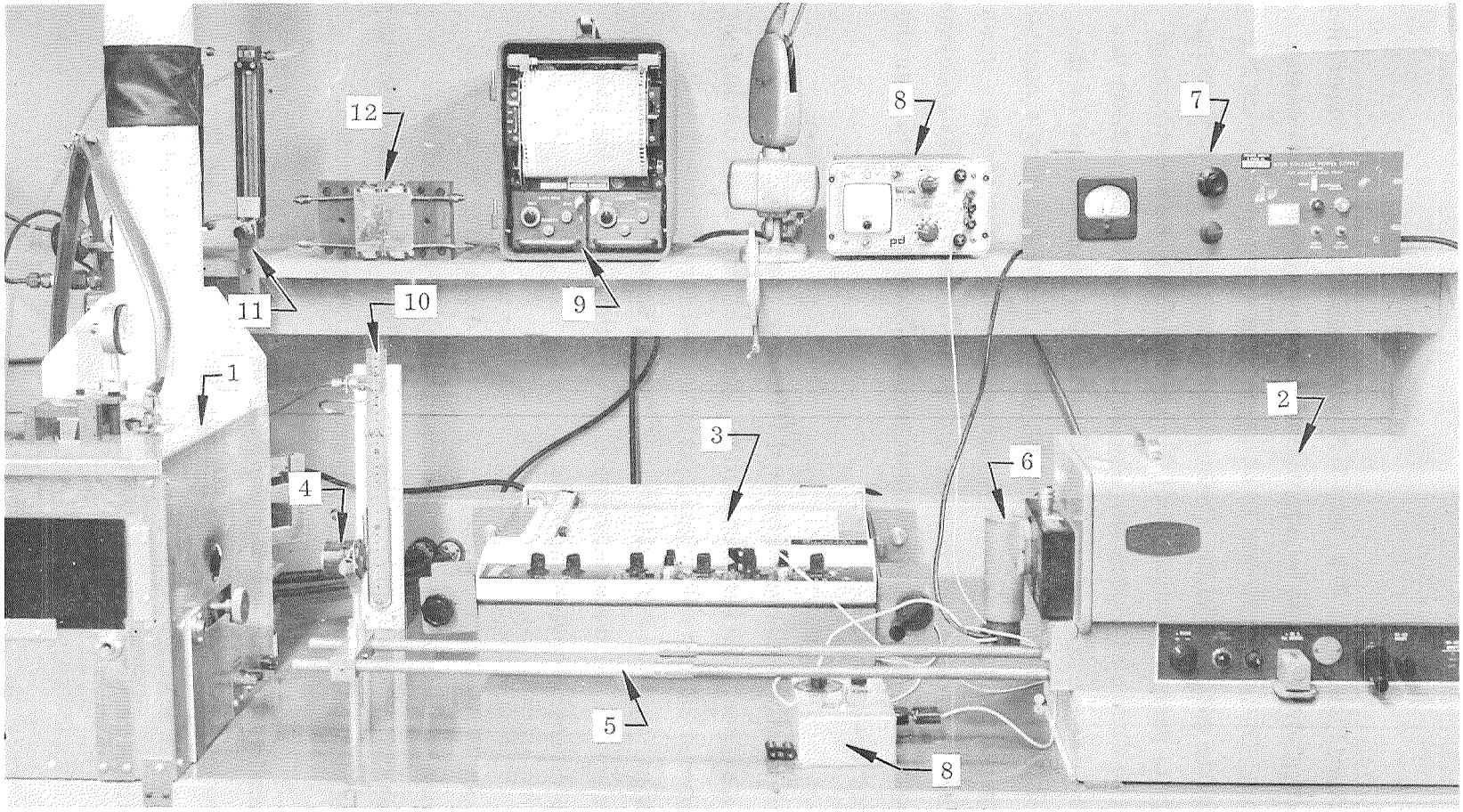

1 Arc Chamber
2 Grating Spectrometer
3 Recorder
4 Projection Lens
5 Optical Bench
6 Photomultiplier
7 Photomultiplier Power Supply
8 Attenuator and Zero Suppressor for Photomultiplier Output
9 Auxiliary Recorder for Photomultiplier
10 Water Manometer
11 Shielding Gas Flowmeter
12 Split-Anode Assembly

Fig. 3-1 Equipment Used for Measuring GTA Characteristics

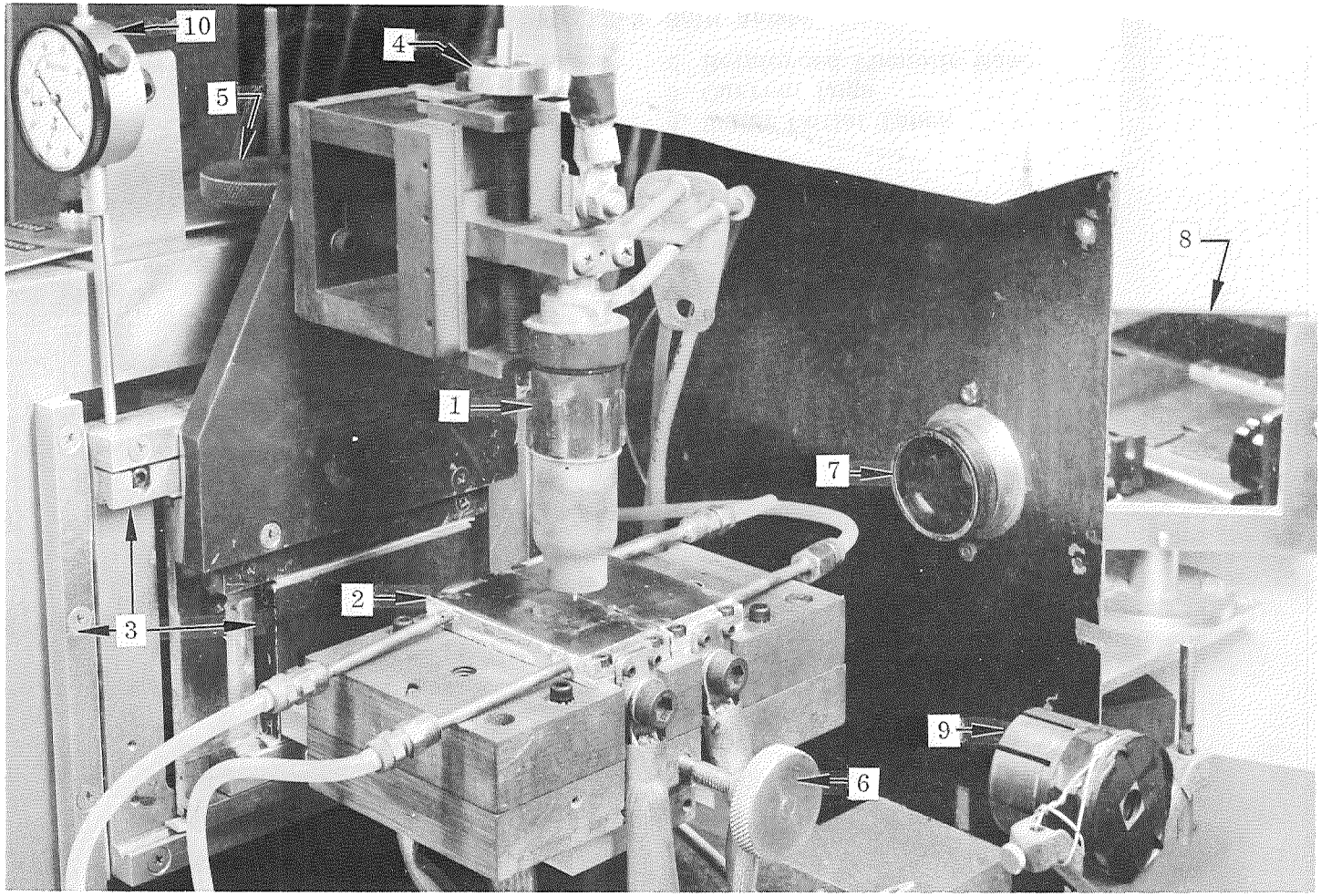

Key:

1 Arc Torch
2 Split Anode
3 Arc-Drive Frame
4 Arc-Length Adjustment
5 Vertical Arc Positioner
6 Longitudinal Arc Positioner
7 Side-View Projection Lens
8 Side-View-Image Mirror
9 Projection Lens for Spectrometer
10 Vertical Position Indicator

Fig. 3-2 View of Opened Arc Chamber

1 Anode Surfaces
2 Splitting Plane
3 Water Inlet Tubes
4 Water Outlet Tubes
5 Current Lugs
6 Reinforced Phenolic Base

Fig. 3-3 Split Anode

paths consist of 1/32-in.-wide channels separated by equally wide copper fins soldered to the copper on lower anode surfaces. Such a fin assembly reduces the flow of current perpendicular to the splitting plane when it is close to the arc axis by providing a downward path for the current instead of requiring it to flow in a thin sheet along the surface.

The finned anode assembly offers another advantage by enhancing heat dissipation to the cooling water. This eliminates local heating (directly beneath the arc) which previously had driven dissolved gases from the water to form many bubbles which seriously interfered with the measurement of water temperature and flow rate.

Continuum intensity measurements on molten aluminum were made with the same setup equipped with a water-cooled plate of 2219 aluminum 1/2-in. thick. All arcs were struck near the plate center and showed no asymmetry suggesting a uniform current distribution in the aluminum anode.

The current leads for the torch and anode assembly were designed and positioned to ensure the elimination of a resultant magnetic field component in the arc perpendicular to its axis. Such a component could cause arc deflection resulting in asymmetry. The magnetic-field free condition was achieved by making the anode leads vertical (parallel to the arc axis) and symmetrically distributed around the arc. The cathode lead was coaxial with the arc for about 14 in. above the torch, and the anode leads extended vertically downward for about the same distance.

Accurate positioning of the arc and setting of the arc length was achieved by means of the image projected upon calibrated grids in conjunction with three precision dial indicators. The bodies of these were secured to the frame supporting the arc assembly and placed in contact to appropriate moving parts to indicate the vertical position of the torch, the vertical position of the anode, and the horizontal position of the anode. The latter were used for making the pressure-probe measurements. One of these indicators is shown in the accompanying figures.

The motion of the anode relative to the torch and the motion of the assembly relative to the optic axis for the early experiments were effected by two 1-rpm synchronous motors connected through speed-reducing gear trains to screw drives which resulted in a scan rate of 26 mils/min, only 1 mil/min faster than used by Nestor (Ref. 12). Phase III experiments, where higher power densities were encountered, were made with a 90 mils/min scan speed to minimize anode melting. No heat flux measurements were made at this speed because of thermal lag.

Figure 3-4 is a view of the drive mechanism located behind the torch assembly shown in Fig. 3-2. The synchronous motors were geared down to rotating nuts which traveled on fixed screws to provide a scan speed of 26 mils/min or 90 mils/min in either direction. Limit switches were provided on each drive as a safeguard. A remote control switching arrangement permitted stopping, starting, and reversing of the individual motors as well as stopping or starting the motors simultaneously as required for coincident current, heat, and continuum scanning.

3.3.2 Calorimetry

The rate of heat flow into the monitored anode section was determined by setting a constant water flow rate through the anode and recording the change in water temperature as the anode passed into the arc. Variations in water flow rates were eliminated by means of a pressure regulator in the input lines to the anode (to block variations in the line pressure) and by filtering the water to ensure clean, unrestricted lines.

Two chromel-alumel thermocouples connected in opposition were used to indicate the rise in cooling water temperature. The inlet water thermocouple was immersed in the feed-line water and the outlet thermocouple was soldered to a thin brass sleeve in the exhaust line, electrically isolated from the anode and wrapped in thermal insulation to eliminate errors caused by heat lost to the surrounding air. Electrical insulation was necessary to prevent electrical interaction between the power source and the recording potentiometer used to monitor the thermocouple output.

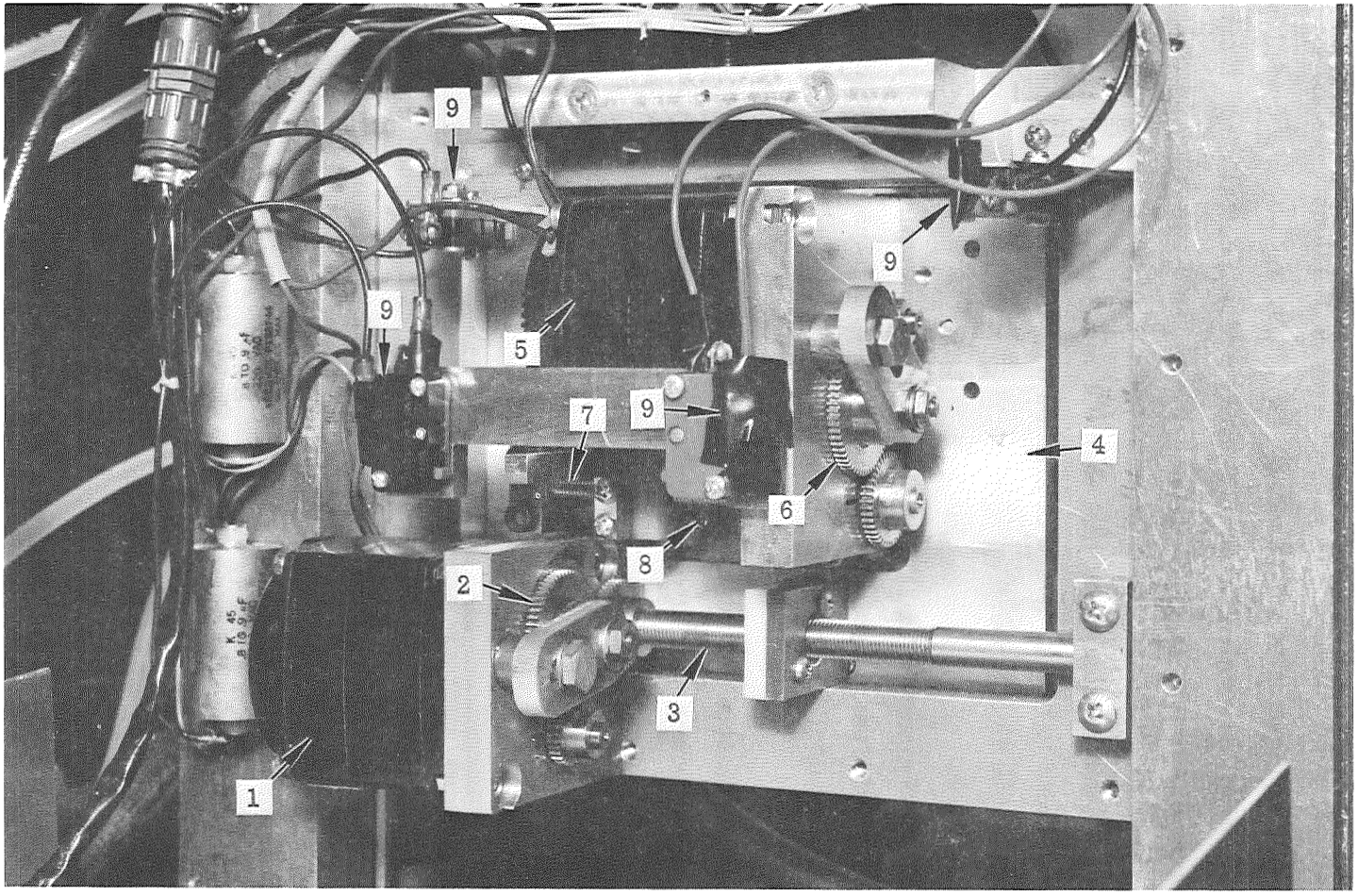

Key:

1 Arc Assembly Drive Motor
2 Arc Assembly Drive Reducing Gears
3 Arc Assembly Drive Screw
4 Arc Assembly Support Plate
5 Anode Assembly Drive Motor
6 Anode Assembly Drive Reducing Gears
7 Anode Assembly Drive Screw
8 Anode Assembly Support Plate
9 Limit Switches

Fig. 3-4 Arc-Drive Mechanism (View From Rear)

3.3.3 Continuum Intensity

Continuum intensity traces were obtained by means of a Jarrell-Ash half-meter Ebert-type spectrometer equipped with a 1180-grooves/mm grating which provided a 16 A/mm reciprocal linear dispersion in the first order and a spectral range from 2000 to 8000 A. An achromatic lens (Figs. 3-1 and 3-2) was used to project an image of the arc at about 3 times magnification onto the entrance slit of the spectrometer. The slit width and length were maintained at less than 0.5 mm to obtain measurements from regions of the arc close to the anode and of minimum volume in the plasma, i.e., as close as possible to a time line probe.

The continuum intensity was sensed by a 1P21 photomultiplier operating with 120 VDC across each dynode supplied from a Furst Electronics high-voltage power supply modified by adding a fine control for the adjustable voltage output.

Phase II continuum measurements were made with the arc operating on the split anode. For Phase III, when higher power densities could damage the surface, a water-cooled anode with a replaceable top was used.

3.3.4 Instrumentation

The three measured functions, current, heat flux, and continuum, were initially recorded by a Honeywell multipoint recording potentiometer. More refined Honeywell 520 X-Y plotters operating in the time-base mode were used for Phase III measurements. Since the three function outputs were not all the same, it was necessary to provide amplification or attenuation either to produce a significant deflection or to bring the maximum deflection within the recorder range for the multiprint recorder.

For the current measurements it was necessary only to incorporate, across the current shunt terminal, a precision voltage divided with an attenuation ratio selected to provide near 1 mV peak output for the particular arc current under investigation.

The peak thermocouple output was generally less than 1 mV. Hence, a dc amplifier was required to produce sufficient gain to give a potentiometer deflection of nearly full scale with the maximum water temperature difference for a given current. A Leeds and Northrup microvolt-indicating amplifier with several amplification factors was used for this purpose.

Measurement of the continuum intensity required auxiliary equipment to perform several functions. First, the peak photomultiplier voltage change had to be reduced to the order of 1 mV with a simple voltage divider providing the proper input impedance to the recorder. Second, a bias was needed to bring the "dark" photomultiplier voltage to within the recorder range. With this arrangement it was possible to obtain the maximum photomultiplier sensitivity.

The pressure probe anode was of the same general shape as the original split-anode but was made in one piece; that is, without a splitting plane. A 0.013-in.-diameter hole drilled at the center, perpendicular to the surface, was soldered to a small diameter tube through the water-filled anode body and out through the cylindrical wall. This was in turn connected to a water manometer by means of a plastic tube. Since the measurements were made near the center of the 3-in.-diameter anode surface which carried all of the arc current, there was no magnetic arc deflection as in the case of measurement with the split anode.

The water manometer used for the pressure measurements was designed of 4-mm glass tubing and was connected to the probe hole in the anode by means of a 1/16-in.-diameter copper tube about 20-in. long. Selection of these materials was made to minimize the gas volume in the device thereby providing a good response time despite the small diameter of the probe hole.

3.3.5 Power Supply

The arc current was supplied by a Vickers electronically controlled constant current full-wave rectifier equipped with high frequency starting. Arc voltage was measured with a Weston Model 931 precision voltmeter connected between the torch and anode.

3.4 EXPERIMENTAL PROCEDURE

3.4.1 Arc Measurements

Most of the current, heat flux, and continuum measurements were simultaneously recorded to ensure that any variations in characteristics from arc to arc operating under the essentially same conditions would not complicate attempts to correlate the measured curves.

In preparation to obtaining data curves for one set of conditions, a low current arc was started near the center of the unmonitored anode and adjusted to the proper length and current. The inputs were then connected to the instrumentation from which they were originally disconnected to prevent damage by the high-frequency high-voltage used to start the arc. The gear drives of the scanning mechanism were disconnected and the splitting plane position relative to the arc axis was adjusted so that half of the total arc current was delivered to the monitored anode. This, in effect, placed the arc axis in the anode splitting plane.

Next, the entire arc assembly was moved horizontally until the maximum photomultiplier deflection was observed and the drive gears were reengaged. This made the centers of the traces on the multipoint recorder practically coincident, thereby facilitating comparison of the traces on a cursory basis. Also, it placed the image of the splitting plane over the spectrometer slit.

Simultaneous scanning of current and heat flux with continuum intensity was accomplished by driving the anode assembly in one direction relative to the arc axis and the entire assembly in the opposite direction. In this way, the arc image moved at a constant rate across the spectrometer slit while the anode image remained fixed with the splitting plane coincident with the slit. Prior to actual monitoring of the run, both drives were backed off to the zero reading point and reversed to permit recording of a complete trace which could easily be checked for symmetry. All pertinent data, i.e., arc current, length, voltage, cooling water flow rate, and recorder sensitivity were noted on the recorder chart before each run.

Spectrometer wavelength scans were made with each shielding gas (argon, helium, helium-argon) and the auxiliary recorder shown in Fig. 3-1 to identify regions of the continuum free from lines. A similar precaution was taken for continuum intensity traces on molten aluminum. A check of the possible lines was made from published spectra. The wavelengths of 4089 A and 4095 A were unobstructed and used for argon and helium, respectively, and 4080 A was used for the Phase III measurements when additions were made to the shielding gas.

3.4.2 Data Reduction (Phase II)

Experimental data curves were drawn smoothly through appropriate points on the strip chart records. The center of the current trace was established in all cases as the half-current value. Since the heat-flux was simultaneously recorded using the same anode, its center was taken at the same place. The continuum center did not always coincide with the previous centers since its flat peak prevented exact alignment at the start of each run. Consequently, it was determined by locating the half-width at various intensities.

Values for numerical inversion were obtained from the data curves as follows.

The data curves for the continuum intensity attain a zero value at a well defined distance from the arc axis. In this case, the distance from the curve center to the zero value was geometrically divided into 30 equal intervals and the value on the curve for each point was recorded for computation by the formulas derived in Appendix A. The radial distributions were obtained by means of a Univac 1108 computer and a General Dynamics Electronic Company SC-4020 Plotter.

A modification of this procedure was required for inverting the surface probe data (current and heat) since the formula used (see Appendix A) employs second differences which results in a sensitivity requiring greater input accuracy. To improve on the results, an existing computer program was used to approximate the data by a

best-fit curve of degree up to 7 using the method of least squares. In this way it was possible to increase the accuracy from 3-place to 8-place. This resulted in smooth radial distribution curves instead of the meaningless zig-zags obtained without the refinement.

Reduction of the heat-flux data required an additional operation since the data never attain a zero value with the experimental apparatus used. This is due to transfer of heat to the monitored anode by gas-streaming and radiation when the arc axis is as much as 1 cm away. An approximation was used for this tail by requiring it to approach a zero value tangentially at twice the zero-current distance, while having the same value and slope as the data curve where the current becomes zero. The result is a cubic polynomial which "fits" the experimental data cut-off point and attains a zero value in a well-behaved manner. A derivation of the general cubic and a procedure for determining the coefficients is given in Appendix B. Since the measured values are small in this region, the error introduced near the arc axis is also small.

The modified heat-flux data curves were smoothed by applying the least-squares curve fitting described previously and points from the resulting curves (60 intervals long) were used for the inversion program to obtain the radial distribution curves.

All of the radial distributions were then replotted after converting the abscissa values from interval numbers to actual radial distance from the arc axis.

In the case of continuum intensity measurements, the original data curves were normalized to a peak value of 100 since no standard was employed to obtain absolute intensity values. No usefulness is lost by this since the curve shapes can be compared with the current or heat-flux distributions to determine how close a correlation exists between them. For example, the half widths and curve shapes can be compared in a strictly quantitative manner. Also, for simplicity, the square root of the intensity

was not calculated in every case although it is necessary to produce a result more nearly proportional to the electron density distribution. The reason for eliminating this step is that the relative location of the half-widths would be unaffected and the results would still be valid for determining if arc modifications tested in Phase III produced any contraction of the plasma core, that is, any increase in power density. A further simplification also applied in Phase III is described in the corresponding section.

3.5 RESULTS AND DISCUSSION

The results presented are the radial distributions only for the current density, heat-flux, continuum intensity, and the plasma-stream pressure. Raw data for the first three have been excluded since they are of little interest. Metric units have been used throughout to facilitate computation, although dimensions such as those for the cathode are in English units. Plasma-stream pressures are in centimeters of water at 20°C, as measured, since the curves are for comparison only, which requires only consistent units.

All the data curves are valid within experimental error with the possible exception of those for the current and heat-flux distribution. In both of these cases, the numerical inversion scheme results in anomalous results when very small variations appear in the raw data, as will be shown. Much effort has been devoted to improving the results as described in subsection 3.4, and the curves presented are greatly improved compared to those obtained initially. An additional modification of the inversion scheme which may produce more meaningful radial distributions was tried for the case of a 3-mm, 150-A arc in argon. It is not certain if the current and heat-flux distribution curves shown are truly representative because they differ significantly from the continuum intensity traces and from similar curves shown in the literature (Ref. 12).

3.5.1 Current Density

Radial current density distributions are shown in Figs. 3-5 through 3-8 for arc lengths of 1, 2, and 3 mm and currents of 150, 200, 250, and 300 A, in argon flowing at 18 cfh, operating between a water-cooled copper anode and a 2% thoriated tungsten cathode 3/16-in. in diameter ground to a 10° taper with a flat tip 55 mils in diameter. This cathode configuration, designated here as 3/16"-10°-55 has a 39-mil smaller tip diameter than the NASA tip.

The curves exhibit an expectable form well away from the axis but appear anomalous at distances less than about 0.2 cm. A typical current density curve shows inconsistent radial variations such as rounded off-axis maxima and sharp maxima or minima on the axis. There appears to be a consistent change in peak current density for the 1-mm arcs at all currents. Figure 3-9 shows that these peak values fall very close to a straight line in the arc-current interval studied. The slope is 15.8 A cm^{-2} increase in peak current density for each ampere increase in arc current. However, this is less than the 22 A cm^{-2} per ampere which would obtain if doubling the arc current doubled the peak density, It appears that more current is carried in the outer portions of the arc as the current increases.

The more consistent form of the distribution at the shortest arc length suggests that the plasma is perturbed at the splitting plane when the arc is longer and less stiff.

The behavior of the current density distributions near the axis appears too erratic to be real, particularly for the longer arcs. This and the well-behaved form of the continuum intensity distributions suggest another cause which will be argued subsequently. Also, the heat and current curves for the same arc are not always consistently similar or dissimilar, suggesting some distortion of the data. Similarities are described in greater detail in the next subsection.

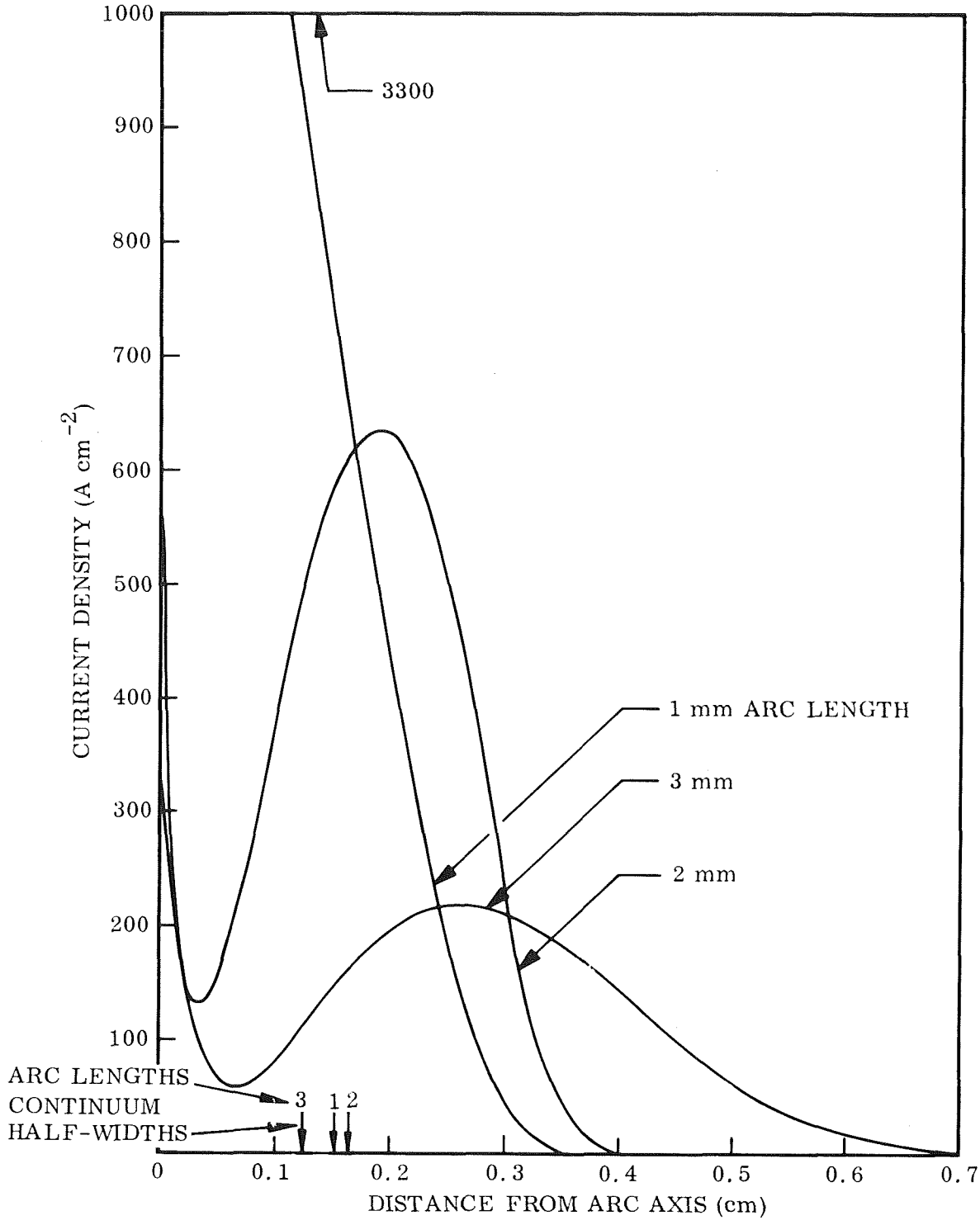

Fig. 3-5 Radial Current Density Distribution for "Normal" DCSP-GTA's in Argon With: Anode – Water-Cooled Copper; Gas Flow – 18 cfh Through No. 12 Cup With Gas Lens; Arc Length – 1, 2, and 3 mm; Current – 150 A

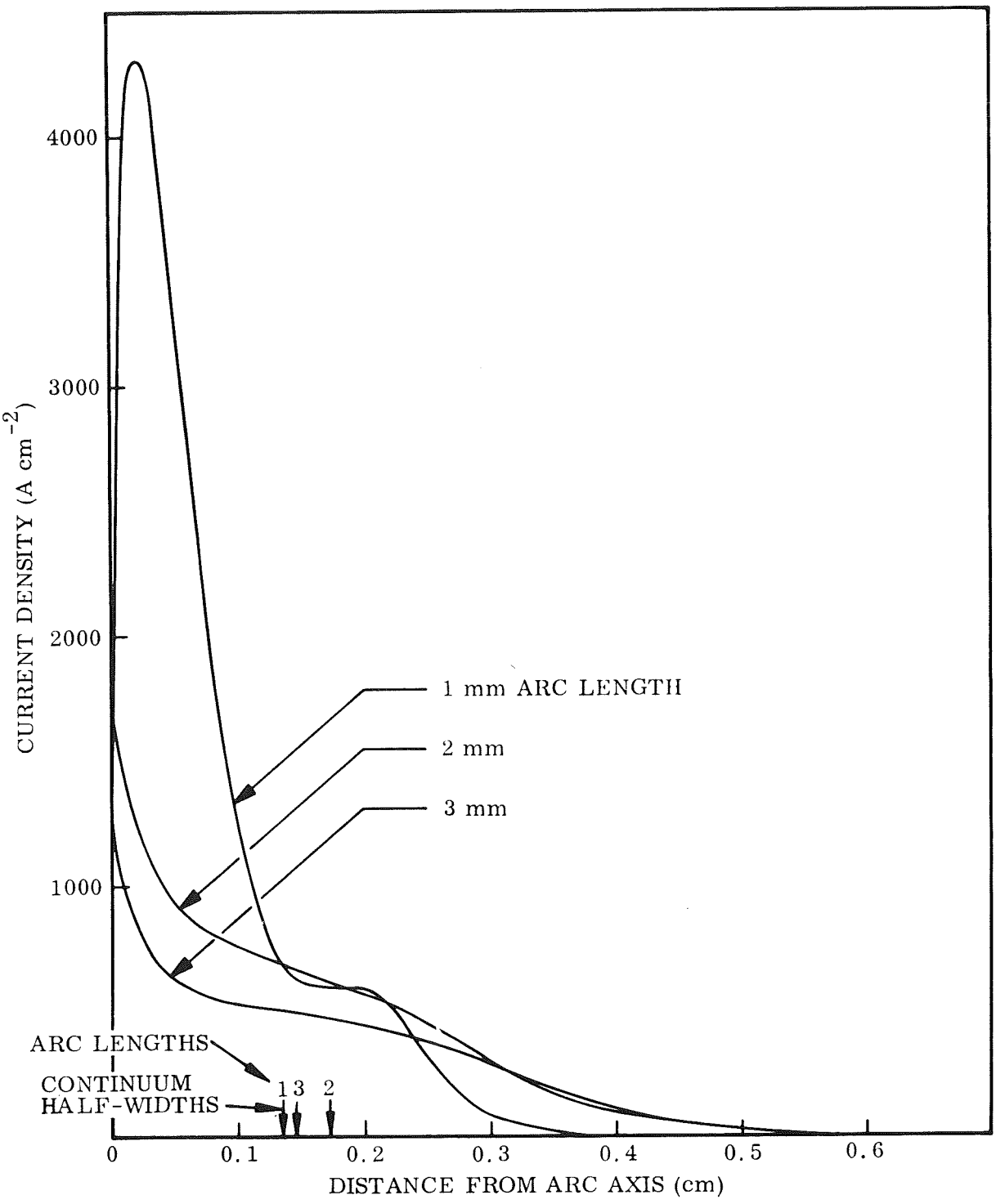

Fig. 3-6 Radial Current Density Distribution for "Normal" DCSP-GTA's in Argon With: Anode – Water-Cooled Copper; Gas Flow – 18 cfh Through No. 12 Cup With Gas Lens; Arc Length – 1, 2, and 3 mm; Current – 200 A

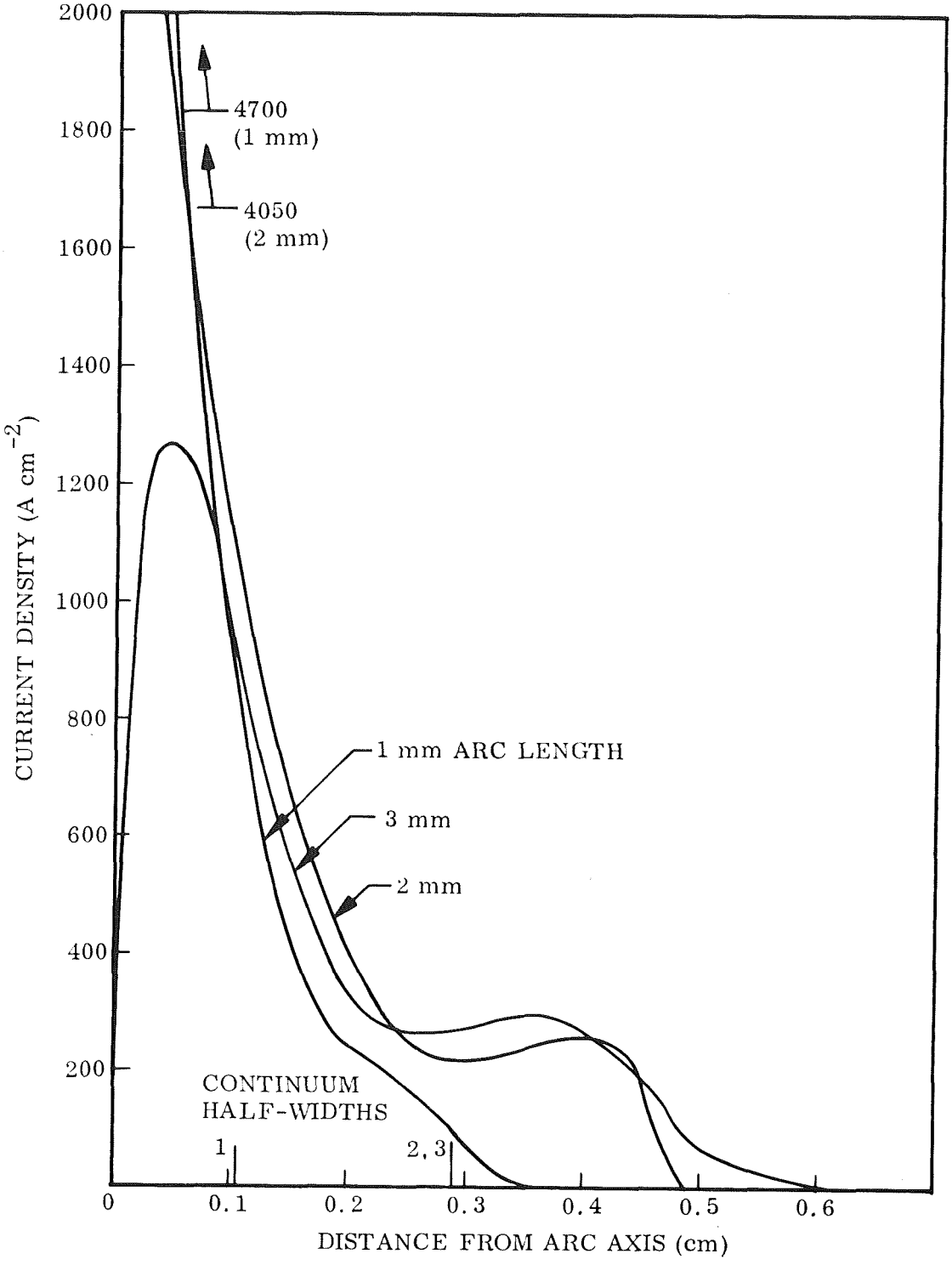

Fig. 3-7 Radial Current Density Distribution for "Normal" DCSP-GTA's in Argon With: Anode – Water-Cooled Copper; Gas Flow – 18 cfh Through No. 12 Cup With Gas Lens; Arc Length – 1, 2, and 3 mm; Current – 250 A

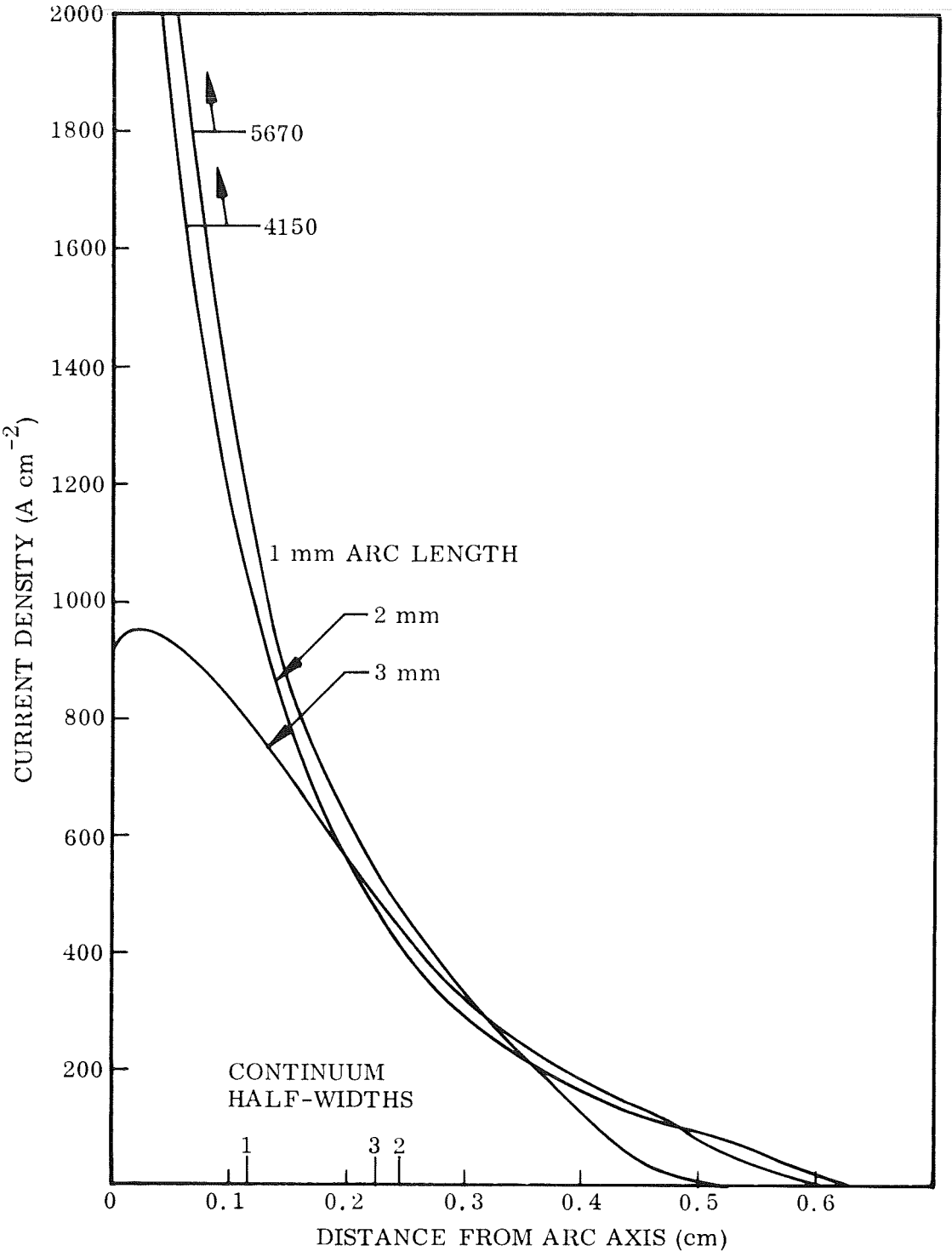

Fig. 3-8 Radial Current Density Distribution for "Normal" DCSP-GTA's in Argon With: Anode – Water-Cooled Copper; Gas Flow – 18 cfh Through No. 12 Cup With Gas Lens; Arc Length – 1, 2, and 3 mm; Current – 300 A

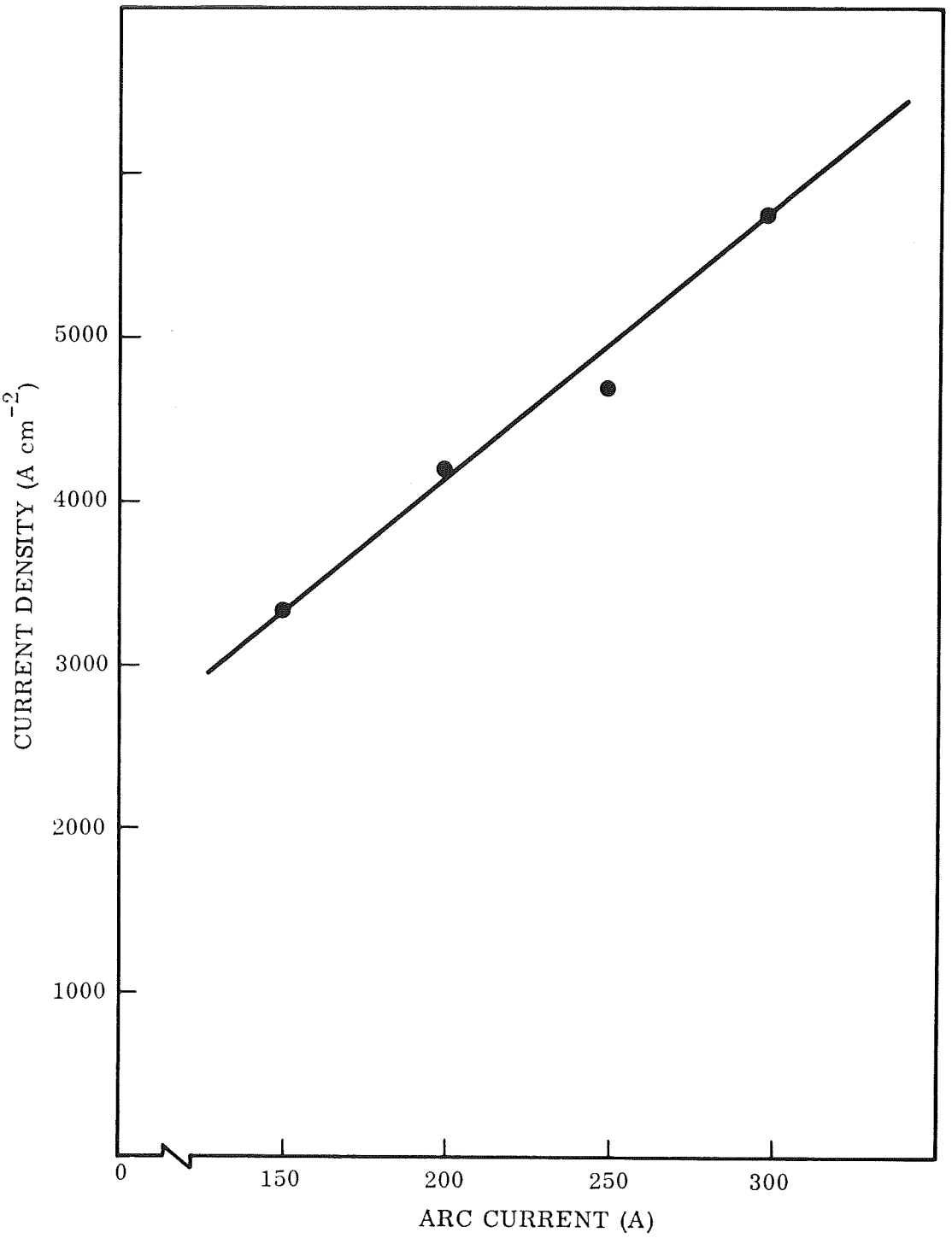

Fig. 3-9 Peak Current Density Versus Total Arc Current for a 1-mm "Normal" GTA on a Water-Cooled Copper Anode

3.5.2 Heat-Flux

Figures 3-10 through 3-13 show the radial distribution of heat-flux intensity for the same arc conditions mentioned in the previous section. Again, the behavior of the curves appears reasonable for radial distances greater than about 0.2 cm. For smaller radii, however, there occur off-axis rounded maxima and sharp maxima or minima on the axis. The maxima are positioned similarly to those for the current intensity but there is no correlation between the on-axis maxima or minima except for the 250- and 300-A arcs. This can be seen more clearly by referring to Table 3-1 which shows the positions of the current and heat flux maxima for all cases.

Table 3-1

MAXIMA POSITIONS OF CURRENT AND HEAT-FLUX RADIAL DISTRIBUTION CURVES FOR ALL CASES

Arc Current (A)	Arc Length (mm)	Peak Positions (cm)	
		Current Density	Heat Flux
150	1	0	0.035
	2	0, 0.19	0.08
	3	0, 0.26	0, 0.175
200	1	0.025	0
	2	0	0.075
	3	0	0
250	1	0	0
	2	0	0
	3	0.05	0.075
300	1	0	0
	2	0	0
	3	0.025	0.075

A plot of the peak heat flux intensities versus current (Fig. 3-14) shows a linear dependence similar to that found with the current except for the 300-A value. The

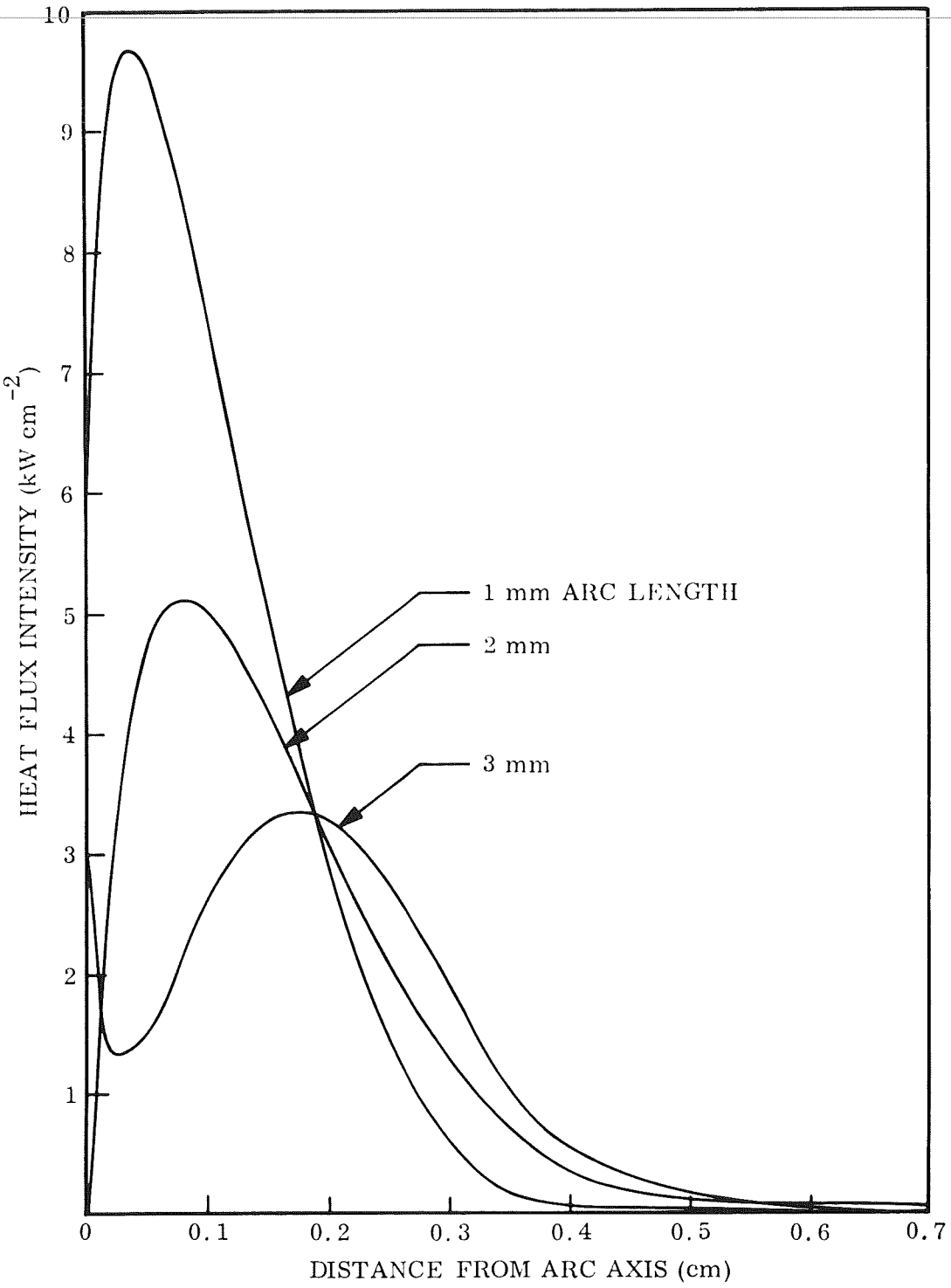

Fig. 3-10 Radial Heat-Flux-Intensity Distribution for "Normal" DCSP-GTA's in Argon With: Anode – Water-Cooled Copper; Gas Flow – 18 cfh Through No. 12 Cup With Gas Lens; Arc Length – 1, 2, and 3 mm; Current – 150 A

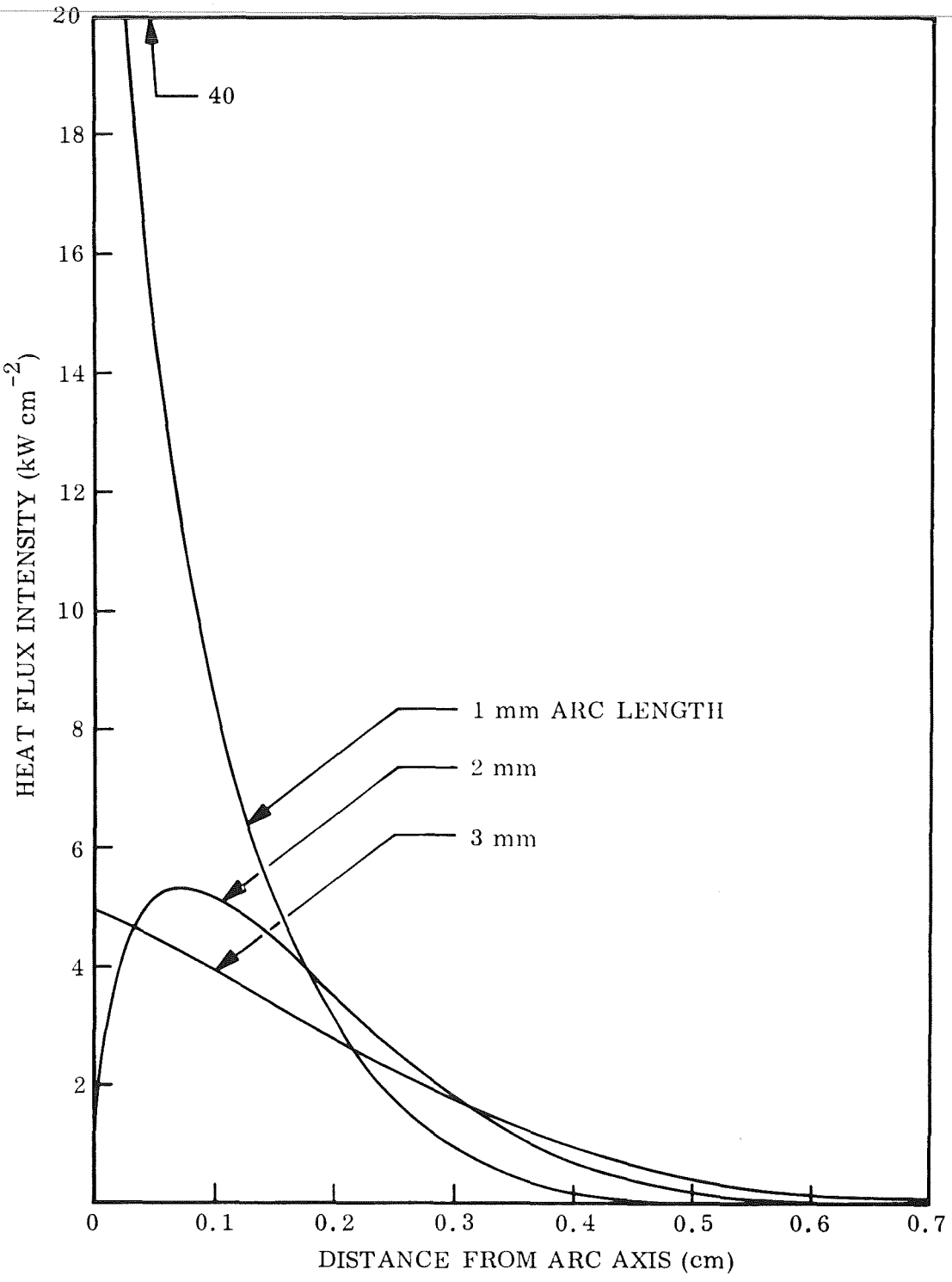

Fig. 3-11 Radial Heat-Flux-Intensity Distribution for "Normal" DCSP-GTA's in Argon With: Anode – Water-Cooled Copper; Gas Flow – 18 cfh Through No. 12 Cup With Gas Lens; Arc Length – 1, 2, and 3 mm; Current – 200 A

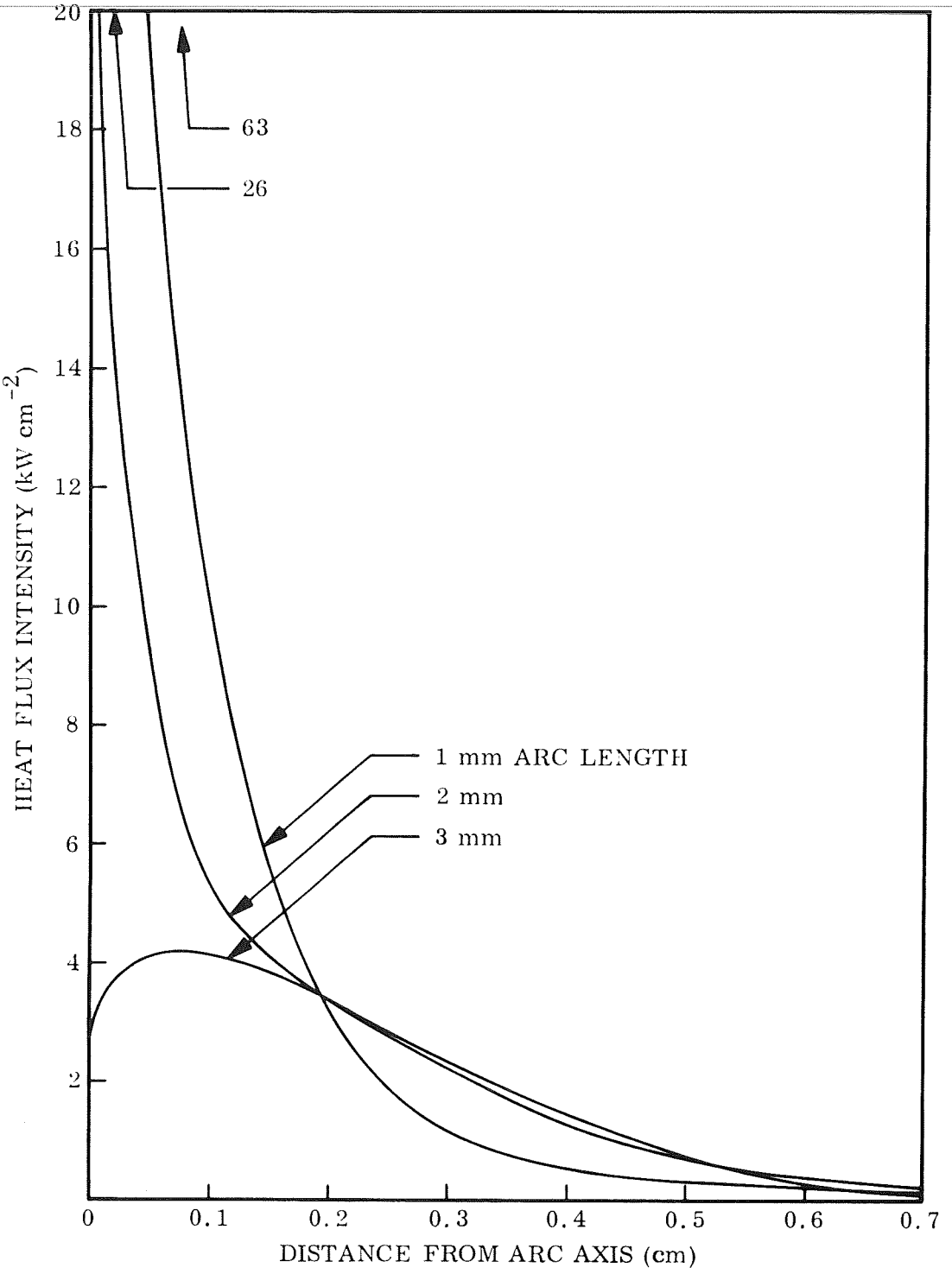

Fig. 3-12 Radial Heat-Flux-Intensity Distribution for "Normal" DCSP-GTA's in Argon With: Anode – Water-Cooled Copper; Gas Flow – 18 cfh Through No. 12 Cup With Gas Lens; Arc Length – 1, 2, and 3 mm; Current – 250 A

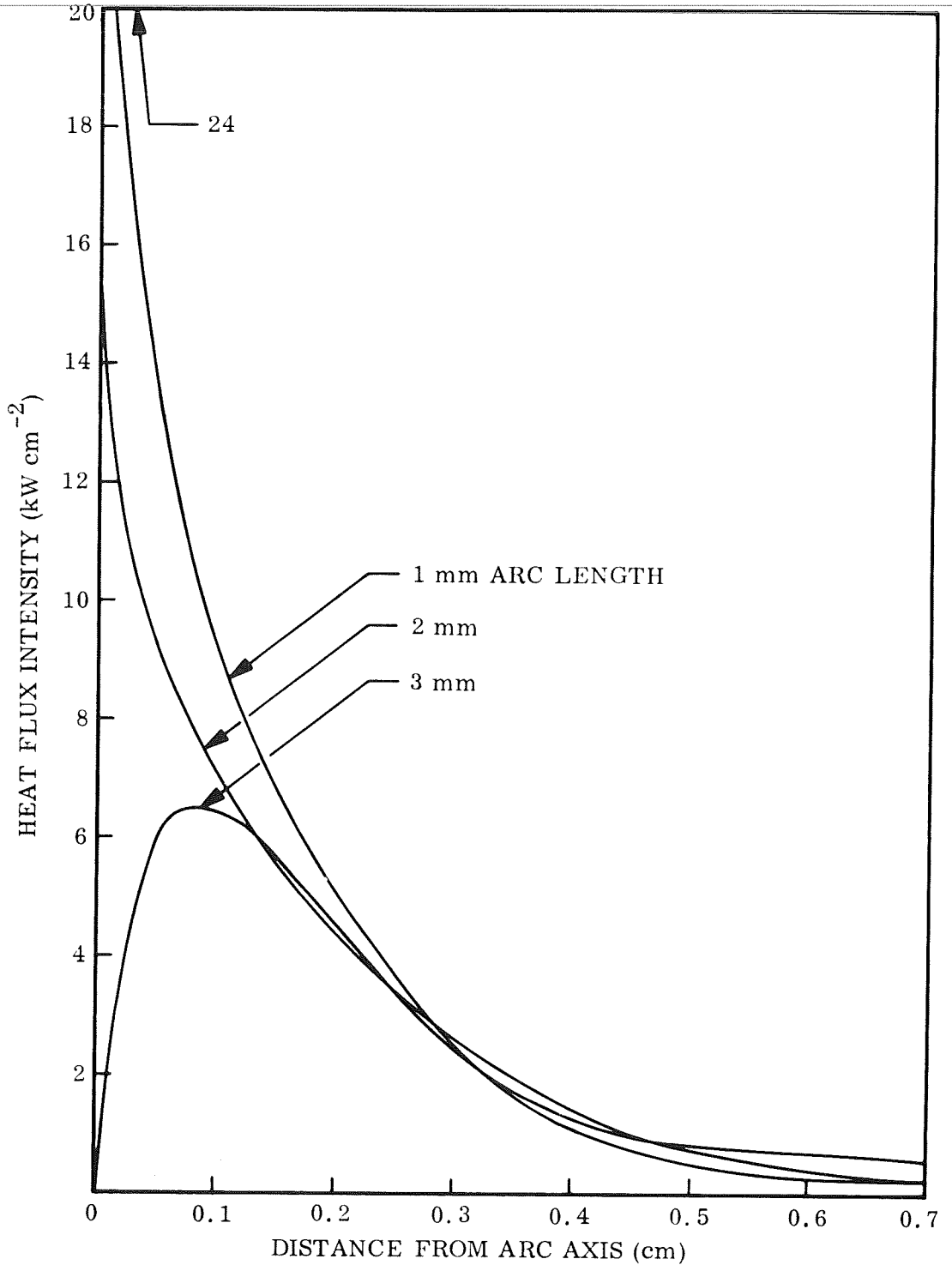

Fig. 3-13 Radial Heat-Flux-Intensity Distribution for "Normal" DCSP-GTA's in Argon With: Anode – Water-Cooled Copper; Gas Flow – 18 cfh Through No. 12 Cup With Gas Lens; Arc Length – 1, 2, and 3 mm; Current – 300 A

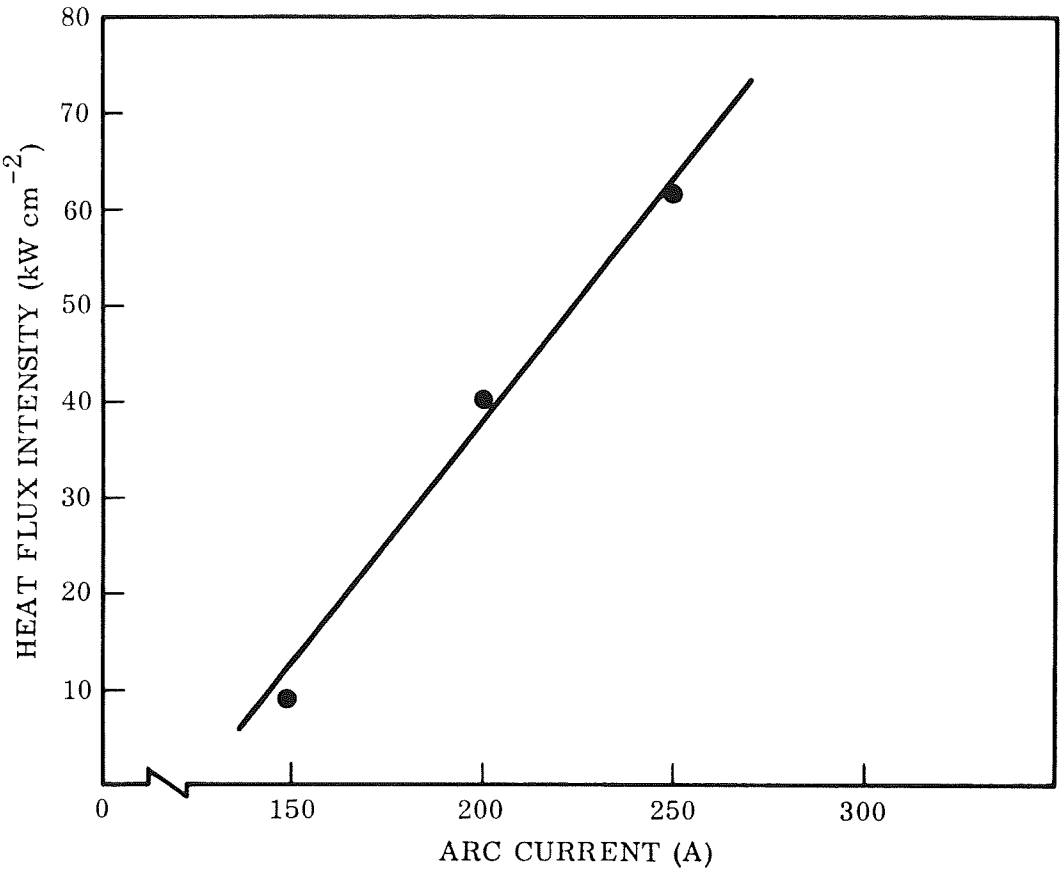

Fig. 3-14 Peak Heat Flux Intensity Versus Total Arc Current for a 1-mm "Normal" GTA on a Water-Cooled Copper Anode

slope, however, is 22 as compared to 18.5. If electron condensation were the dominant anode heating factor, and if the anode drop were independent of current, the slopes should be identical. This suggests several possibilities: (1) the anode voltage changes with current and (2) plasma streaming contributes more to heat transfer at higher currents.

The apparent lack of consistency for the results with greater arc lengths is probably due to splitting plane effects as in the case of the current density distribution.

The heat-flux curves also differ from those developed by Nestor, particularly with respect to the sharp on-axis maxima for the smaller lengths. The difference may be real and due to the particular cathode geometry used.

In an effort to resolve the apparent inconsistencies, the sensitivity of the numerical inversion scheme to variations in the form of the experimental heat-flux data was checked for 150 A and 3-mm arc length. Values from the 7th-degree least-squares approximation were used to compute a 3rd-degree and a 2nd-degree approximation, also by the method of least squares. These curves were smoothed to give a tangential approach to zero at the 60th interval to more closely approximate the true behavior. Values from these two curves were then used in the numerical inversion program to yield radial distributions.

Figure 3-15 shows the shape of the three polynomial approximations for the experimental data. On the scale used, the difference between the 7th-degree approximation and the experimental points is barely perceptible. Radial distributions corresponding to these approximations are shown in Fig. 3-16. The sensitivity of the numerical inversion procedure to small variations in the input function is readily apparent, particularly near the axis. Although a detailed error analysis has not been performed, it appears that the extreme sensitivity results from the use of second differences inherent in the scheme.

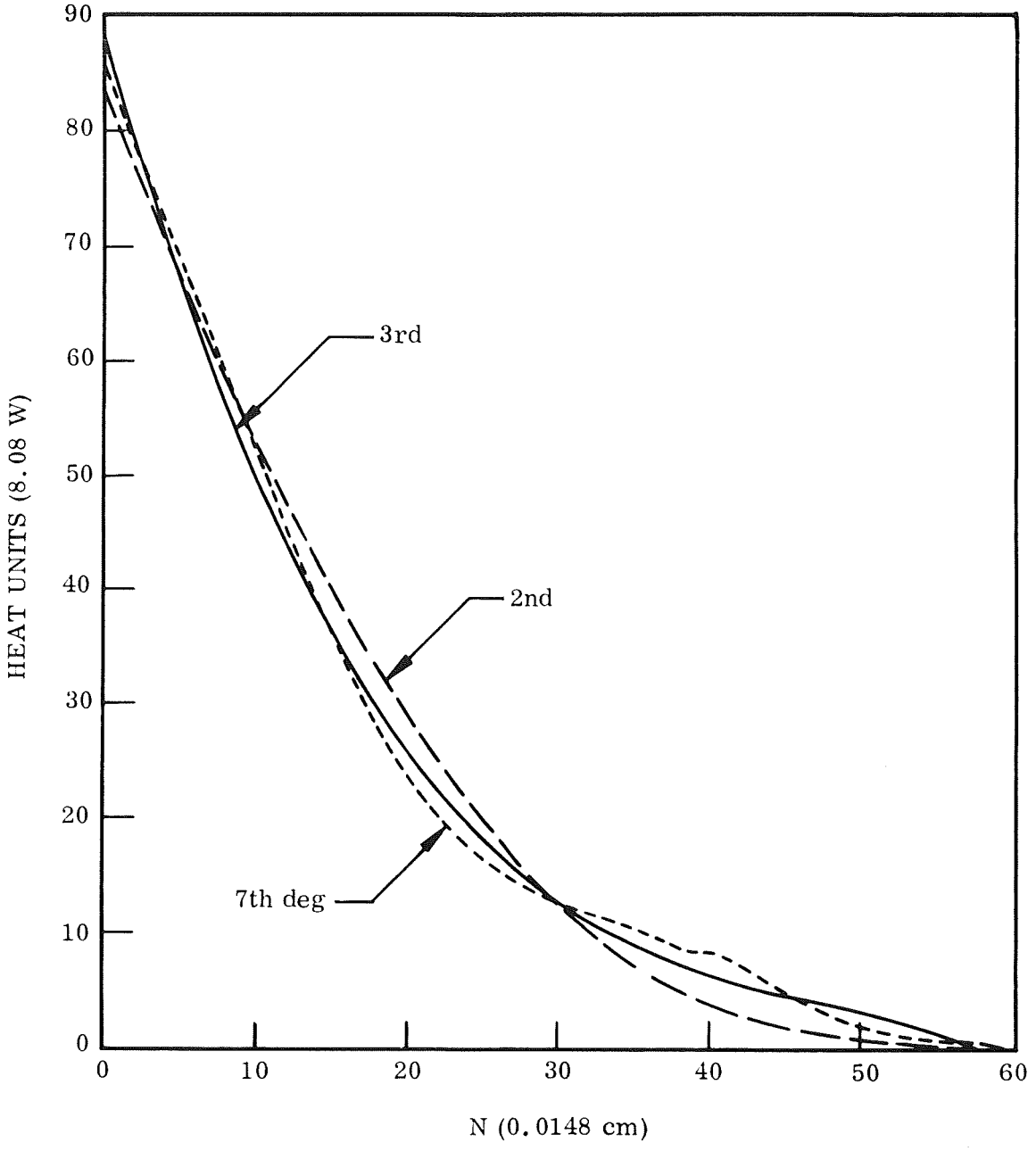

Fig. 3-15 Three Slightly Different Input Data Curves for Determining the Sensitivity of Surface-Probe Inversion Program Used to Obtain Heat-Flux-Intensity Radial Distribution for 150 A, 3-mm Arc

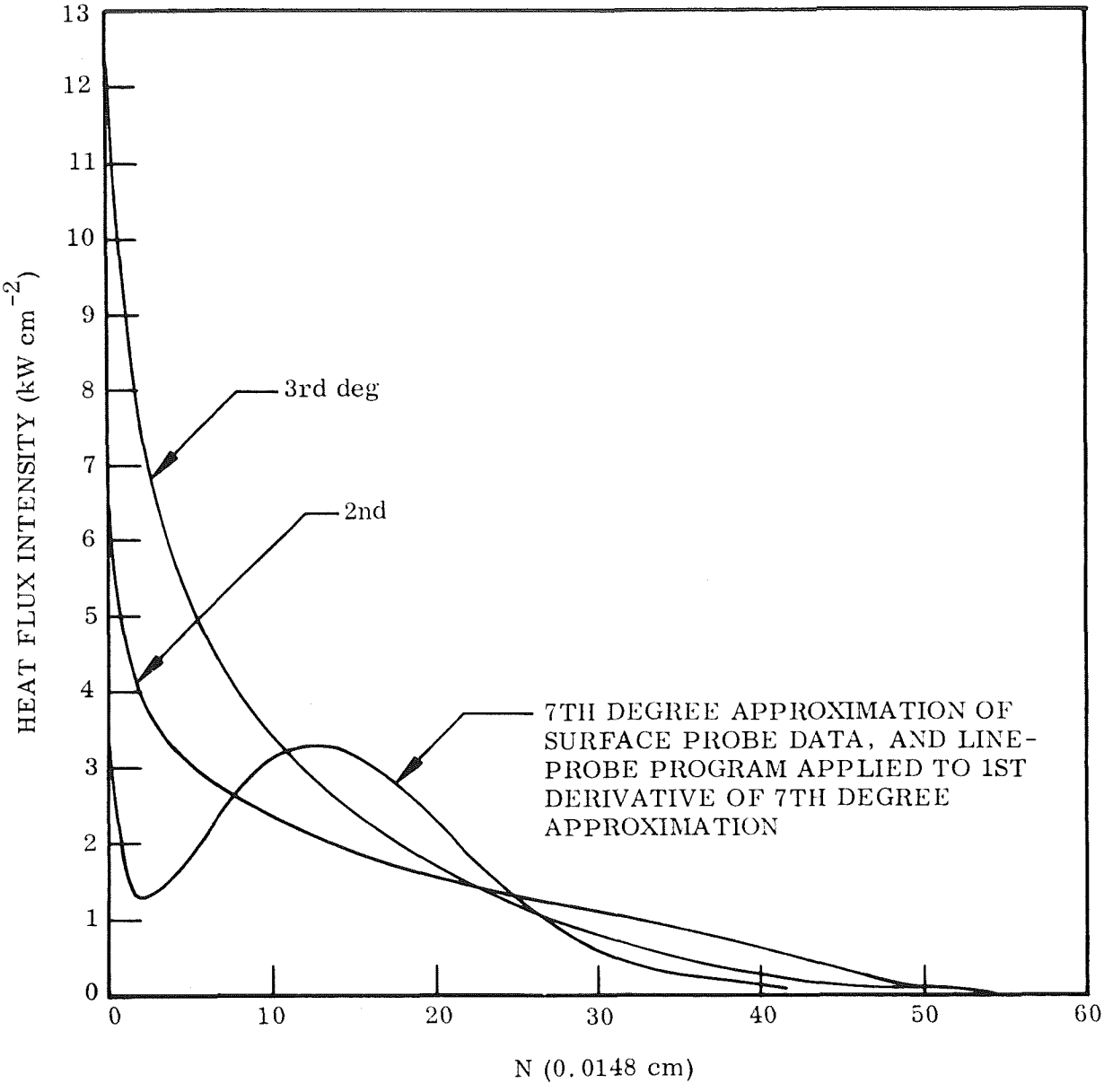

Fig. 3-16 Heat-Flux-Intensity Radial Distributions for Input Curves in Fig. 3-15, Obtained by Application of Line-Probe Inversion Program to First Derivative of 7th Degree Polynomial Approximation

A second check of the surface probe inversion scheme was made by obtaining the derivative of the approximating polynomial for the experimental data and using values from the resulting curve (Fig. 3-17) in the inversion program for the line probe. The radial distribution obtained for this method is included in Fig. 3-16. It is evident that the general shape of the curve is not significantly altered from the one derived by the surface probe scheme using the 7th-degree polynomial approximation suggesting that the apparent anomalies are either real or result from insufficient experimental accuracy.

3.5.3 Continuum Intensity

Radial distributions of the relative continuum intensity for the same arcs used in the current density and heat-flux intensity studies are shown in Figs. 3-18 through 3-21. These curves are all well behaved in the sense that the intensity peaks with zero slope at the arc axis and decreases monotonically with increasing distance from the axis, reaching a zero value tangentially at a well-defined distance which is practically the same as observed in the current distributions for each case.

The continuum intensity theory predicts that the intensity is proportional to the square of the electron concentration. To check this, the square root of the radial distribution curves for 1- and 2-mm arcs at 250 A were normalized to 100 and plotted in Fig. 3-20. The curve shapes are not greatly altered though the half-widths are increased to the extent they no longer approximate those for the radial distributions of current density of heat flux intensity. It is therefore concluded that the half-width of the continuum intensity radial distribution is more representative of the power density than its square root.

It is not possible to compare the continuum intensity half-width with those for the current distribution since the latter curves are not bell-shaped. That the distributions differ greatly between these two measurements can be realized with the aid of the continuum half-widths indicated on the abscissa of the corresponding current distribution curves. The number over each line indicates the arc length for the particular half-width.

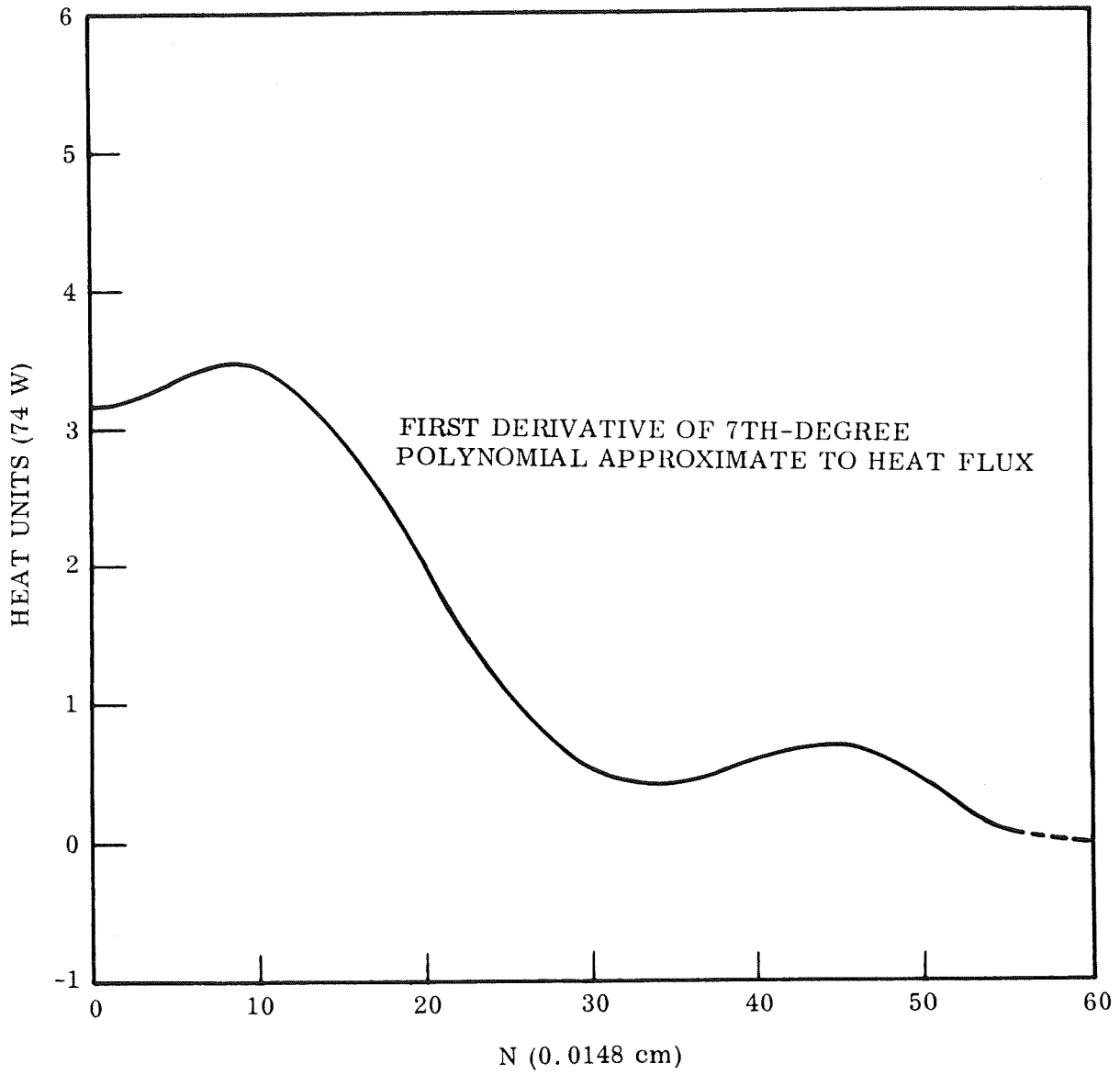

Fig. 3-17 First Derivative of 7th Degree Polynomial Approximation for Heat-Flux Data Used to Obtain Radial Distribution Shown in Fig. 3-16

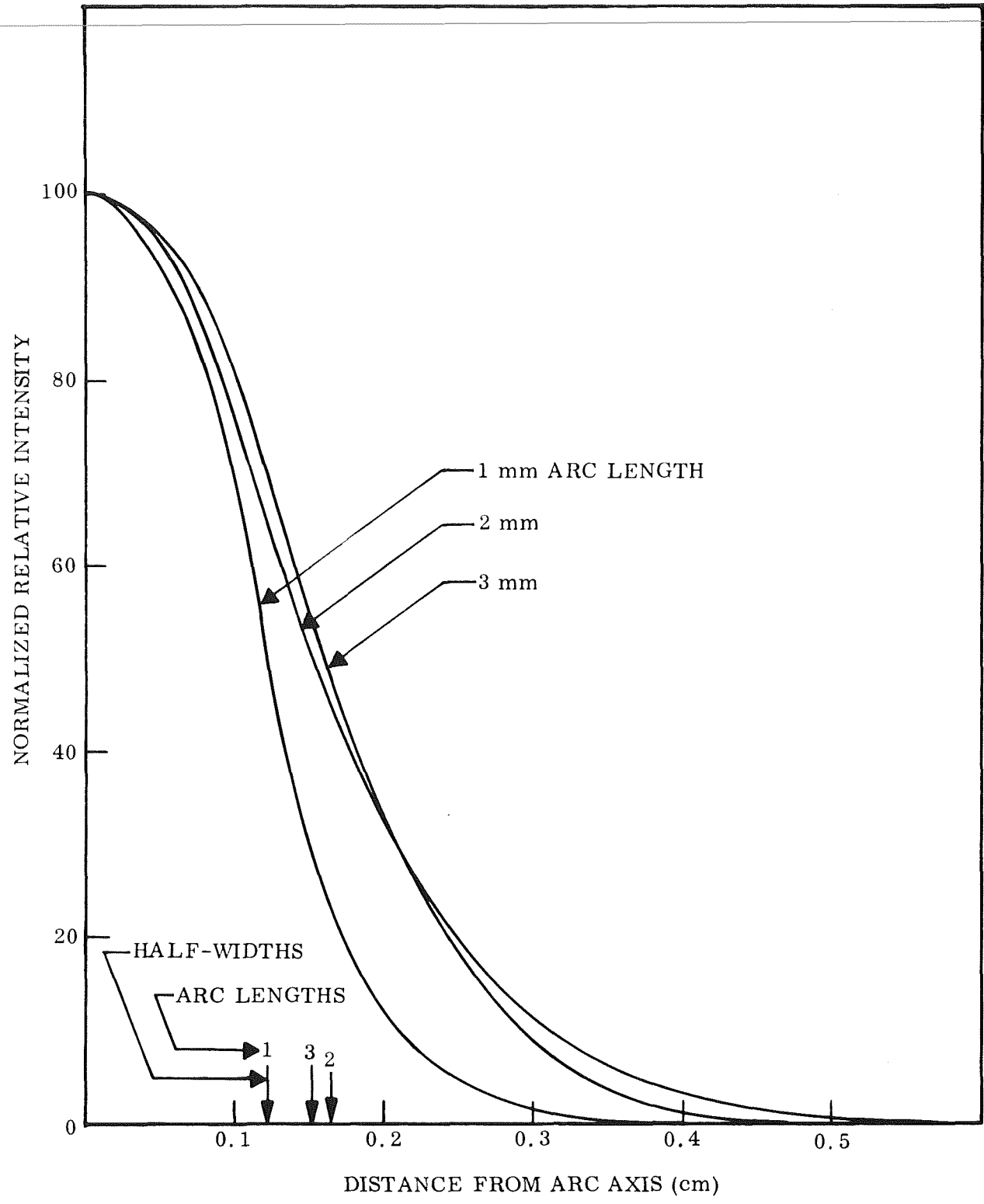

Fig. 3-18 Normalized Radial Distributions of Continuum Intensity for DCSP-GTA's With Argon – 18 cfh; Arc Length – As Indicated; Current – 150 A

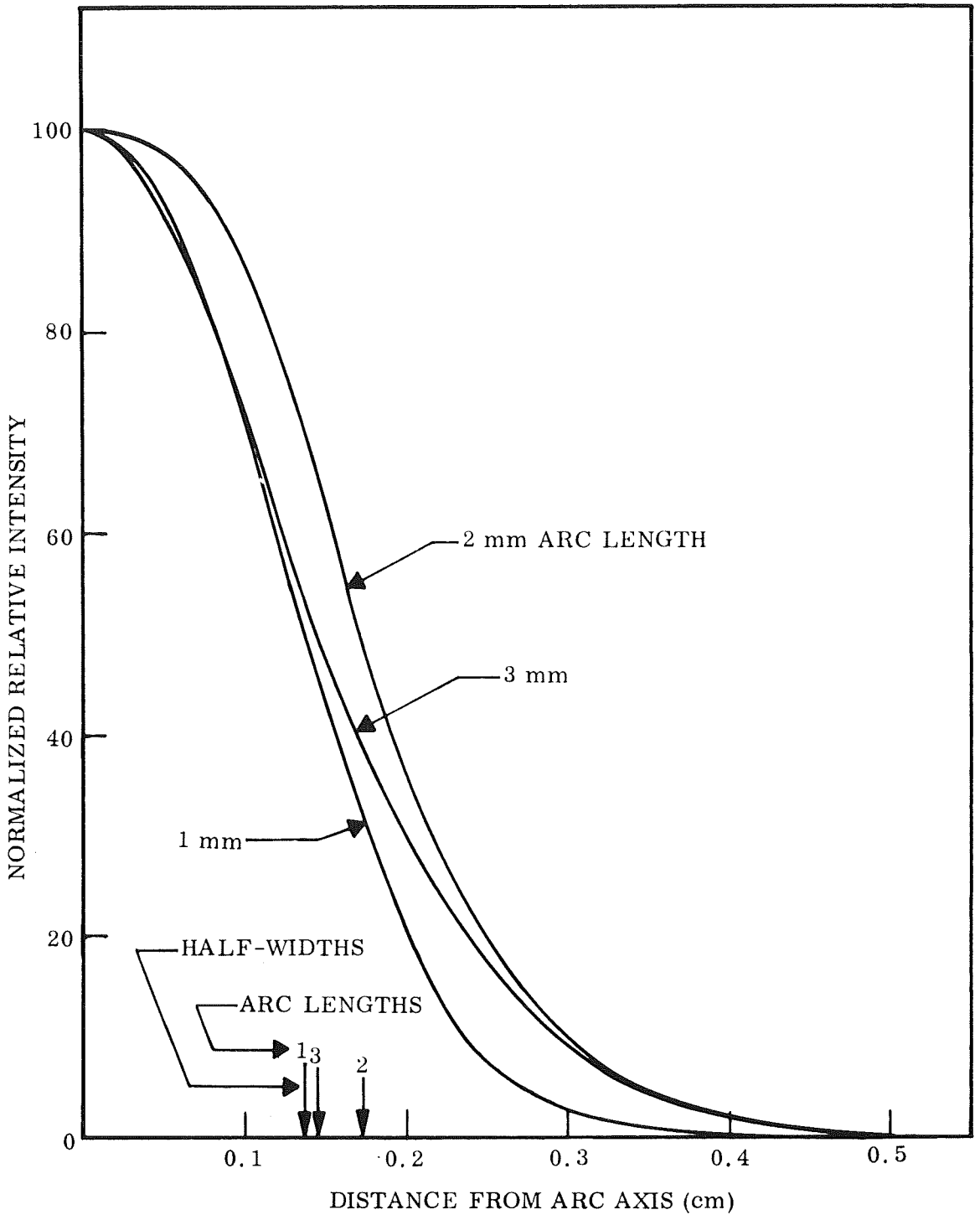

Fig. 3-19 Normalized Radial Distributions of Continuum Intensity for DCSP-GTA's With Argon – 18 cfh; Arc Length – As Indicated; Current – 200 A

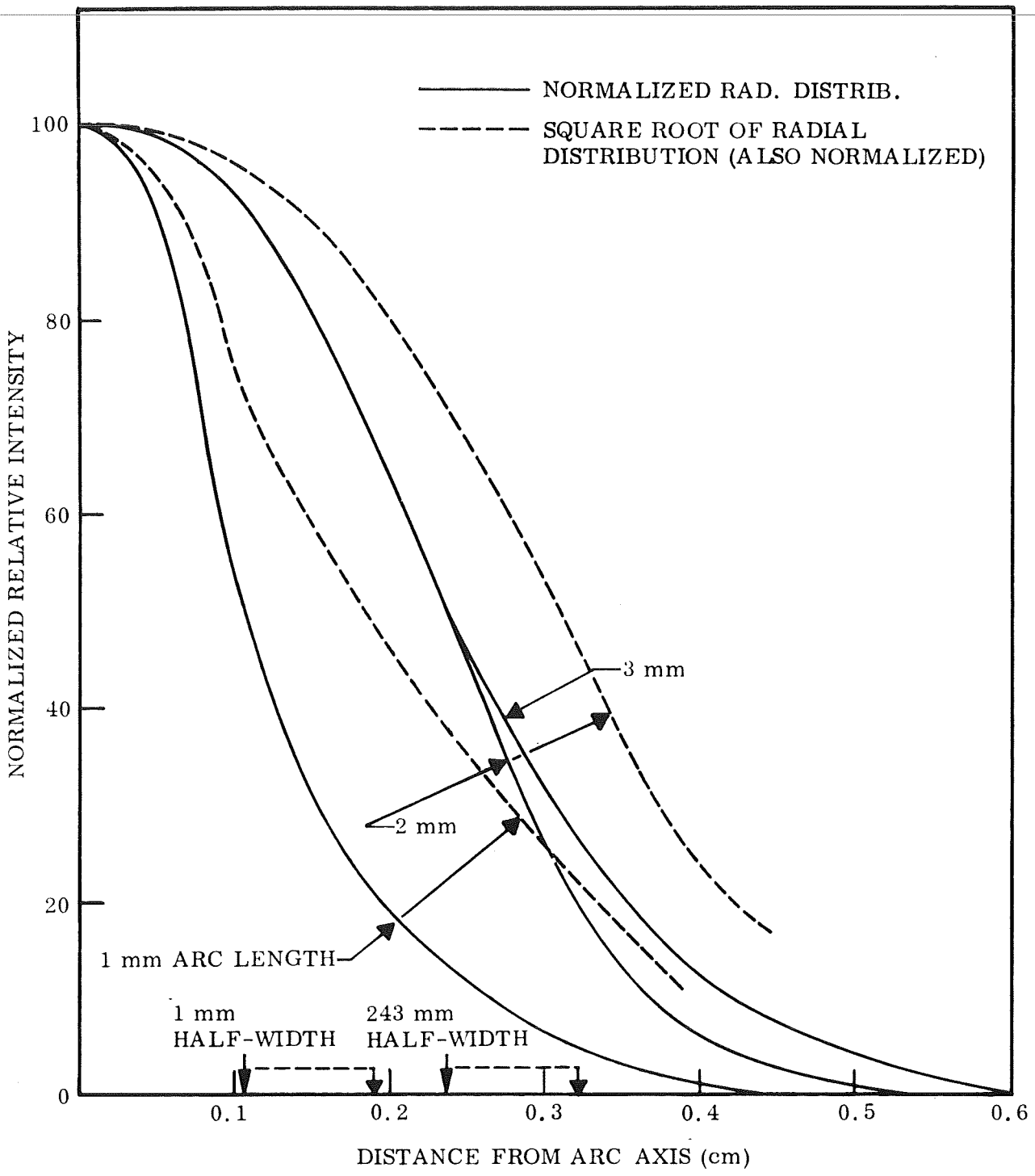

Fig. 3-20 Normalized Radial Distributions of Continuum Intensity for DCSP-GTA's With Anode – Water-Cooled Copper; Gas – Argon at 18 cfh; Arc Length – As Indicated; Current – 250 A

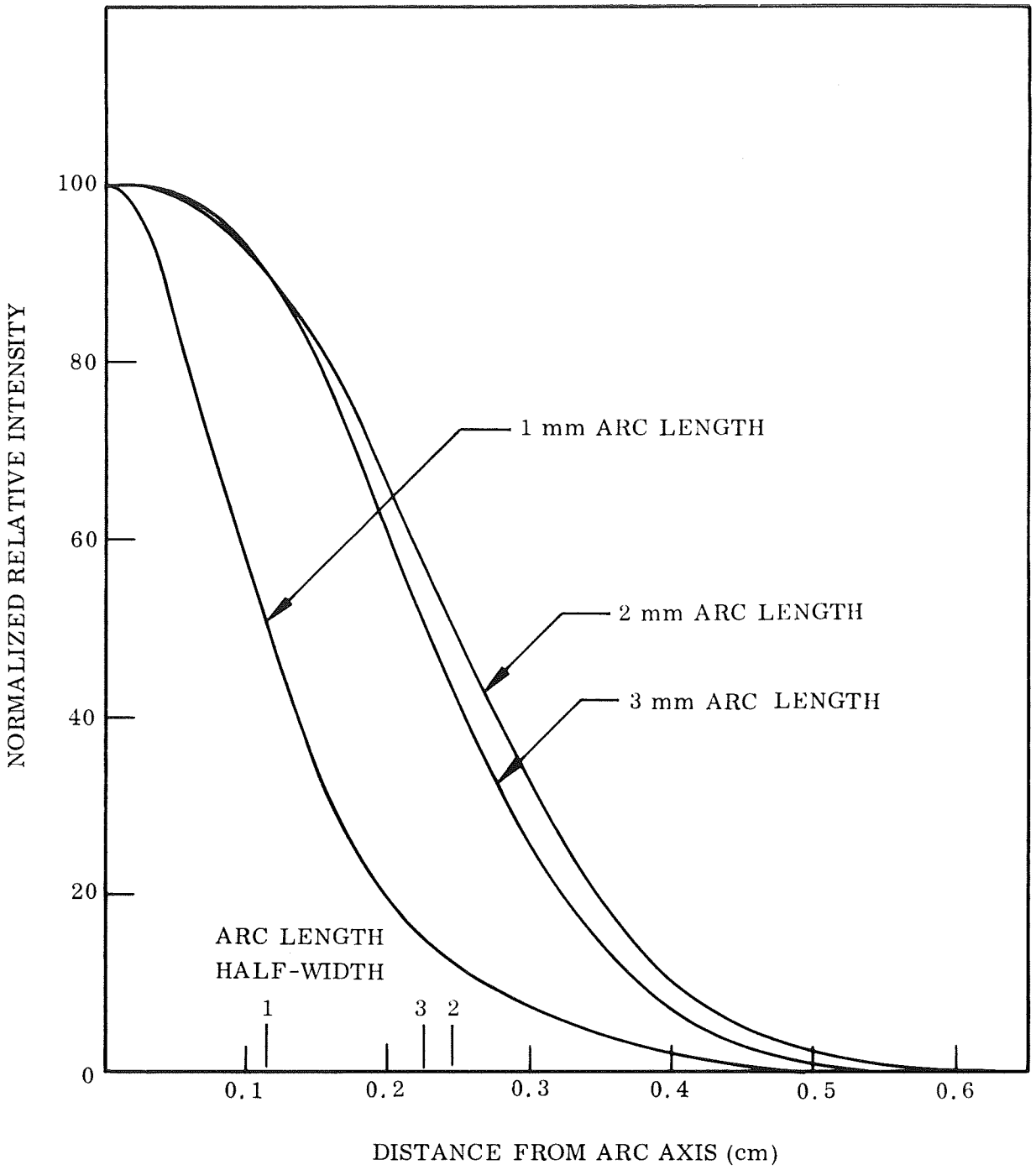

Fig. 3-21 Normalized Radial Distributions of Continuum Intensity for DCSP-GTA's With: Argon – 18 cfh; Arc Length – As Indicated; Current – 300 A

A significant similarity exists for the 1-mm curve at each arc current studied. Their half-widths are very close to 0.1 cm for all except the 200-A arc where the half-width is 0.135 cm. Increasing the current with 2- and 3-mm arc lengths causes an increase in the half-width which appears to reach a constant value of between 0.225 and 0.250 cm for currents of 250 A or greater. If the continuum half-widths were proportional to those for the current and/or heat-flux distributions, this would verify that consistently better power density results from shorter arc lengths as has been demonstrated in practice. Whether or not the intensity distribution for the continuum and that for the current, and/or the heat flux, correlate can be determined only after establishing with certainty that the data reduction scheme for the surface probe and the accuracy of the experimental technique result in truly representative distributions.

Additional continuum measurements were made with the arc on a molten 2219 aluminum anode with the 3/16"-10°-55-2% thoriated tungsten cathode. The purpose was to ascertain to what extent the plasma core, not too close to the anode, changes shape as the arc length is increased. Figure 3-22 shows the observed variation of the normalized continuum intensity with distance from the axis, 2 mm from the cathode, of 150-A arcs operating in argon at 35 cfh. There is little difference between the half-width of the trace as the arc length is increased from 5 to 6 mm. These are 0.115 and 0.105, respectively, a value very close to the half-width of the radial continuum intensity distribution for 1-mm arcs in argon at currents from 150 to 300 A. Figure 3-23 shows a similar result for 200-A arcs of length from 4 to 6 mm at 17.5 and 35 cfh argon. The results for 250-A arcs in helium at 110 cfh, at 1 and 2 mm from the cathode tip are shown in Figs. 3-24, and 3-25, respectively. At 2 mm the half-width is 0.09 and 0.11 cm for 5- and 4-mm arc length, respectively, slightly less than for the case of argon. At 1 mm from the cathode, the half-widths are 0.09, 0.095, and 0.075 cm for arcs 3-, 4-, and 5-mm long. The greater half-widths for the shorter arcs reflect a distortion of the arc by the interaction of the plasma stream with the nearby anode.

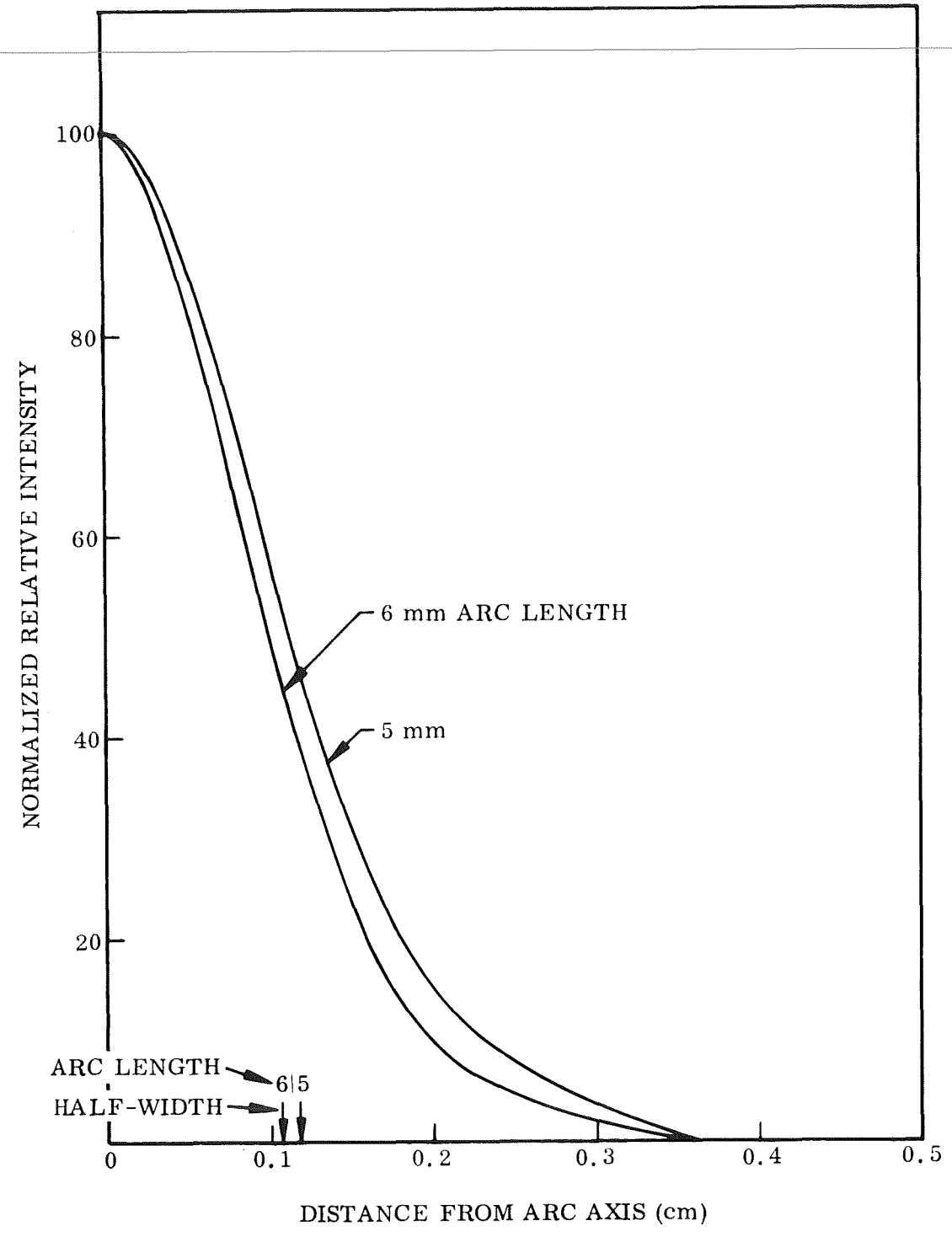

Fig. 3-22 Observed Continuum Intensity Distribution (Normalized) 2-mm From Cathode Tip for DCSP-GTA's Under the Following Conditions: Cathode – W-2%ThO_2, 3/16-in. Diameter With 10° Taper to 55-mil Diameter Flat Tip; Anode – Molten Crater on Water-Cooled Aluminum; Gas – Argon at 35 cfh; Arc Length – As Indicated; Current – 150 A

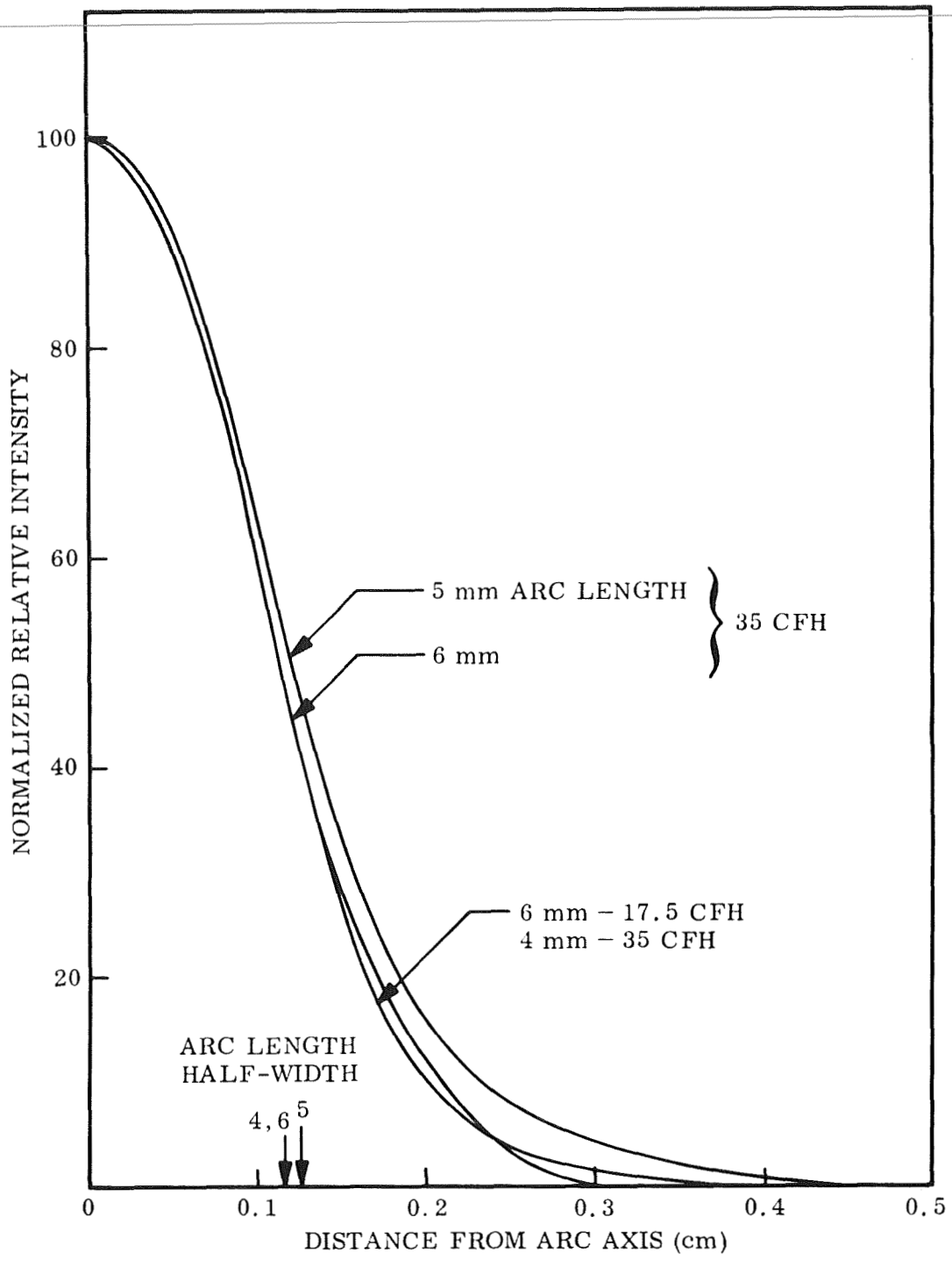

Fig. 3-23 Observed Continuum Intensity Distribution (Normalized) 2-mm From Cathode Tip for DCSP-GTA's Under the Following Conditions: Cathode – W-2%ThO_2, 3/16-in. Diameter With 10° Taper to 55-mil Diameter Flat Tip; Anode – Molten Crater on Water-Cooled Aluminum; Gas – Argon at 35 and 17.5 cfh; Arc Length – As Indicated; Current – 200 A

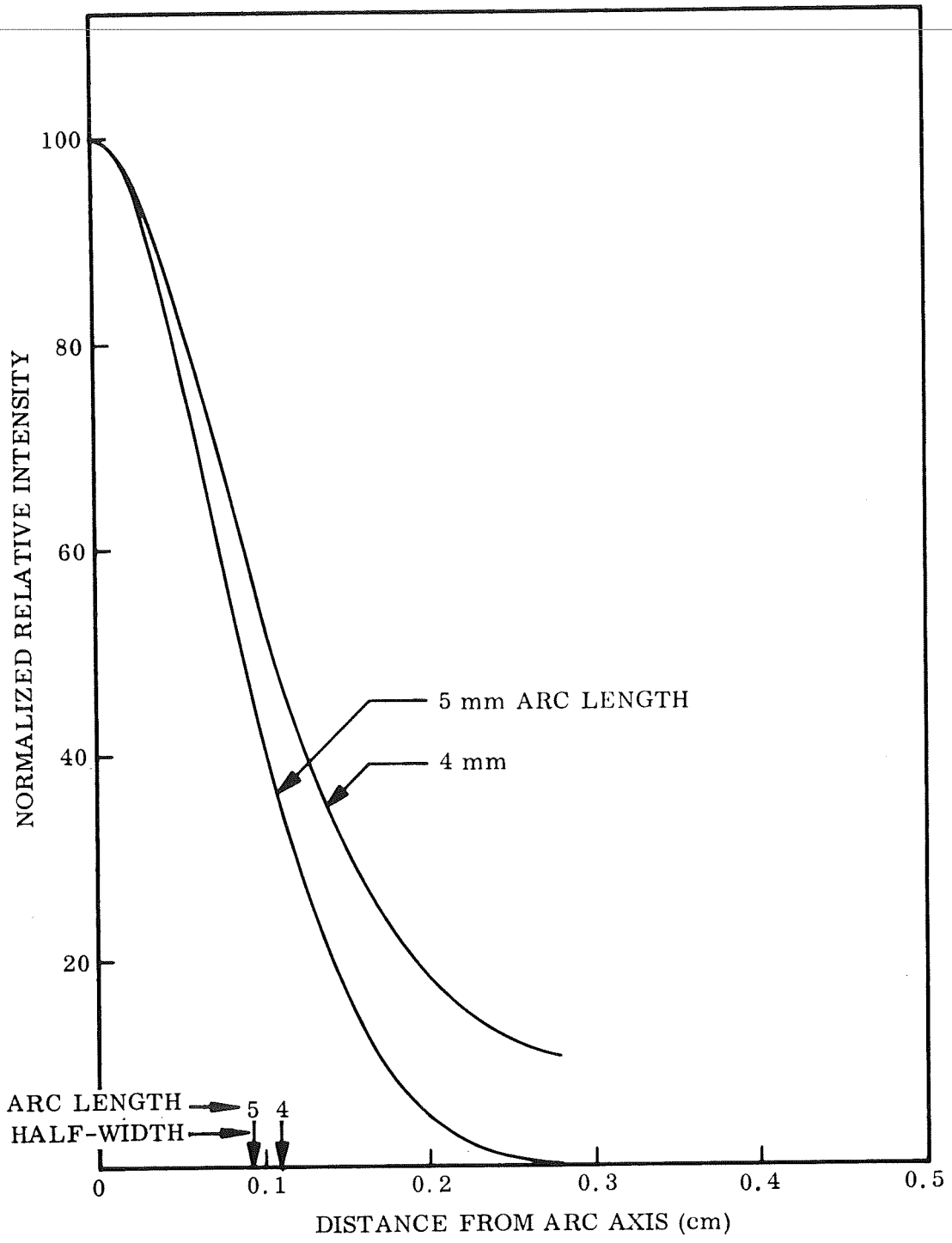

Fig. 3-24 Observed Continuum Intensity Distribution (Normalized) 2-mm From Cathode Tip for DCSP-GTA's Under the Following Conditions: Cathode – W-2%ThO_2, 3/16-in. Diameter With 10° Taper to 55-mil Diameter Flat Tip; Anode – Molten Crater on Water-Cooled Aluminum; Gas – Helium at 110 cfh; Arc Length – As Indicated; Current – 250 A

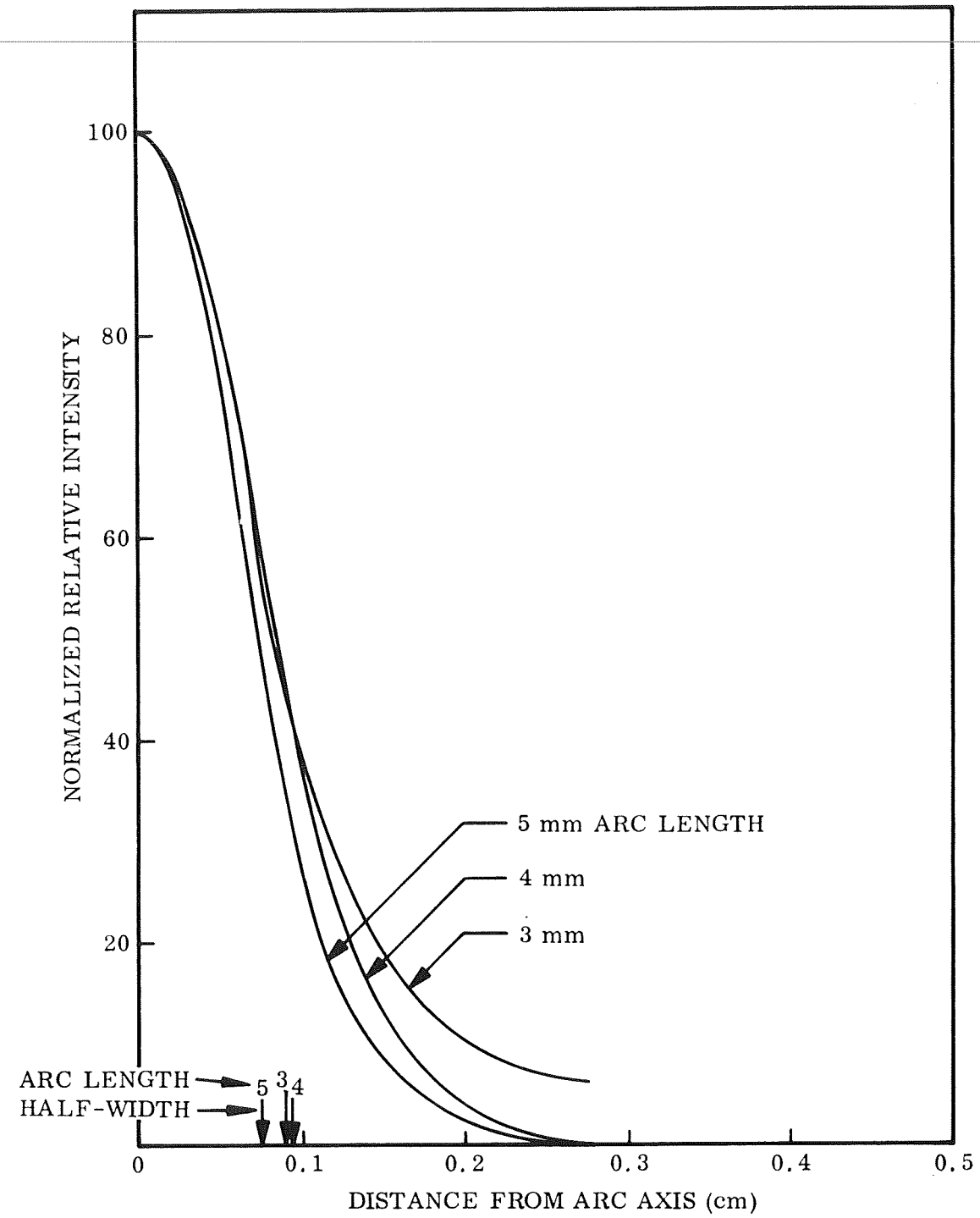

Fig. 3-25 Observed Continuum Intensity Distribution (Normalized) 1-mm From Cathode Tip for DCSP-GTA's Under the Following Conditions: Cathode – W-2%ThO_2, 3/16-in. Diameter With 10° Taper to 55-mil Diameter Flat Tip; Anode – Molten Crater on Water-Cooled Aluminum; Gas – Helium at 110 cfh; Arc Length – As Indicated; Current – 250 A

Figure 3-26 shows the plots of observed relative continuum intensities versus distance from the arc axis for several distances below the cathode of 250-A arcs, 3- and 4-mm long, operating in helium at 110 cfh. These are presented to demonstrate the limitations of continuum intensity distribution measurements near the anode caused by the distorting effect of the arc crater.

3.5.4 Plasma-Stream Pressure

The results of pressure probe measurement at the anode surface of arcs with various currents and lengths, and operating in argon or helium show that: (1) the pressure is higher in argon than helium for other conditions equal, (2) in argon the peak pressure varies linearly with current while in helium it rises more rapidly, and (3) the peak pressure is weakly dependent on arc length in the range from 2 to 6 mm and more strongly dependent between 1 and 2 mm. The half-widths are close to those for the continuum intensity and the radius at which the pressure becomes zero is generally larger than the radius for zero continuum intensity.

Figures 3-27 and 3-28 show the radial distribution of pressure for 1- and 3-mm arcs, respectively, in argon at currents from 150 to 300 A. The linear dependence of peak pressure on arc current is readily evident for the 3-mm arc. It is also interesting to note that the half-widths increase with arc length and vary only slightly with current in an inconsistent manner that may be within the limits of experimental error.

Pressure distributions for arcs 2- and 3-mm long in helium are shown in Figs. 3-29 and 3-30, respectively. The peak pressures are about half the value found in argon arcs under the same conditions, and the half-width is about twice as large. No values were obtained at less than 0.1 cm from the axis at 2-mm length and 250 A since the intense heating of the anode surface caused melting which sealed the probe hole.

The dependence of peak pressure on arc length for various currents in argon and in helium are shown in Fig. 3-31. These values were obtained by positioning the probe

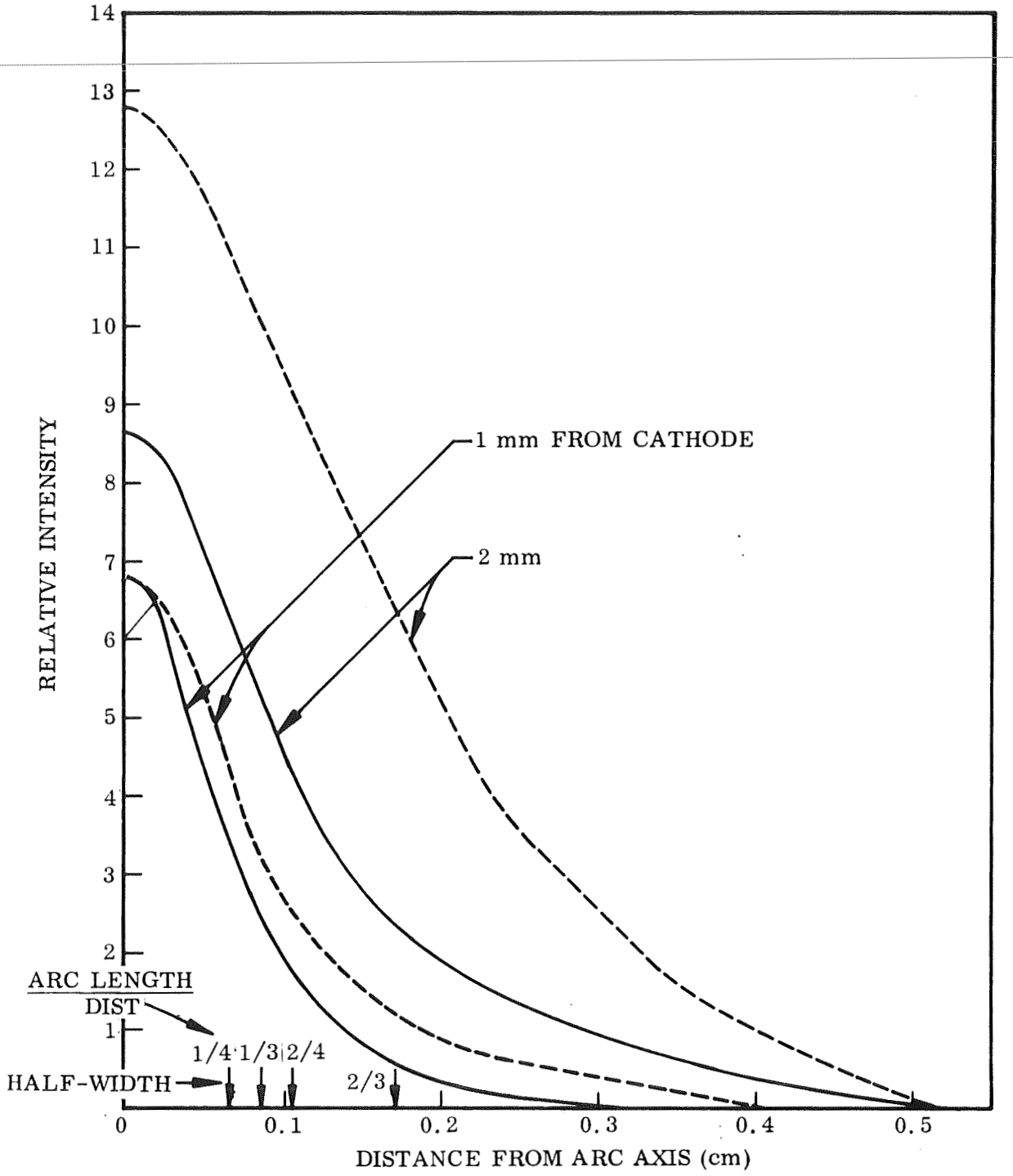

Fig. 3-26 Observed Continuum Intensity Distribution for DCSP-GTA's Under the Following Conditions: Cathode – W-2%ThO_2, 3/16-in. Diameter With 10° Taper to 55-mil Diameter Flat Tip; Anode – Molten Crater on Water-Cooled Aluminum; Gas – Helium at 110 cfh; Arc Length – 4 mm (——), 3 mm (---); Distance From Cathode Tip – As Indicated; Current – 250 A

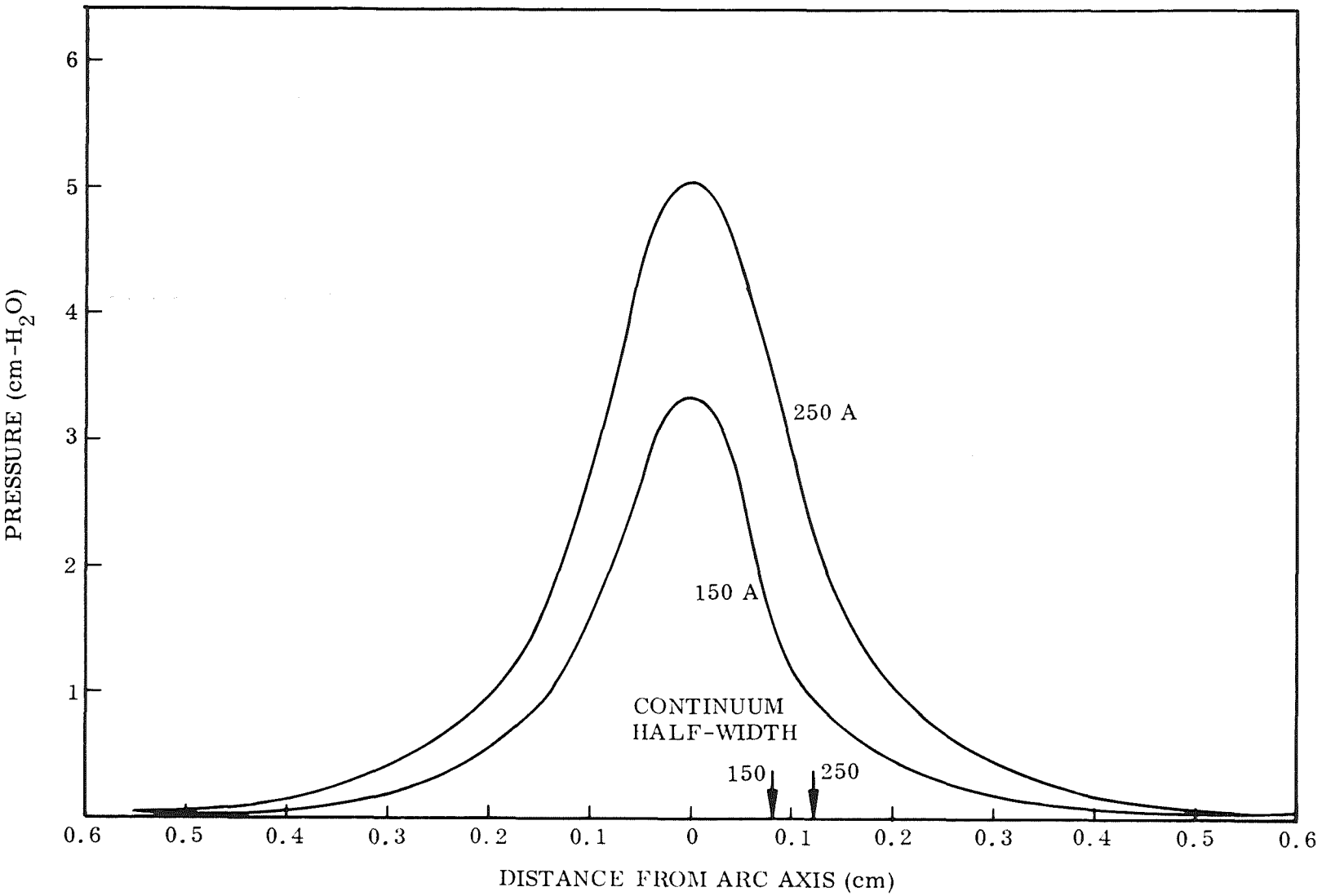

Fig. 3-27 Pressure Distribution for 1-mm DCSP-GTA's With: Anode – Solid Water-Cooled Copper; Gas – Argon at 18 cfh; Current – As Indicated

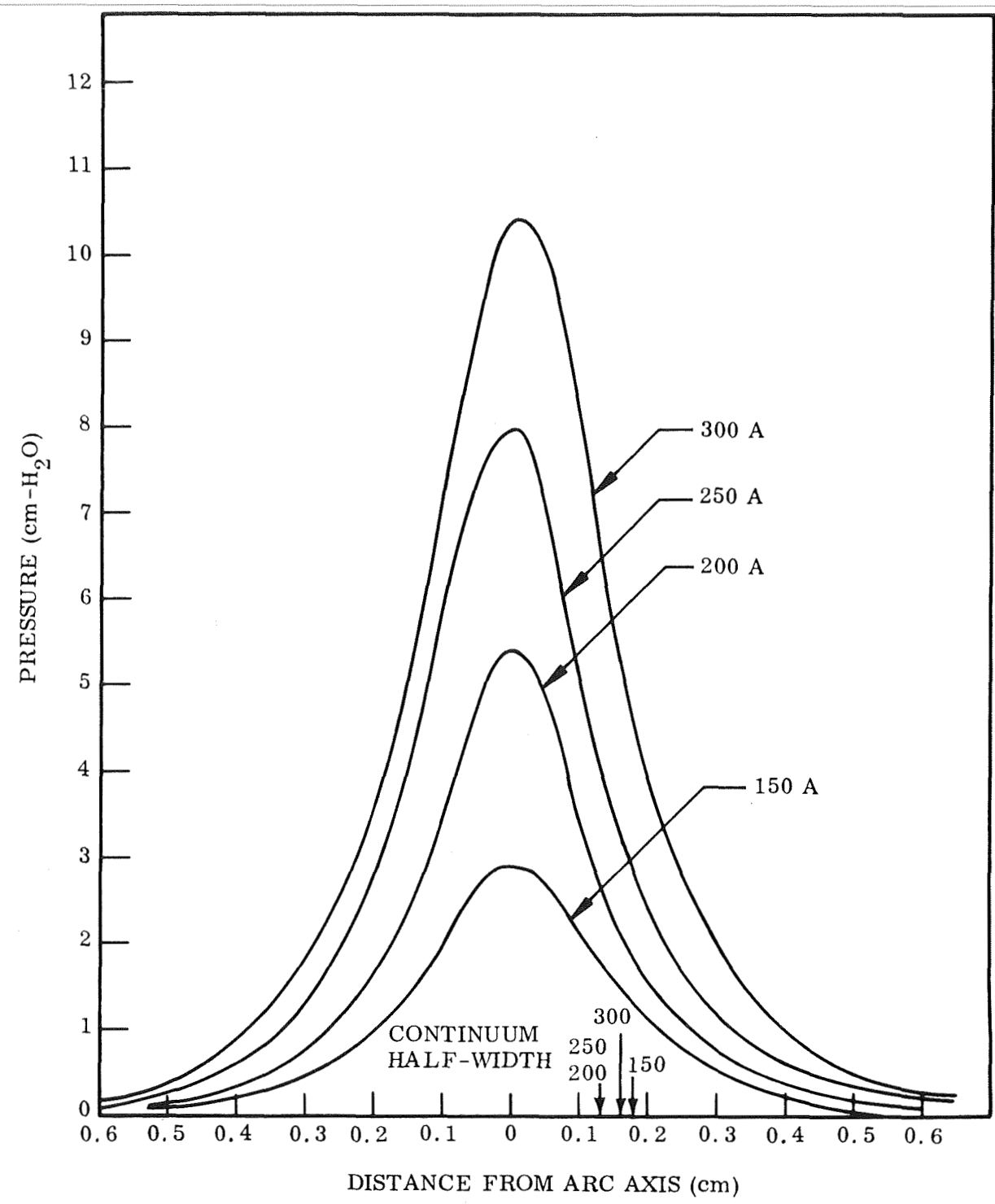

Fig. 3-28 Pressure Distribution for 3-mm DCSP-GTA's With: Anode – Solid Water-Cooled Copper; Gas – Argon at 18 cfh; Current – As Indicated

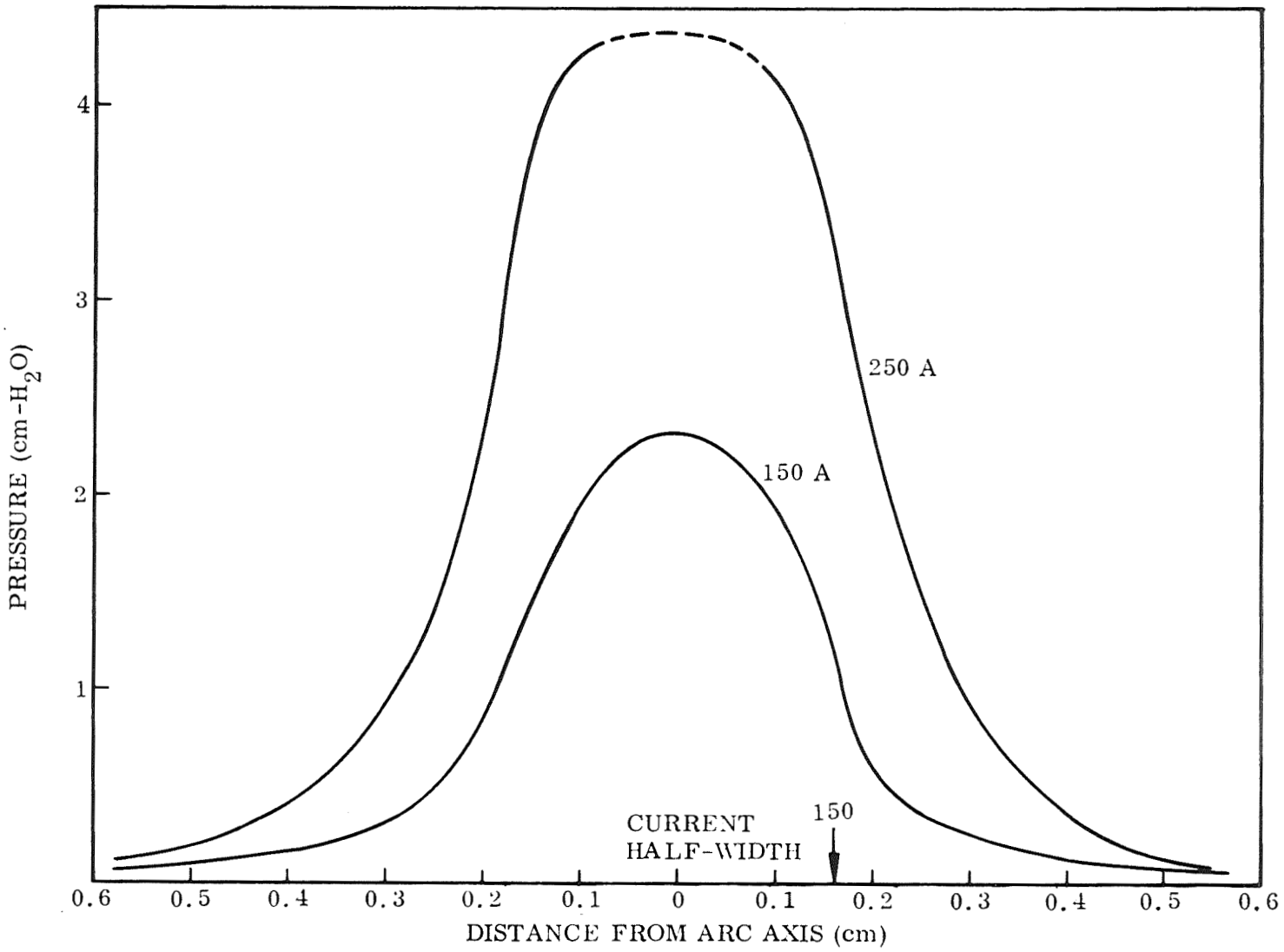

Fig. 3-29 Pressure Distribution for 2-mm DCSP-GTA's With: Anode – Solid Water-Cooled Copper; Gas – Helium at 110 cfh; Current – As Indicated

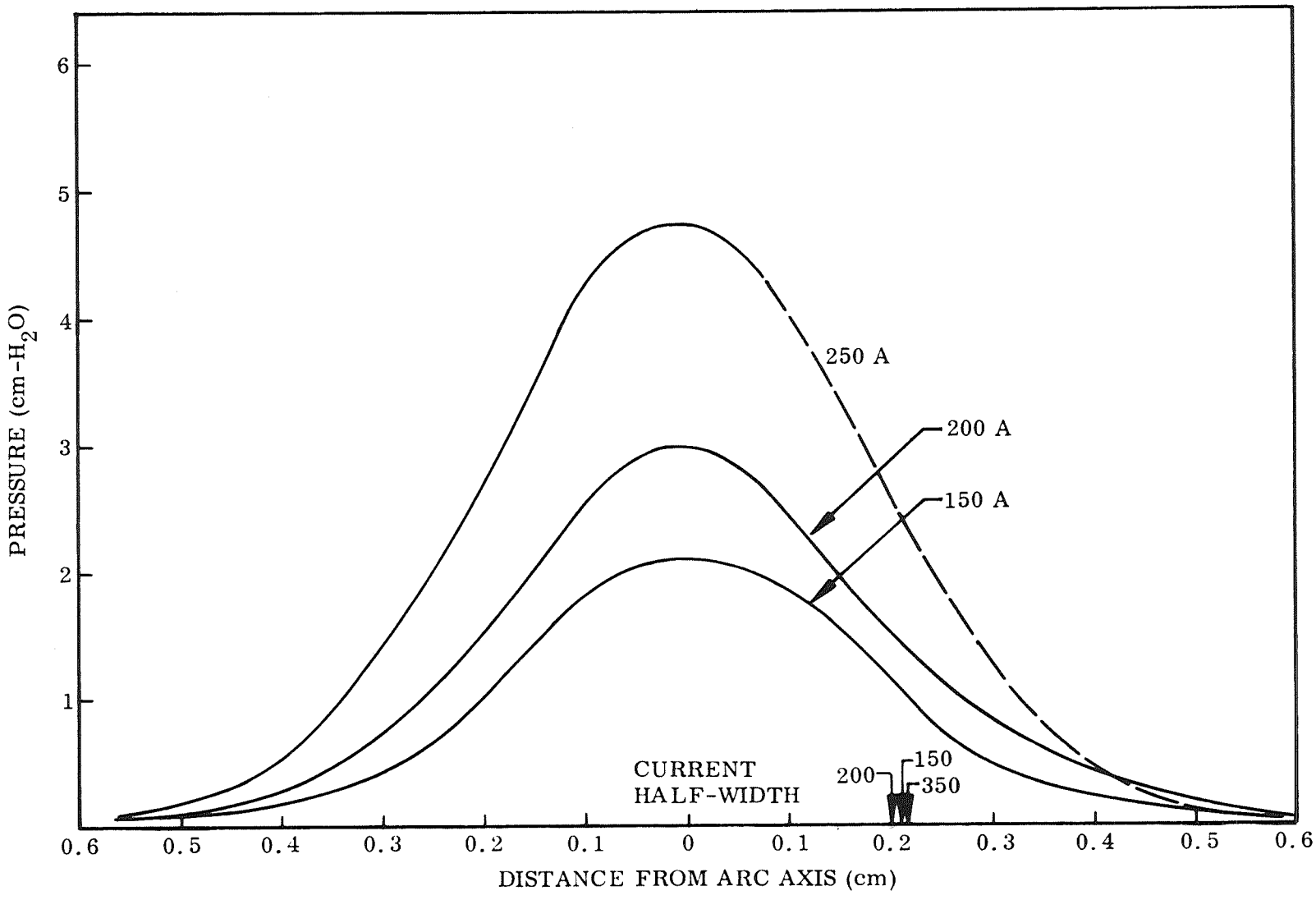

Fig. 3-30 Pressure Distribution for 3-mm DCSP-GTA's With: Anode – Solid Water-Cooled Copper; Gas – Helium at 110 cfh; Current – As Indicated

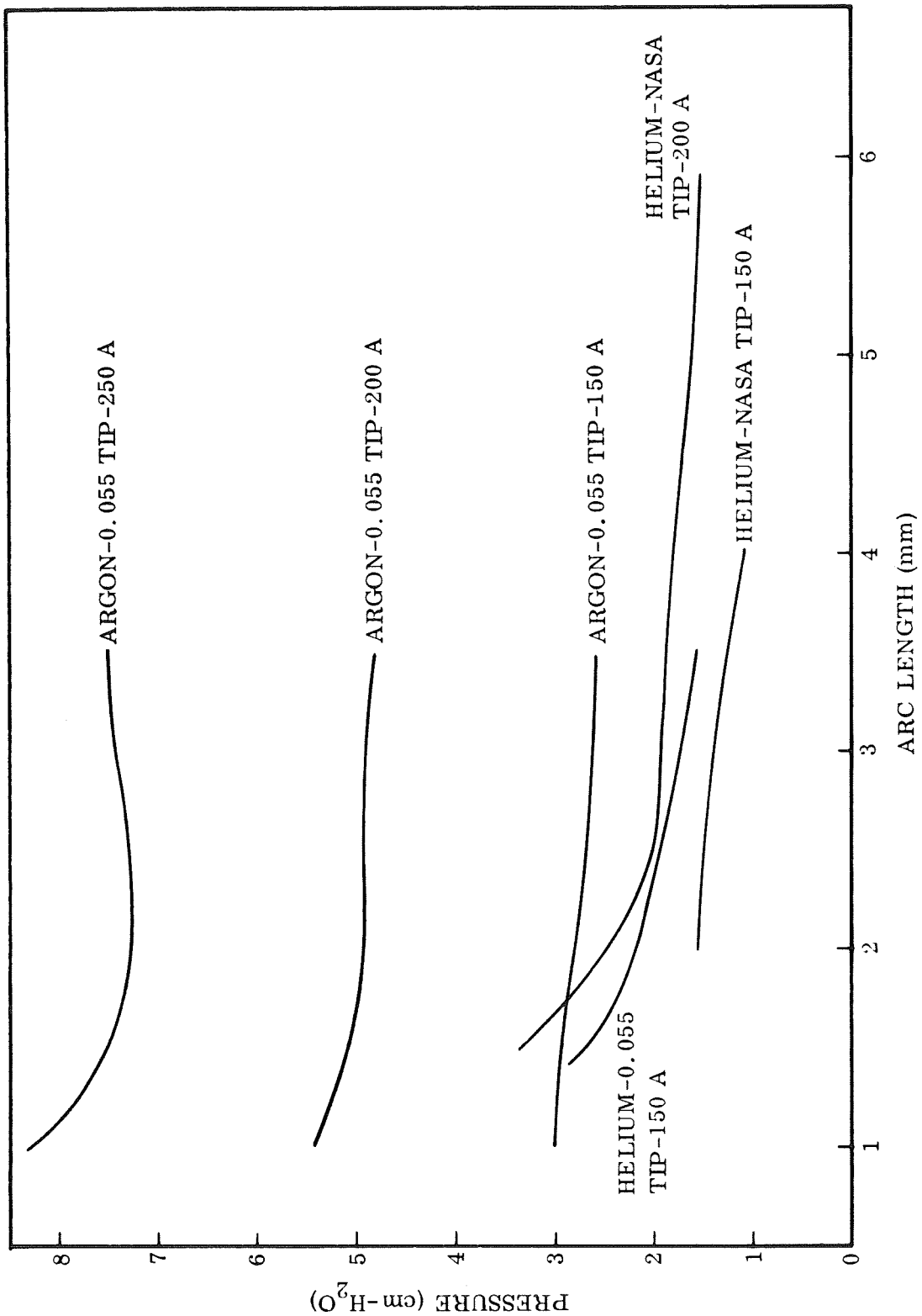

Fig. 3-31 Variation of Peak DCSP-GTA Pressure on Solid Water-Cooled Anode With Arc-Length for Various Conditions Indicated

for a maximum and varying the arc length. The greater peak pressure in argon gas is immediately apparent. It is also interesting to note that the NASA tip with a 94-mil-diameter flat produces a lower peak pressure than the 55-mil tip which was used because of its stabilizing influence when operating on a water-cooled copper anode.

3.5.6 Miscellaneous Relevant Observations

On the surface, the experimental techniques used for determining the current and heat-flux distributions appear straightforward and simple. Yet several observations made during the experiment indicate that there are two or more factors not previously considered which can influence the accuracy of the technique. These are (1) the interaction of the arc current (electrons) with magnetic fields produced by currents in the anode, (2) variations in the cathode tip configuration caused by redistribution of tungsten to produce asperities which alter the plasma shape, and (3) instability and anode melting with helium shielding gas.

A small magnetic deflection has been observed with the anode used for the current and heat-flux measurements despite precautions to eliminate magnetic fields which would produce such a deflection. The arc was deflected a small but detectable amount toward the splitting plane when the arc axis was about 1 mm from the plane and the amount of deflection increased slightly as the distance from the plane to the axis was decreased. When the arc axis was receding from the splitting plane on the other anode section, the deflection direction was reversed, i.e., also toward the splitting plane. Also, there appeared to be a small amount of "drag" as the arc axis crossed the splitting plane.

The influence of the magnetic deflection in the measurements was sometimes observed as an asymmetry in the current and heat traces. Surprisingly, however, the continuum traces were relatively symmetrical even when made simultaneously with the asymetric traces.

A qualitative analysis of the current flow within the anode as the arc approaches the splitting plane shows that a deflection of the arc, however small, will occur even with a hypothetical anode designed to produce the minimum magnetic field perpendicular to the arc axis. Consider the currents within a quarter-infinite conducting block as a line source on one surface approaches the edge. (This configuration is similar to one anode section but infinite extent in the plane of the anode surface and in thickness.) There will be a divergence of the current into the block which has a component parallel to the anode surface and directed away from the splitting plane. This will produce a magnetic field with a component perpendicular to the arc axis with a direction determined by the vector product of the radius to the point in the arc and the current. The force on the electron current (flowing from the cathode to the anode), given by the vector product of the electron velocity and the magnetic field, is directed away from the anode as was observed.

Complete elimination of the arc-deflecting magnetic field by altering the anode design does not appear possible. However, it may be possible to mask the effect by superimposing a small longitudinal magnetic field through the arc. While this would not eliminate the transverse component from the anode current, it could greatly reduce the effect on the measurements. The influence of such a field on the arc shape could be determined by measuring the distributions caused by various field strengths.

Change of the cathode tip shape was observed in several instances. This occurred when small whiskers grew on the flat end or the edge of the tungsten cathode during the approximately 20 min required for arc data scan. Generally, such a growth became the center of the arc attachment and a deflection of the axis resulted. Scans were terminated and the data were discarded when this occurred.

Current and heat-flux distributions were not obtained with helium because of difficulties in maintaining arc stability and a clean unmelted anode surface. It was possible to avoid surface melting with currents less than 250 A, but the plasma would not rigidly attach to the 94-mil-diameter tip, resulting in asymmetry which precludes the use of the data inversion scheme required to obtain radial distributions since axial symmetry is essential. Application of longitudinal magnetic fields may improve the symmetry adequately.

It was not possible to achieve the 11.0-V arc potential required for the "normal" operating conditions with the 94-mil NASA tip. This voltage is a condition for practical welding and apparently results from the arc operating with the tip below the metal surface where the plasma consists in large part of aluminum, a condition impossible to obtain on solid water-cooled copper. If the arc is shortened in an attempt to attain this low voltage on the copper anode, melting invariably results and the split configuration becomes inoperative.

3.6 CONCLUSIONS

The primary consideration in evaluating the results of this phase was which of the measured characteristics (current distribution, heat-flux distribution,continuum intensity distribution, or pressure distribution on the anode) can be best used to characterize the practical GTA's in terms of power density. A correlation between the current distribution and the continuum distribution was also sought.

The heat-flux distribution is necessarily related to the current distribution but previous experiments reported in the literature have not yielded sufficient data to quantitatively indicate its relative importance accurately. Other contributions are from electron condensation, electron kinetic energy, heating from the plasma stream, and possibly the plasma stream pressure. It is important to know quantitatively the relative contribution of these sources of heat, not only to gain familiarity with how energy in an arc is transferred to the anode, but also to provide insight as to how the transfer efficiency can be improved. If electron condensation dominated, for example, it would appear more feasible to improve the arc efficiency by increasing the current density than by augmenting the gas streaming velocity or its temperature. Conversely, if a considerable portion of the heating is from the plasma stream, means of increasing this transfer should be studied.

A brief description of two experiments which may illuminate the question of energy partition at the anode surface is included in subsection 3.7.

The difficulties encountered in applying the numerical inversion technique for the surface probe, as described by Olsen and Nestor (Ref. 72), permit only tentative conclusions to be made regarding the radial distribution of current density and heat-flux intensity and their relationship to the continuum intensity distribution. There is, however, evidence indicating which of the characteristics measured is significantly related to an arc's ability to produce a weld with good penetration. Further experiments, from which the role of each characteristic can be more clearly delineated, are suggested by the results of this study. These will be described in the following section.

3.6.1 Current Densities

Definite conclusions about the importance of current on heat-transfer efficiency in DCSP-GTA's cannot be made on the basis of this work alone until improved data and/or reduction procedure is applied to all the experimental conditions, or until additional experiments can be made to verify these results. With the use of data from the literature (Ref. 12), however, some tentative conclusions are possible.

- Peak (axial) current density varies inversely with arc length
- Peak (axial) current density varies directly with total arc current at least to 300 A
- Half-width of the radial distribution current density varies directly with arc length
- Half-width of the radial distribution of current density varies directly with arc current
- Peak current densities (on axis) from 3300 to 5670 A cm^{-2} are attained with 1-mm arcs in argon as the current is increased from 150 to 300 A
- Peak current densities generally become much lower as the arc length is increased from 1 to 2 mm
- For arcs 1-mm long, the bulk of the current is carried within a radius of 1 mm for currents from 150 to 300 A
- It may not be possible to construct a split anode with sufficient cooling to prevent surface melting for the power density produced by 3-mm arcs at 150 A in He. Nestor (Ref. 72) did not use less than 6.3 mm and more than 200 A.

Furthermore, it is concluded that measuring the current by the split anode techniques may require more refinements than were made in this work in order to ensure that the resulting radial distributions are truly representative. The most important modification required is to ensure that the arc is not perturbed as the splitting plane is approached. This can probably be best accomplished by making the anode sections sufficiently thick so that there is a minimum divergence of the return currents within the anode when the arc is near the slit or by connecting a return current lead adjacent to the slit.

3.6.2 Heat-Flux

Conclusions about the influence of the parameter studied on the heat flux must remain in part tentative until (1) the present results are verified by repeat experiments or (2) the experimental procedures are further refined. The distributions obtained appear to indicate the following conclusions:

- Peak (axial) heat-flux density varies inversely with arc length
- Peak (axial) heat-flux density varies directly with arc current
- Half-width of the radial heat-flux intensity distribution remains essentially constant for arc lengths from 1 to 3 mm
- Half-width of the radial heat-flux intensity distribution remains essentially constant for currents from 150 to 300 A
- Peak (on axis) heat-flux intensities for 1-mm arc length increase with current in the range studied (150 to 300 A) from about 10 kW cm^{-2} to 63 kW cm^{-2}, the 300-A case excepted
- Bulk of the heat for a 1-mm arc length is deposited on an area 2 mm in diameter in all cases except at 150 A
- Peak heat-flux intensities are reduced by about 50% as the arc length is increased from 1 to 2 mm for currents from 150 to 300 A

As in the case of the current-density measurements, it appears that the split-anode technique by which these results were obtained requires more refinements and/or further use to repeat the results to ensure that the resulting radial distributions are truly representative.

3.6.3 Continuum Intensity

The general shape of the normalized continuum intensity distributions suggest that the technique by which the results were obtained requires no better experimental accuracy than was used. Analysis of the radial distributions obtained in conjunction with the current and heat-flux data permits the following conclusions for DCSP-GTA's in argon with the 55-mil-diameter flat tip.

- The radial distribution of continuum intensity is more nearly related to the current density than to its square root.
- For 1-mm arc length and all currents, the continuum half-width is related to the radial distance encompassing most of the current.
- Continuum half-width increases with increased arc length to 2 mm in much the same manner as the current distribution appears to increase.
- Local continuum intensity in helium may not be proportional to the local current density.
- Continuum intensity half-width (uninverted) 1 and 2 mm from the cathode is essentially independent of arc length as it is greater than 4 mm in argon and about 3 mm in helium for arc currents of 200 to 250 A.
- Continuum intensity half-width (uninverted), for 4- and 5-mm arc lengths increases slightly with distance from the cathode to 2 mm for 250-A arcs in helium.
- Continuum intensity half-width (uninverted) 2 mm from the cathode of a 250-A arc in helium, 3-mm long, is about double the half-width 1 mm from the tip

It appears that the continuum-intensity distribution half-width may be a workable means of estimating the current distribution half-width 1 mm or more above a molten metal

pool. More measurements of both the current and continuum intensity distributions made under a variety of conditions are required before a more definite conclusion can be reached. Considering the consistency among the various continuum distributions obtained, particularly as compared to the corresponding current distributions simultaneously obtained, the method appears to have distinct advantages if the correlation can be unequivocally demonstrated. However, metal vapors from the pool and the shape of the crater may alter the current distribution such that the method is not applicable for predicting the penetration a given arc will produce. Application of the continuum intensity technique for characterizing actual welding arcs will probably be most seriously complicated, if not made altogether impossible, by the fact that most practical welding arcs operate with a length of 1 mm or less, which means that the continuum scan would be made at or above the cathode tip.

3.6.4 Plasma-Stream Pressure

These relatively simple measurements suggest that if the plasma-stream pressure is a significant factor determining penetration, argon arcs should produce greater penetration than arcs in helium at essentially the same arc length and power. Since the contrary is the case, it must be concluded that the plasma-stream pressure plays no more than a secondary role among the factors causing penetration. Furthermore, the following general statements can be concluded from the results presented.

- Half-width of the pressure distribution curves is essentially the same as for the continuum intensity in the case of DCSP-GTA's in argon.
- Axial pressure (peak) is proportional to the current for DCSP-GTA's in argon.
- Axial (peak) pressure is less with DCSP-GTA's in helium than for the same arc conditions in argon.
- Half-widths of the pressure distribution for DCSP-GTA's in helium is about 30% greater than for the corresponding arcs in argon.
- Peak axial pressures are weakly dependent on arc lengths greater than 2 mm for DCSP-GTA's in argon and helium at currents from 150 to 250 A.
- For a DCSP-GTA operating at 150 A in helium, a greater peak plasma-stream pressure is obtained with a 55-mil-diameter flat tip than with one 94 mils in diameter.

Section 4

EXPERIMENTS TO INCREASE GTA POWER DENSITY

4.1 BACKGROUND

The objective of this phase of the program was to conduct a series of experiments designed to significantly increase GTA power density.

Based on the literature survey, on the results of the Phase II analysis of power density in normal gas tungsten arcs, and on discussions with MSFC personnel, a number of modifications were selected which were believed to show the most promise for increasing GTA power density. Each of these influences a different portion of the arc and can be classified as follows:

(a) Modification of the electrode (cathode)
(b) Modification of the anode (workpiece)
(c) Modification of the shielding gas
(d) Use of magnetic fields to constrict the arc plasma

Modification of the electrode may include changes in the material from which it is constructed, changes in its shape, or changes in the means used to cool it. Emphasis was placed on materials with high thermionic emissivity since they could operate with a smaller cathode spot at a given current and thereby provide a narrower current-conducting path near the cathode. The reported high thermionic emission of lanthanum hexaboride together with its high melting point, 2210°C (4012°F), good electrical conductivity, and stability led to its selection as one of the materials for experimentation. Barium-calcium-aluminate impregnated cathodes were also selected for their high thermionic emission and because of their successful application as electrodes in an arc plasma generator by Neurath and Gibbs (Ref. 34). Accordingly, experiments were made to study these two materials.

At the anode or workpiece in DCSP-GTA welding, there is much less latitude available in which to perform modifications to increase power density; i.e., the composition only can be changed and only in very small amounts. A fourfold difference in penetration due to trace amounts of chlorine reported by Ludwig (Ref. 28) was justification for further investigation of this phenomenon in this program. Several experiments with halogen additions to the anode region were made.

The marked effect of shielding gas composition on arc voltage, power density, and thermal efficiency reported in the literature indicated a potential for significant improvement in GTA power density. Additions of the diatomic gases – hydrogen, nitrogen, oxygen, and chlorine – were selected for study as showing particular promise. It was anticipated that hydrogen and nitrogen could be studied in all concentrations whereas oxygen and chlorine, because of possible degradation of the cathode, would be limited to about 1% by volume.

An arc plasma such as used for GTA welding diverges from the cathode to the anode as the result of a form of thermal diffusion called ambipolar diffusion. This phenomenon occurs when the more mobile electrons, formed near the cathode by ionization, diffuse radially outward more rapidly than the larger, more massive positive ions. The charge separation produced results in a radial electrostatic field which retards the motion of electrons and simultaneously increases the force driving the positive ions outward. If the electrons could be restrained from their rapid outward flight, the plasma divergence could be decreased, effectively constricting the arc in the anode region. One means of inhibiting the outward motion of electrons would be by the application of a longitudinal magnetic field through the arc. Such a field would be expected to cause small circular motions of the electrons between collisions in contrast to the interrupted linear motion that normally occurs. Longitudinal magnetic fields of the order of 20 to 50 G had been used to stabilize the gas tungsten arc and to provide "stiffness." Somewhat higher field strength (100 G) has been reported to provide a "focussing" action on the arc. Therefore, a study was conducted of longitudinal magnetic fields of up to 300 G to determine their effect on arc power density.

Constriction of the arc plasma by means of a water-cooled orifice has been shown to greatly increase arc power density and forms the basis of the plasma-arc welding process. However, no experiments were made with this process since it was explicitly excluded from the scope of this effort.

4.2 MEASUREMENT PROCEDURE – PHASE III

The techniques employed for evaluating the various experiments and for analyzing the results were essentially as described previously in Section 3. There were two major differences, however. First, bead-on-plate tests were made to establish whether a correlation exists with the power density measurement techniques and a real welding situation. Second, analysis of the current density and continuum intensity data was greatly simplified to give only qualitative results, adequate for screening purposes and at the same time sufficiently inexpensive to permit the completion of a large number of tests at a small cost. Heat-flux intensity distribution measurements were not made since the long response time of the apparatus requires slow scan rates which would cause deterioration of the anode at the anticipated high power density levels.

4.2.1 Current Density, Continuum Intensity, and Pressure Measurements

Data for current density distribution were obtained with the split anode and arc drive mechanism described in Section 3, with the drive speed increased from 26 mils/min to 90 mils/min, to minimize degradation of the anode surface at the greater power densities anticipated. These measurements were made to determine the influence of longitudinal magnetic fields on the arc but not for the other modifications since the extremely stable arc operation required could not be achieved on the split anode in the absence of the magnetic field.

Continuum intensity measurements were not made of the bead-on-plate (BOP) test for two reasons. First, acceptable welds are possible only with relatively short arc lengths; i.e., the electrode less than about 80 mils (2.0 mm) from the workpiece surface. With such a short spacing, the molten metal in the pool rises sufficiently

far above the workpiece surface to almost completely obscure the arc when viewed perpendicular to the arc axis. Second, the staker used for BOP tests has a movable head and the work is stationary, so that the arc cannot be continuously focused on the spectrometer slit.

Continuum intensity data for the modified arcs were obtained as before but with the faster scan rate and with the arc operating on a one-piece flat copper anode (Fig. 4-1). The spectrometer was set at 4080 Å and the arc image was positioned so that the scan was made at about 10 mils (0.25 mm) above the anode surface. In some instances, when surface melting of the anode interfered with the measurements, the scan was made at 20 mils (0.5 mm) above the anode surface. These measurements were made with all of the arc modifications tested except those to the anode.

The plasma-stream pressure distribution was measured directly by means of a water manometer modified from the earlier design by greatly reducing the gas volume between the probe aperture and liquid level. This facilitated data taking by decreasing the manometer response time.

4.2.2 Data Analysis (Current and Continuum)

The experimental techniques used for current density and continuum intensity yield data which must be treated mathematically to obtain the radial distributions, as described in Section 3. Since this procedure requires very accurate data and is very time consuming, it was decided to eliminate the data reduction and instead use the experimental data directly. This is justifiable for qualitative comparisons only, such as are of interest here. It is evident that any significant decrease in the width of the radial distribution will be observable as a decrease in the width of the observed function even though the fractional changes observed may not be the same in each case. Since the tests made during this program phase were primarily for screening, this simplified technique is adequate.

The approximation techniques used were as follows. For the surface probe used to obtain current data, a typical output curve consists of a region where the slope

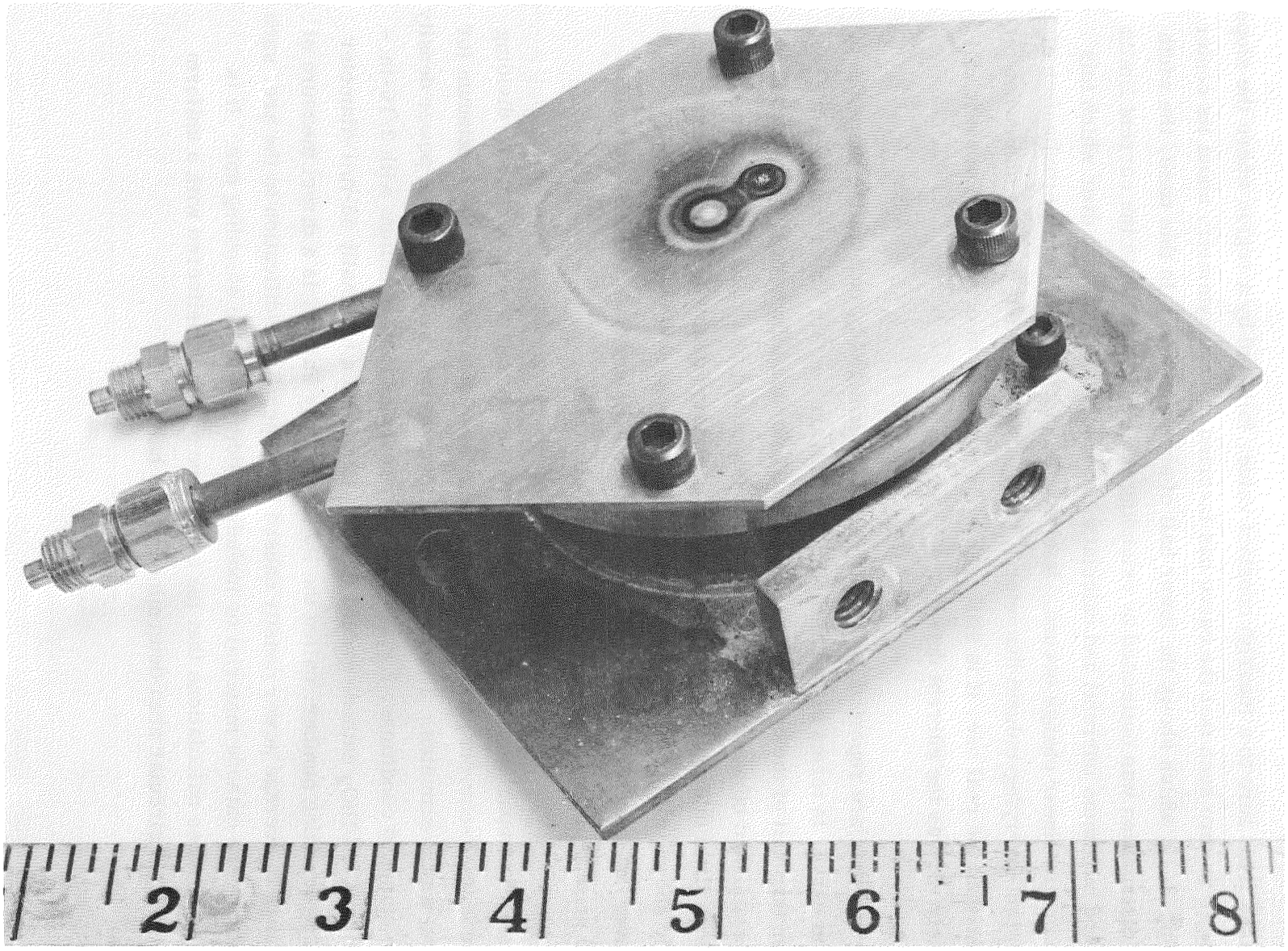

Fig. 4-1 Water-Cooled Copper Anode for Continuum Intensity Measurements. The expendable copper plate permits each run to be made on a new surface

increases from zero to a (nearly) constant value, followed by a region where the slope decreases to zero such that the curve has inverted mirror symmetry about its center. (See Fig. 3-15, which shows the lower half of such a curve.) In this case, the width of the distribution was estimated by extending the linear portion to the current limits (zero and maximum current) and calculating the distance in the arc over which this approximated linear change occurs. In effect the method yields an approximation of the current-carrying-column diameter. Though the estimated value is somewhat smaller than the real one, it is still usable for purposes of comparison since it will obviously vary as the current density.

Continuum data are reported as the half-width determined by calculating the width of the data curve, in terms of radial distance in the arc, within which the intensity is greater than half of the observed maximum. While no mathematical correlation has been established between this estimating procedure and that used for the current distribution, little information is lost since the continuum data can be compared as confidently shown in Fig. 4-5. The continuum and current data should correlate, moreover, at least with respect to trends, i.e., a reduction in the current width should produce a decrease in the continuum half-width.

For ease of comparison, the data are converted to average power density by dividing the arc voltage-current product by the circular area obtained from the continuum (or current) width estimates. These values are then divided by the average power density for the standard conditions, i.e., for an arc operating in pure helium with 3/16-in.-diameter W-2%ThO_2 cathode ground to a 10° taper and a nominally 55-mil-diameter tip. The resulting number, called the Power Density Factor, is a direct measure of the change in average power density caused by a specific modification to the arc, such as changing the cathode material or including additives to the shielding gas. It is assumed in these calculations that the entire arc power is delivered with a uniform density over a circular area determined by the half-width.

4.2.3 Bead-On-Plate Tests

In evaluating various modifications to the gas-tungsten-arc to produce increased power density, it is necessary to establish whether a measured increase in power density can produce a useful result under conditions simulating actual welding practice. Variables such as the shape of the weld crater under the arc, vaporization of metal in the weld pool, the influence of convection currents and electromagnetic stirring, and variation in the shape of the weld pool with travel speed will all have some influence on the efficiency of arc energy transfer to the weld. Therefore, bead-on-plate tests were performed to evaluate the "effective" power density of the various arc modifications.

A commercial-type Airline welding positioner (staker) and a Linde HW-27 torch mounted to an automatic voltage-controlled head were used for the bead-on-plate welds. The head could be locked to provide constant electrode-to-work distance if required. Welding power was supplied by the same Vickers WP-600 three-phase, full-wave rectified dc power source used for the arc studies (Section 3).

Bead-on-plate welds were made on test plates 6-in. wide and 10-in. long held in copper tooling. Some preliminary welds were run on copper but the majority of the tests were made on 1/4-in. type 304 stainless steel or 1/2-in. 2219-T87 aluminum.

Evaluations included arc stability, effect on the electrode, bead surface appearance, and contour. In addition, cross sections were taken and depth of penetration, bead width, and shape of the bead noted.

4.3 EXPERIMENTAL PROCEDURES AND RESULTS

The four major arc modifications studied during this program phase were selected to produce effects on different portions of the arc. Operating an arc with a low-work-function high-emissivity cathode could increase the power density at the anode by providing a narrower current-conducting path. Additives to the shielding gas could

cause any of several effects. The plasma column diameter could decrease, the enthalpy of the plasma could increase, the heat-transfer efficiency to the anode could increase by diatomic recombination, and the penetration could be increased by increasing the plasma-streaming pressure. Anode material modifications (or surface additives) could produce effects similar to gaseous additives but confined to a thin region above the anode surface. Finally, the use of longitudinal magnetic fields was studied to determine if the Lorentz force on outwardly diffusing mobile electrons would have a confining effect.

The specific procedures for evaluating the various modifications tested included continuum intensity measurements, arc photography, bead-on-plate tests, voltage measurements, and measurement of plasma-stream pressure. For the studies of superimposed magnetic fields, current-density distribution measurements were also performed. The results of the tests made are given in the following sections.

4.3.1 Modification of the Electrode

The two materials selected for evaluation based on their low thermionic work function and high emissivity were lanthanum hexaboride and porous tungsten impregnated with barium-calcium aluminate. Gas tungsten arc welding electrodes were fabricated by brazing small tips of the material to short lengths of 3/16-in.-diameter tungsten rod. These composite electrodes were then mounted in the GTA torch in the same manner as conventional electrodes and evaluated.

4.3.1.1 Lanthanum Hexaboride Electrodes

Two configurations of lanthanum hexaboride tipped electrodes were investigated and are illustrated in Fig. 4-2. One closely resembles a normal GTA electrode configuration, whereas the other consists of a 0.050-in.-diameter LaB_6 rod brazed into a hole in a larger electrode.

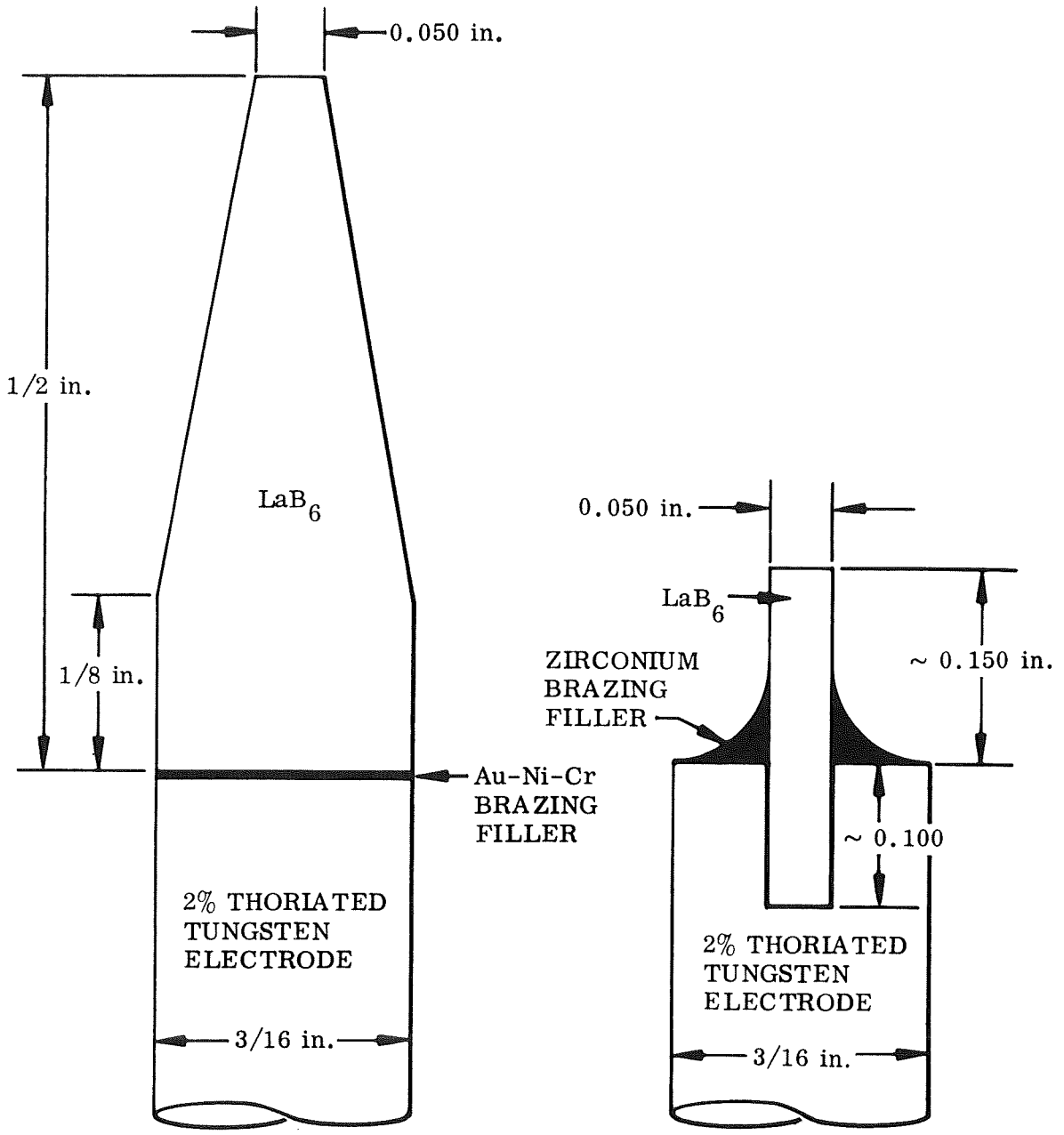

Fig. 4-2 Configurations of LaB_6 Tipped Electrodes

Both configurations of LaB_6 were procured from Haselden, Inc., San Jose, California. They were pressed from high-purity powder and sintered in a hydrogen furnace at about 1800°C (3270°F) to give a dense material which was then finished to contour by diamond grinding.

A search of the literature provided no information on brazing procedures. It was recognized that the 0.050-in.-diameter LaB_6 inserts would require a high-melting braze alloy, whereas the conical tips with the braze joint 1/2-in. away from the tip could possibly be silver brazed to a copper or tungsten rod.

An attempt was made to torch braze a conical LaB_6 insert to a copper rod using a lithium-containing silver braze alloy (Lithobraze 925) to promote wetting of the LaB_6, but it was not possible to get proper wetting and flow of the brazing alloy.

To improve wetting, a film of zirconium was vacuum vapor deposited on the surface of the LaB_6. The tips were masked to obtain plating only on the 3/16-in.-diameter end. Each was then placed in contact with the tungsten rod and successfully electron-beam brazed using a gold-nickel-chromium alloy.

The insert-type electrode was fabricated by EDM drilling a 0.052-in.-diameter hole approximately 0.100-in. deep in the end of a 3/16-in.-diameter tungsten rod and vacuum brazing a 0.050-in.-diameter LaB_6 insert into the hole. Because of the high operating temperature at the joints, a diffusion barrier was used to retard diffusion of boron from the LaB_6 into the tungsten. This was accomplished by electron-beam depositing a film of tantalum on the inserts followed by a carbon layer. The parts were heated in vacuum to form tantalum carbide. A film of zirconium was then vapor deposited over the TaC to enhance wetting. A small ring of zirconium or titanium wire filler was placed around the insert as shown in Fig. 4-3, and the assembly was heated with a defocused electron beam until the filler melted and flowed.

Continuum intensity measurements were made at 100, 150, and 200 A with the 0.050-in. LaB_6 inserts. During the runs it was noted that the insert melted at currents over 100 A. The 3/16-in.-diameter conical tips (tapered to 0.050-in.-diameter) also

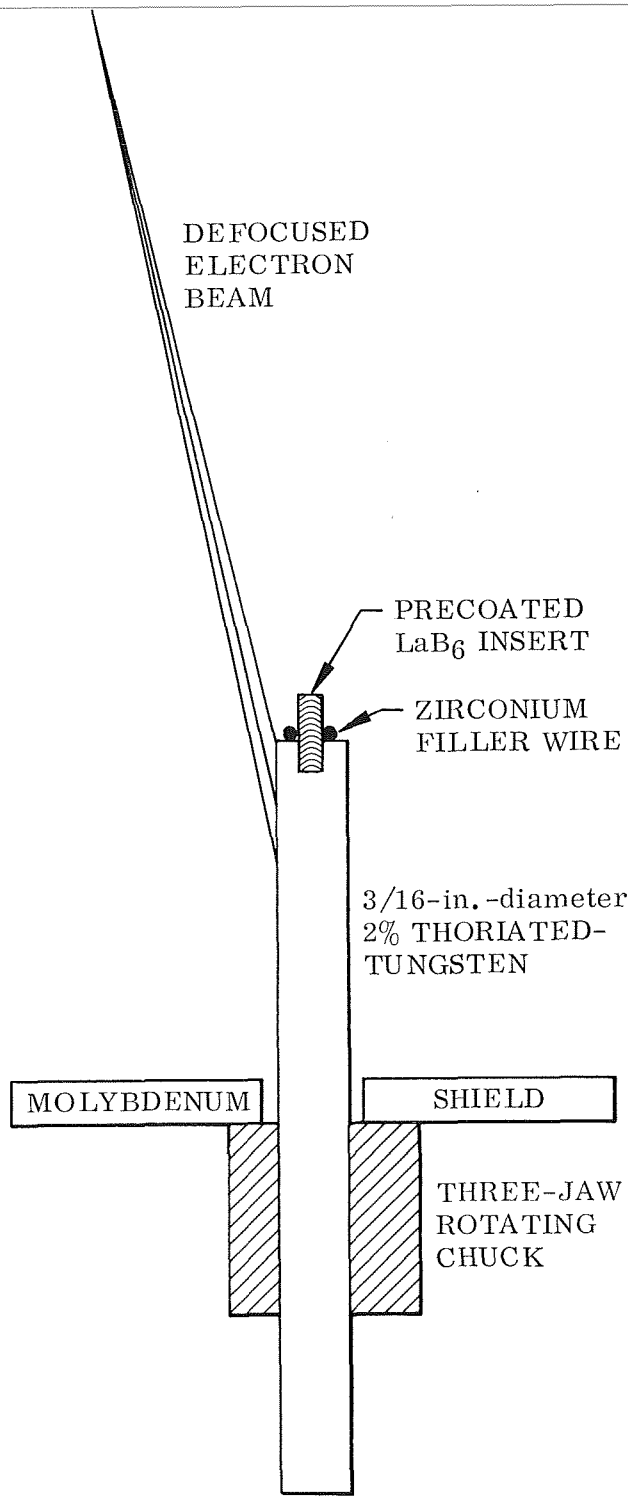

Fig. 4-3 Method of Electron Beam Brazing LaB_6 Insert Electrodes

melted back; in addition, they were very sensitive to thermal shock. Continuum data are presented in Table 4-1. The various modifications were evaluated by comparing the power-density factors, i.e., the factor by which the power is increased as compared to the normal arc operating with all other conditions identical. The effects of using LaB_6, on the power-density factor is shown in the Table. Values greater than 1 occur at 100 and 250 A with smaller than 1 values for the intermediate currents of 150 and 200 A. The greatest value observed was 1.49 for the 100-A arc. It should be noted that some error may exist in these data since the LaB_6 cathode configuration was not comparable to the thoriated tungsten configuration. This shape difference came about because of the difficulty in machining the LaB_6 and as a result of the change in the LaB_6 tip shape observed during operation at the higher currents.

Some bead-on-plate runs were made with 0.050-in. insert tips in which the zirconium brazing alloy coated the o.d. surface of the tip. The LaB_6 tended to melt back inside the zirconium "shell," but provided sufficient emission to carry up to 250 A. An improvement in depth/width ratio of about 25% was noted. Data are given in Table 4-2.

Because of the melting of the lanthanum hexaboride tips, it appears that another method of utilizing the high emissivity of lanthanum at the electrode surface is needed. One possibility is to use powder metallurgy techniques. This would involve the pressing and sintering of tungsten powders mixed with lanthanum hexaboride or lanthanum oxide powders. An order was placed for 2% thoriated-tungsten tips containing 3% lanthanum hexaboride. Tips containing 3% lanthanum oxide were also ordered. Unforeseen difficulties were encountered by the vendor in fabricating these materials, however, and they were unavailable for evaluation.

4.3.1.2 Barium-Calcium-Aluminate Impregnated Electrodes

This type of cathode is widely used in the electronic industry for high power applications and have been reported by Neurath and Gibbs to operate well as a cathode in an arc-plasma generator. Electrodes of the configuration shown in Fig. 4-4 were obtained from Semicon Associates, Inc. (Division of Varian Associates). Fabrication

Table 4-1

DATA SHOWING THE EFFECT OF ELECTRODE (CATHODE) MATERIAL ON ARC-POWER-DENSITY IN 2 mm HELIUM ARCS ON WATER-COOLED COPPER

Current (A)			Voltage (V)	Arc Power (kW)	Continuum Half-Width (in.)	Average Power Density* ($kW/in.^2$)	Power-Density Factor		
W-ThO_2[a]	Ba-Ca[b] Aluminate	LaB_6[c]					W-ThU_2	Ba-Ca Aluminate	LaB_6
150	—	—	15.9	2.38	0.125	194	1	—	—
—	150	—	15.1	2.26	0.129	173	—	0.89	—
—	—	150[d]	16.0	2.40	0.142	152	—	—	0.78
200	—	—	15.2	3.04	0.131	225	1	—	—
—	200	—	14.3	2.86	0.137	193	—	0.86	—
—	200	—	14.5	2.90	0.134	206	—	0.92	—
—	—	200[e]	16.0	3.20	0.155		—	—	0.76
250	—	—	15.1	3.78	0.155	200	1	—	—
—	250	—	14.5	3.62	0.156	189	—	0.95	—
—	250	—	14.5	3.62	0.139	239	—	1.3	—
—	—	250[c]	16.0	4.00	0.140	259	—	—	1.30
100	—	—	17.5	1.75	0.139	115	1	—	—
—	—	100[f]	17.0	1.70	0.117	158	—	—	1.38
—	—	100[d]	17.8	1.78	0.115	171	—	—	1.49
—	150[g]	—	14.9	2.24	0.137	151	—	0.78[h]	—
—	200[g]	—	15.3	3.06	0.145	185	—	0.82[h]	—
—	250[g]	—	16.3	4.08	0.137	277	—	1.38[h]	—

(a) 60°−50 mil tip and 100 cfh gas flow.
(b) 60°−50 mil tip and 50 cfh gas flow.
(c) Tip as shown in Fig. 4-2b and 100 cfh gas flow.
(d) Cathode tip rounded.
(e) Cathode tip melted back to tungsten holder.
(f) Cathode tip with sharp corners.
(g) 30°−45 mil tip and 50 cfh gas flow.
(h) Compared to 60°−50 mil W-ThO_2 tip at same currents.

*Measured 0.25 mm (10 mil) above anode surface.

Table 4-2

BEAD-ON-PLATE TESTS WITH LANTHANUM HEXABORIDE ELECTRODES[(a)]
ON 1/2-in. 2219 ALUMINUM PLATE
(100 cfh Helium Shielding)

Arc Current (A)	Arc Length (in.)	Arc Voltage	Travel Speed (ipm)	Heat Input (kJ/in.)	Depth of Penetration (in.)	Bead Width At Top (in.)	Depth-to-Width Ratio
100	0.025	12.0	15	4.8	0.072	0.190	0.380
100	.060	14.0	15	5.6	.069	.220	.314
200	.025	11.5	15	9.2	.160	.265	.605
200	.025	11.5	15	9.2	.196	.322	.610
200	.060	13.5	15	10.8	.157	.398	.394
250	.025	13.0	15	13.0	.198	.315	.630
280	.025	13.5	15	15.0	.190	.382	.497
200	~.020	11.0 (Set)	15	8.8	.184	.277	.665
200	~.020	11.0 (Set)	10	13.2	.204	.320	.637
250	~.020	11.0 (Set)	15	11.0	.259	.331	.783
250	~.020	11.0 (Set)	10	16.5	.256	.382	.670
CONTROL WELD – Standard 3/16-in. Diameter, 10°–0.055-in. 2% Thoriated Tungsten Electrode							
250	.025	14.0	15	14.0	.232	.374	.620

(a) 0.050-in. LaB_6 insert brazed into 3/16-in.-diameter tungsten.

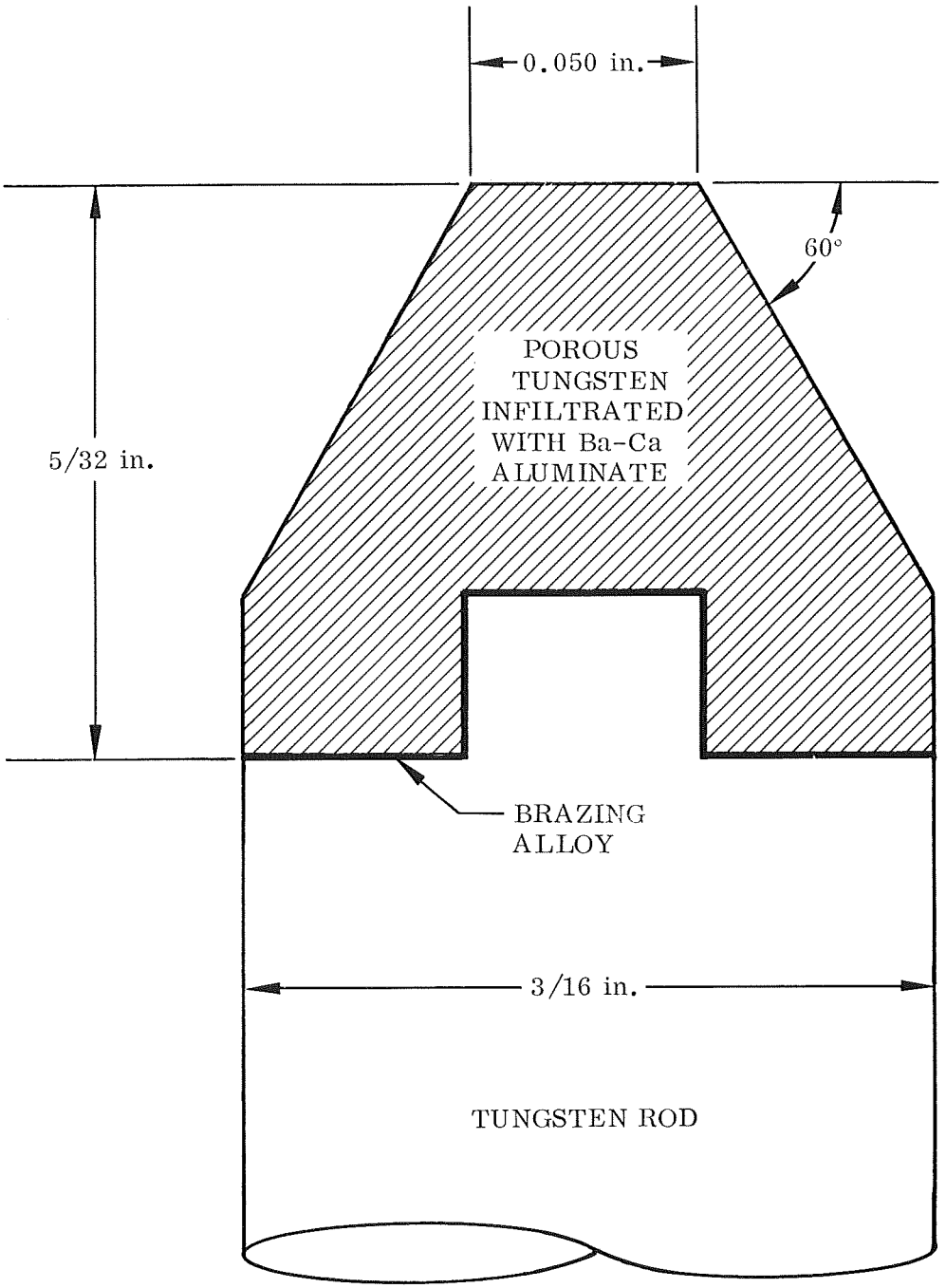

Fig. 4-4 Configuration of Ba-Ca-Aluminate Impregnated Electrodes

consisted of first pressing and sintering a 3/16-in.-diameter porous tungsten cylinder and infiltrating the matrix by placing the porous tungsten in a molten mixture of Ba-Ca-aluminate. The special tips were then machined to contour and furnace brazed to 2-in.-long tungsten rods.

Continuum intensity measurements were made on the water-cooled copper anode at 150, 200, 250, and 300 A and two tip contours; a 60° included angle with a 0.053-in.-diameter flat, and a 30° included angle with a 0.045-in.-diameter flat. The "normal" 10° – 0.055-in. shape was not recommended by the vendor because of the fragile nature of the material.

Results of these tests are presented in Table 4-1. The power-density factor (the factor by which the power is increased as compared to the normal arc operating with all other conditions identical) is greater than 1 only at 250 A where the value is 1.38. The trend appears to be for a larger power-density factor at greater currents.

Bead-on-plate tests were run at 250 A with various electrode tip diameters as shown in Table 4-3. Heat input was kept constant by using a preset arc voltage (12 V) and a travel speed of 8 ipm. The 30°–30 mil electrode tip gave the highest depth-to-width ratio for the Ba-Ca-aluminate electrodes but this was less than that obtained with a standard 10°–55 mil 2% thoriated-tungsten electrode. No deterioration of the Ba-Ca-aluminate tips was noted.

4.3.1.3 Summary of Cathode Modification Experiments

Figure 4-5 is a composite plot of all the continuum half-width data obtained with the various electrode materials studied. In addition, two curves from the "normal" arc characterization studies with argon gas shielding are presented to demonstrate the similarity between the half-widths of the raw continuum data (transverse intensity distribution) and the mathematically reduced data (radial intensity distribution). The greatest error observed in this comparison is about 10% at 250 A with the reduced

Table 4-3

BEAD-ON-PLATE TESTS WITH Ba-Ca-ALUMINATE ELECTRODES ON 1/2-in. 2219 ALUMINUM PLATE
(100 cfh Helium Shielding)

Electrode Shape		Arc Current (A)	Arc Voltage (V)	Arc Length[a] (mil)	Travel Speed (ipm)	Heat Input (kJ/in.)	Depth of Penetration (in.)	Bead Width at Top (in.)	Depth-to-Width Ratio
Tip Angle (deg)	Tip Diameter (mil)								
30	15	250	12 (Set)	0 to -10	8	22.5	0.228	0.370	0.616
30	30	250	12 (Set)	0 to +10	8	22.5	.220	.344	.640
30	45	250	12 (Set)	20 to 25	8	22.5	.198	.375	.528
30	55	250	12 (Set)	+40	8	22.5	.202	.362	.559
CONTROL WELD – 3/16-in.-Diameter 2% Thoriated Tungsten 10°–55 mil tip.									
10	55	250	12 (Set)	+10	8	22.5	.224	.314	.712

(a) With reference to plate surface.

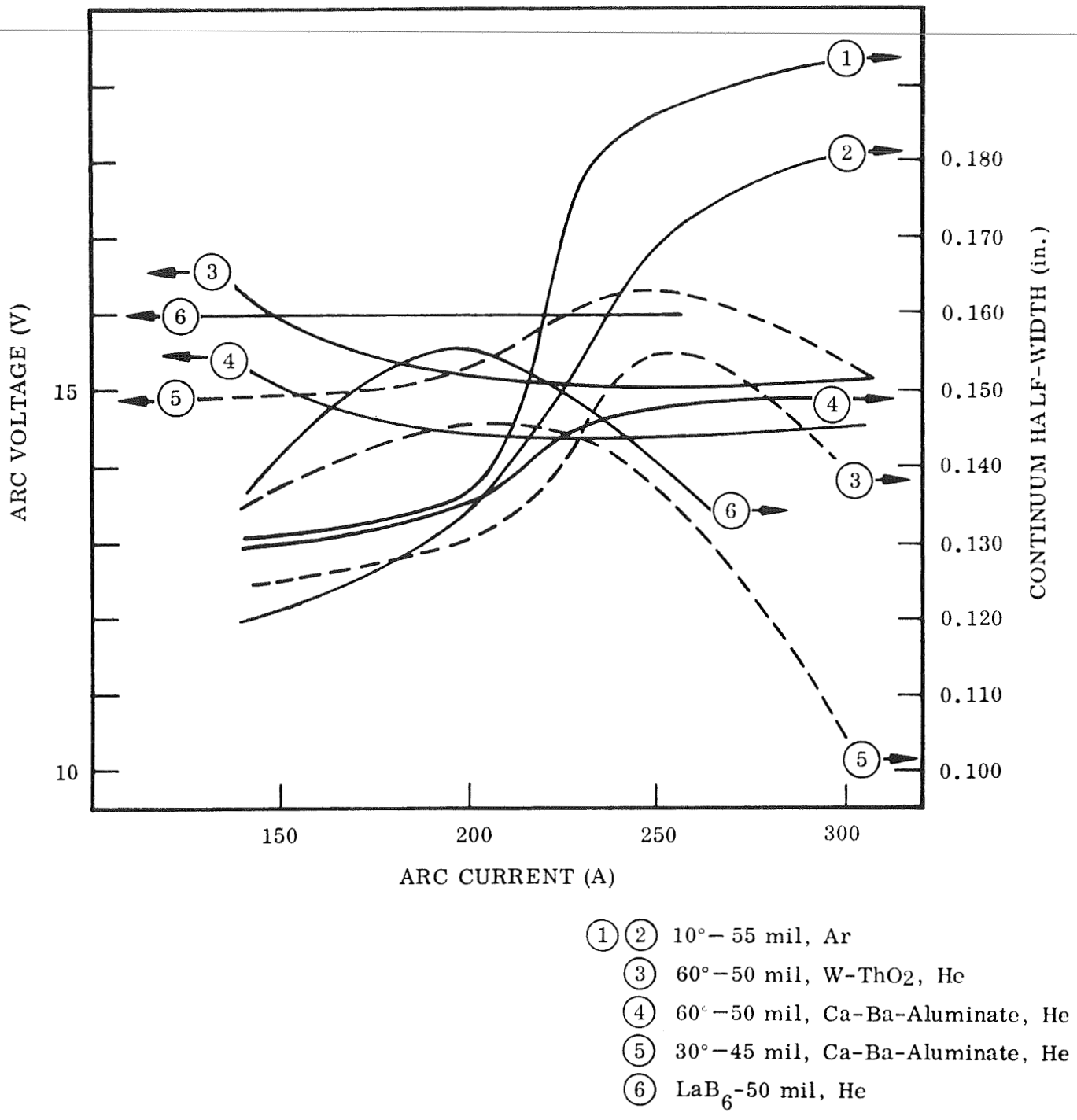

Fig. 4-5 Composite Plot of Continuum Half-Width and Voltage Versus Current for 2 mm GTA's in He With Various Cathode Materials. Also, transverse and radial half-width versus current for 2 mm arc in Ar with 10°– 55 mil thoriated tungsten electrode

half-widths always being the larger. The trend toward greater half-width with increasing current is evident in both the raw and reduced data curves, particularly in the range from 200 to 250 A where the rate of change is greatest. Also, both curves show the same leveling-off of the half-width for currents greater than 250 A.

The half-width data for the 60°−55 mil thoriated tungsten tip, used as a standard for the electrode materials studies, shows a behavior similar to the "normal" arc operating in argon with the exception of a reduction in half-width as the current is increased from 250 to 300 A. This anomaly may be an experimental artifact. For example, the anode may have melted and produced a small mound at the arc axis, and this in turn could reflect radiation from the arc column into the spectrograph.

The 60°−50 mil Ca-Ba-aluminate tip in helium is well behaved but the 30°−45 mil tip is not, in the sense that it departs from the behavior of thoriated tungsten. Its behavior is surprisingly similar to the LaB_6 cathode in that it shows an increase in half width from 150 to 200 A followed by steady decline at a rapid rate for higher currents.

Voltage-current curves for the electrode material studies are also included to demonstrate that the half-width changes truly reflect a change in the overall arc characteristics, for example, as for the 30°−45 mil Ca-Ba-aluminate tip, and the one of LaB_6.

4.3.2 Modification of the Anode

It has been generally assumed that the anode plays little or no part in the arc mechanism. This assumption is true only for low current arcs on water-cooled anodes but not under practical welding conditions where considerable metal vapor enters the arc.

Ludwig (Refs. 26, 28) reported a fourfold difference in penetration of GTA welds in zirconium due to trace impurities either in or on the surface of the material. He attributed the increased penetration to chlorine emanating from the weld pool, attaching electrons and forming negative ions, thereby increasing the negative space charge

and the anode potential drop and thus resulting in higher heat output at the anode. Ludwig suggested small amounts of strongly electronegative materials such as the halogens, and halogen compounds such as sulfur hexafluoride, would be expected to increase anode heat output. Following this suggestion, two experiments were made in which small amounts of halogen compounds were introduced into the anode area and the effect on weld penetration and bead width observed.

Test plates of 1/2-in. 2219 aluminum were machined and degreased and a small quantity of aluminum fluoride was painted on the faying surfaces and permitted to dry. The plates were then assembled into a square-butt joint configuration and welded at 250 A, 12 arc volts, and 8 ipm travel, with 100 cfh helium shielding. A control weld without chemical doping was also run. The welds were sectioned and examined for depth of penetration, bead width, and contour. No improvement in penetration was observed. Moreover, the bead surface was very irregular with some undercutting on one side.

Several additional square-butt joints were welded with a helium-1% sulfur hexafluoride (SF_6) backup gas. A small gap (~ 0.003 in.) was maintained between the plates to introduce the SF_6 into the anode region of the arc. Backup gas flows of 1 to 25 cfh were used and the plates welded at 300 A, 12 arc volts, and 8 ipm travel with 100 cfh helium shielding. Again no improvement in penetration was noted over that of the control weld made with He backup. The effect of adding SF_6 to the shielding gas is covered in the next subsection.

4.3.3 Modifications of the Shielding Gas

Gases selected for evaluation as shielding gas additions include hydrogen, nitrogen, oxygen, and chlorine. Hydrogen was added to both helium and argon for study, whereas helium was used as the carrier gas for the remainder of the experiments. In addition, some experiments were run with sulfur hexafluoride additions to helium.

Evaluation of the shielding gas mixtures was based on their effect on arc voltage, stability, and electrode tip contour as well as continuum intensity distribution. In the bead-on-plate runs, the effect on the weld puddle, surface bead contour, and porosity were noted.

Gases for this portion of the work were blended in the laboratory from high purity components and in some cases they were purchased as a mixture. Table 4-4 gives a list of the gases used and their purity. Precision flowmeters (± 5% of maximum scale reading) were used for measuring the flow of additive gas.

Table 4-4
SHIELDING GASES AND MIXTURES

Nominal Gas Composition	Grade and/or Purity
Hydrogen	Zero-Gas, less than 1 ppm hydrocarbon content, less than -80°F dewpoint
Nitrogen	Zero-Gas, less than 0.5 ppm hydrocarbon content, less than -80°F dewpoint
Oxygen (Electrolytic)	Zero-Gas, less than 1 ppm hydrocarbon content, less than -76°F dewpoint
Helium – 1% Chlorine Helium – 2% Chlorine	Mixture made from high purity (99.995%) helium and high purity (99.5%) chlorine, less than -80°F dewpoint
Helium – 1% Sulfur Hexafluoride	Mixture made from high purity (99.995%) helium and 98.0% minimum sulfur hexafluoride, less than -80°F dewpoint
Helium	High purity welding grade
Argon	High purity welding grade

Several preliminary bead-on-plate welds were made on 2219 aluminum, copper, and type 304 stainless steel with hydrogen, nitrogen, and chlorine additions to evaluate the effect of the additions on arc stability and compatibility with the tungsten electrode, and to establish practical ranges of addition for the subsequent studies. The ranges selected were 1 to 20% hydrogen, 1 to 100% nitrogen, and up to 1% chlorine. During

these runs, the stainless steel appeared to be more tolerant to the various additions and exhibited less weld pool turbulence and porosity. Therefore, it was selected for the majority of the bead-on-plate weld tests.

Continuum and Pressure Measurements. Evaluation of the various additives to the shielding gas was made by measuring the continuum intensity distribution either 0.25 mm (10 mils) or 0.50 mm (20 mils) above the surface of a solid water-cooled copper anode as described in detail in subsection 4.2. Tables 4-5 through 4-8 show the results of these measurements.

It is clearly evident that the greatest power density increase occurs for additions of hydrogen to helium in amounts less than about 20%. At 150 A, some melting of the anode surface was noted at hydrogen levels above 15% and arc instability developed at 20% hydrogen. Photographs of the arc at several levels of hydrogen addition are shown in Fig. 4-6. The arc instability at the 20% hydrogen appears to be due to melting of the electrode.

Additions of nitrogen to helium in amounts larger than 40% resulted in significant increases in power density with power density factors up to 8 for 100% N_2. Small quantities of chlorine (to 0.8%) appear to decrease the continuum width more than comparable amounts of hydrogen.

The greatest power density factor was observed for an addition of only 0.5 vol % of SF_6 to He at 50 cfh, for a 150-A, 2-mm arc. A tenfold increase in the power density was noted.

Additions of oxygen to helium in concentrations up to 0.75 vol % produced a slight apparent increase in power density. However, the data suggest that the observed effect may be within experimental error. Additions of over 0.25% O_2 severely degraded the tungsten electrode. (See Fig. 4-7.)

Table 4-5

DATA SHOWING THE INFLUENCE OF HYDROGEN ADDITIONS TO HELIUM AND TO ARGON SHIELDING GAS ON THE ARC POWER DENSITY AS INFERRED FROM THE OBSERVED CONTINUUM INTENSITY DISTRIBUTION OF ARCS OPERATING BETWEEN A 3/16-IN.-DIAMETER W-2ThO_2 CATHODE WITH A 10° TAPER TO A 55-MIL TIP, AND A WATER-COOLED COPPER ANODE AT A 2-mm ARC LENGTH

Shielding Gas (Vol %)	Arc Current (A)	Arc Voltage (V)	Arc Power (kW)	Continuum Half-Width (in.)	Average Power Density (kW-in.$^{-2}$)	Power Density Factor	Remarks
He(a)	150	15.9	2.38	0.134*	169	1.0	
He-1.0%H_2	150	16.8	2.52	0.125*	206	1.22	
He-1.0%H_2	150	16.5	2.48	0.145*	150	0.89	
He-2.0%H_2	150	17.2	2.58	0.112*	260	1.54	
He-5.0%H_2	150	16.5	2.48	0.091*	382	2.26	
He-10%H_2	150	17.2	2.58	0.086**	445	2.64	
He-10%H_2	150	17.0	2.55	0.054**	1110	6.56	Small molten spot on anode approx. 20 mils high.
He-10%H_2	150	17.1	2.56	0.072*	628	3.72	
He-15%H_2	150	17.3	2.60	0.064**	808	4.79	
He-16.7%H_2	150	17.5	2.62	0.067*	744	4.40	
He-20%H_2	150	17.5	2.62	0.070*	680	4.02	Some melting of anode surface, unstable arc.
He-20%H_2	150	18.5	2.78	0.075**	628	3.71	
He(b)	100	17.5	1.75	0.139*	115	1.0	
H_2(b)	100	19.5	1.95	0.066*	570	4.95	
Ar(c)	150	9.7	1.45	0.094*	210	1.0(1.24)(e)	
Ar-5%H_2(d)	150	12.5	1.88	0.094**	271	1.3(1.60)(e)	
Ar-10%H_2(d)	150	15.0	2.25	0.056*	914	4.35(5.41)(e)	
Ar-20%H_2(d)	150	17.5	2.62	0.058*	992	4.73(5.88)(e)	Some melting of anode surface, considerable spatter of copper.

(a) All He-H_2 tests at 100 cfh.
(b) 10° − 45 mil W-2ThO_2 tip and 100 cfh.
(c) 22.5 cfh.
(d) 25 cfh.
(e) Relative to He.
* Measured 0.25 mm (10 mils) above anode surface.
** Measured 0.50 mm (20 mils) above anode surface.

Table 4-6

DATA SHOWING THE INFLUENCE OF NITROGEN ADDITIONS TO HELIUM ON THE ARC POWER DENSITY AS INFERRED FROM THE OBSERVED CONTINUUM INTENSITY DISTRIBUTION OF ARCS OPERATING BETWEEN A 3/16-IN.-DIAMETER W-2 ThO_2 CATHODE WITH A 10° TAPER TO A 55-MIL-DIAMETER TIP, AND A FLAT WATER-COOLED COPPER ANODE AT A 2-mm ARC LENGTH

Shielding Gas (Vol %)	Gas Flow (cfh)	Current (A)	Voltage (V)	Arc Power (kW)	Continuum Half-Width* (in.)	Average Power Density ($kW\text{-}in.^{-2}$)	Power Density Factor
He	100	150	15.9	2.38	0.134	169	1.0
He-5%N_2	100	150	15.0	2.25	0.114	220	1.3
He-10%N_2	100	150	15.0	2.25	0.080	447	2.64
He-10%N_2	100	150	15.2	2.28	0.088	375	2.22
He-20%N_2	100	150	15.6	2.34	0.080	466	2.76
He-50%N_2	100	150	16.3	2.45	0.070	637	3.78
N_2	100	150	17.7	2.66	0.048	1470	8.7
N_2	25	150	16.5	2.48	0.064	772	4.56
He-42%N_2	60	150	15.5	2.32	0.046	1400	8.3

*Measured 0.25 mm (10 mils) above anode surface.

Table 4-7

DATA SHOWING THE INFLUENCE OF ADDING CHLORINE OR SULFUR HEXAFLUORIDE TO HELIUM SHIELDING GAS, ON THE ARC POWER DENSITY AS INFERRED FROM THE OBSERVED CONTINUUM INTENSITY DISTRIBUTION, OF ARCS OPERATING BETWEEN W-ThO_2 CATHODES, WITH THE CONFIGURATIONS INDICATED, AND A FLAT WATER-COOLED COPPER ANODE AT A 2-mm ARC LENGTH

Shielding Gas (vol %)	Gas Flow (cfh)	Current (A)	Voltage (V)	Arc Power (kW)	Continuum Half-Width (in.)	Average Power Density ($kW\text{-}in.^{-2}$)	Power Density Factor
He[a]	50	150	15.8	2.37	0.134*	168	1.0
He-0.02%Cl_2	50	150	16.0	2.40	0.145*	145	0.87[b]
He-0.8%Cl_2	50	150	17.0	2.55	0.105*	294	1.75[b]
He[c]	50	100	17.8	1.78	0.155*	95	1.0
He-0.4%Cl_2[c]	50	100	18.0	1.80	0.125*	147	1.55
He-0.4%Cl_2[c]	50	100	18.0	1.80	0.142*	114	1.20
He[a]	50	150	15.8	2.37	0.127*	187	1.0
He-0.1%SF_6	50	150	17.0	2.55	0.134*	181	0.97
He-0.5%SF_6	50	150	16.5	2.48	0.041*	1870	10.0
He[a]	100	150	16.0	2.40	0.121**	199	1.0
He-0.01%SF_6[a]	100	150	16.7	2.52	0.105**	290	1.45
He-0.10%SF_6	100	150	17.25	2.59	0.097**	350	1.75
He-0.20%SF_6	100	150	18.2	2.73	0.094**	394	1.97
He-0.50%SF_6	100	150	16.8	2.52	0.067**	714	3.57

(a) 3/16-in.-diameter cathode with a 10° taper to a 55-mil-diameter tip.
(b) Anode badly contaminated after run.
(c) Same as (a) with a 45-mil-diameter tip.
* Measured 0.25 mm (10 mils) above anode surface.
** Measured 0.50 mm (20 mils) above anode surface.

Table 4-8

DATA SHOWING THE INFLUENCE OF OXYGEN ADDITIONS TO HELIUM SHIELDING GAS ON THE ARC POWER DENSITY AS INFERRED FROM THE OBSERVED CONTINUUM-INTENSITY DISTRIBUTION, OF ARCS OPERATING BETWEEN A 3/16-IN.-DIAMETER W-2ThO_2 CATHODE AND A FLAT WATER-COOLED COPPER ANODE AT A 2-mm ARC LENGTH

Shielding Gas (vol %)	Gas Flow (cfh)	Current (A)	Voltage (V)	Arc Power (kW)	Continuum Half-Width* (in.)	Average Power Density ($kW\text{-}in.^{-2}$)	Power Density Factor
He	50	150	16.5	2.48	0.139	163	1.0
He-0.25%O_2	50	150	16.3	2.44	0.113	254	1.56
He-0.50%O_2	50	150	16.0	2.40	0.117	223	1.37
He-0.75%O_2	50	150	15.9	2.38	0.137	162	1.0

*Measured 0.25 mm (10 mils) above anode surface.

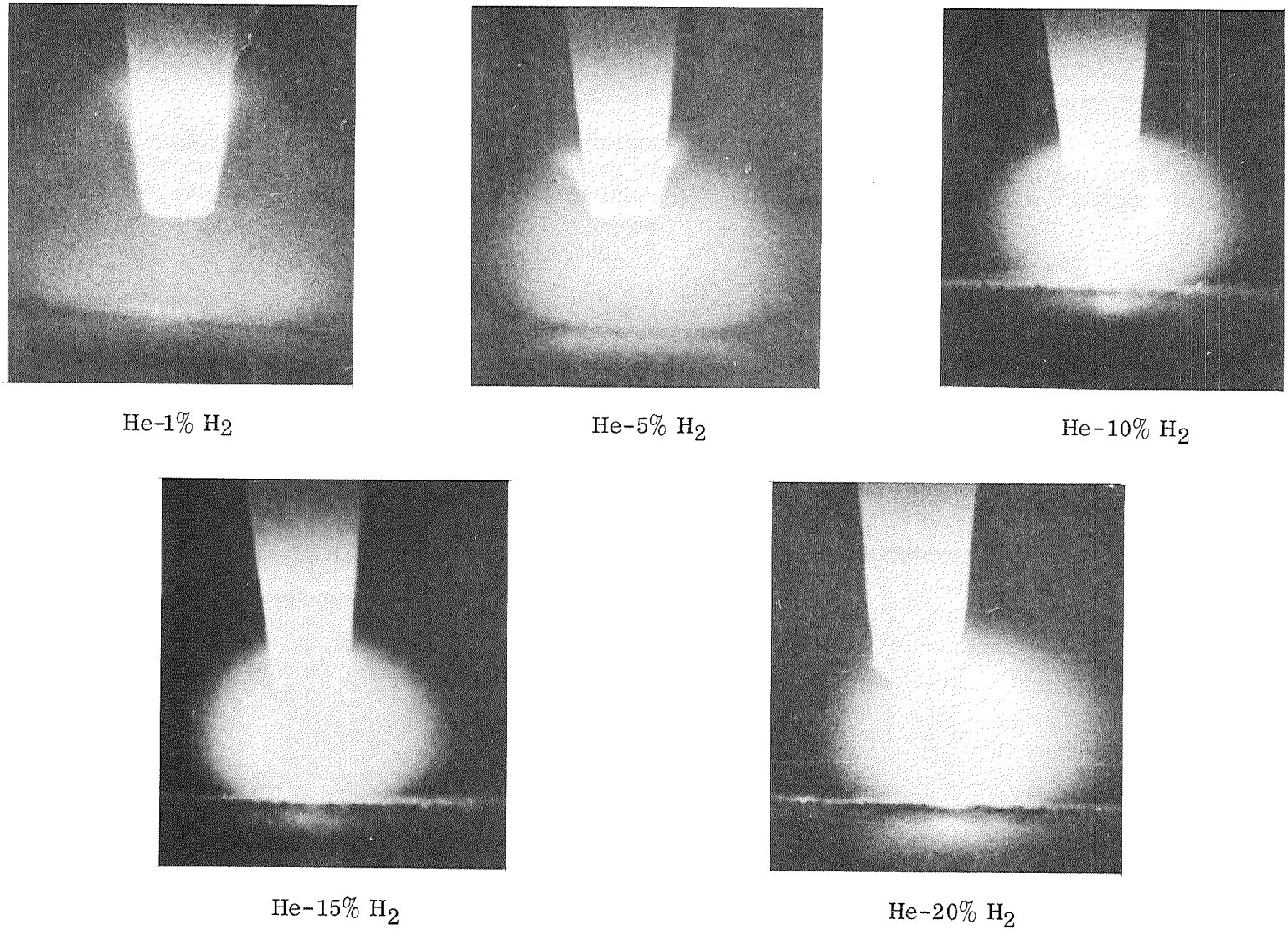

Fig. 4-6 Photographs of the GTA at 150 A on a Water-Cooled Copper Anode at Several Levels of Hydrogen Addition to the Helium Shielding Gas; 2-mm Arc Length

Fig. 4-7 Effect of Oxygen Additions on Electrode Contour. 3/6-in.-diameter 2% thoriated tungsten electrode, 10° taper to 0.055-in.-diameter tip; flat water-cooled copper anode; arc length 0.080 in.; current 150 A, DCSP; various He-O_2 mixtures 50 cfh total gas flow

Measurements of the plasma-stream pressure on a solid water-cooled copper anode were made for two levels of hydrogen added to argon and for one level each of nitrogen and hydrogen added to helium. The peak pressures observed in these tests are listed in Table 4-9.

Table 4-9

PEAK PLASMA-STREAM PRESSURE FOR SEVERAL ADDITIONS TO ARGON AND HELIUM SHIELDING GAS, 10°−55 mil, W-2ThO_2 CATHODE, 2-mm ARC LENGTH

Shielding Gas (vol %)	Gas Flow (cfh)	Current (A)	Peak Pressure (cm H_2O)
Ar	25	150	2.8
Ar-5%H_2	25	150	3.35
Ar-8.2%H_2	25	150	3.35
He	100	150	2.3
He-2.5%H_2	100	150	0.60
He-10%N_2	100	150	4.05

It appears from these results that plasma-stream pressure probably has a minor influence on the penetration characteristics of the arcs. This is evident since additions of hydrogen to either argon or helium shielding gas increase the penetration depth on 2219 Al, as well as decreasing the continuum half-width while the peak pressure is decreased in one case and increased in the other. Also, the peak pressure increases when nitrogen is added to helium while the penetration decreases.

Bead-On-Plate Tests. Several series of bead-on-plate welds were made to evaluate the effectiveness of the various shielding gas additions under actual welding conditions and to compare the results obtained with the continuum data. Welding conditions were selected to penetrate part-through the test plate and the depth-to-width ratio was used as a criterion of effective weld power density.

A summary of the data for welds made on 1/4-in. type 304 stainless steel plate is given in Table 4-10. The greatest increase in weld penetration and depth-to-width ratio was obtained with a helium-20% hydrogen mixture at a flow of 100 cfh. This increase was relatively small compared to the increase in power density measured by the narrowing of the continuum. Moreover, additions of hydrogen to helium of 5% or greater caused severe erosion of the tungsten electrode as a result of contamination by vapors from the weld pool (Fig. 4-8).

Additions of hydrogen to argon provided a significant increase in penetration, but since they also increased the bead width, the depth-to-width ratio was only slightly improved.

Nitrogen additions to argon slightly increased penetration and depth-to-width ratios, whereas they decreased penetration in the case of helium. It was not possible to use greater than 50% nitrogen because of severe porosity and underbead cracking.

Chlorine additions to helium increased the depth of penetration and decreased the bead width resulting in an improvement in depth-to-width ratio.

A series of bead-on-plate welds were made on 2219-T87 aluminum at 200 A current, 0.060-in. arc length, and 15 ipm travel with additions of hydrogen, chlorine, or sulfur hexafluoride to the helium shielding. A summary of the data is given in Table 4-11. As in the case of stainless steel, the 20% hydrogen addition provided the greatest increase in penetration and depth-to-width ratio. However, the bead surface was rough and the weld cross section exhibited considerable porosity. No difficulty with electrode contamination was noted. The chlorine additions increased the depth of penetration and decreased the bead width giving a small increase in depth-to-width ratio. Sulfur hexafluoride additions resulted in penetrations and depth-to-width ratios similar to those of chlorine additions, but caused greater contamination of the electrode (Fig. 4-9).

Because of the extremely high continuum power density factor observed previously for SF_6 addition, it was decided to conduct further bead-on-plate studies. These are summarized in Table 4-12. Welds were made at three levels of SF_6 addition with the heat

Table 4-10

BEAD-ON-PLATE TESTS WITH VARIOUS SHIELDING ADDITIONS[a]

Shielding Gas Mixture (Vol %)	Gas Flow (cfh)			Arc Voltage	Heat Input (kJ/in.)	Depth of Penetration (in.)	Bead Width at Top (in.)	Depth-to-Width Ratio
	Carrier	Additive	Total					
Ar	25 Ar	–	25	8.75	7.0	0.060	0.217	0.276
Ar-10%H_2	22.5 Ar	2.5 H_2	25	14.5	11.6	0.096	0.314	0.305
Ar-20%H_2	20 Ar	5 H_2	25	18.0	14.4	0.102	0.376	0.272
Ar-40%H_2	15 Ar	10 H_2	25	20.0	16.0	0.136	0.374	0.364
He	50 He	–	50	13.5	10.8	0.115	0.248	0.464
He-10%H_2	45 He	5 H_2	50	18.0	14.4	0.120	0.320	0.375
He-20%H_2	40 He	10 H_2	50	19.0	15.2	0.136	0.348	0.548
He-50%H_2	25 He	25 H_2	50	22.0	17.6	0.133	0.332	0.400
He	100 He	–	100	13.5	10.8	0.124	0.271	0.458
He-10%H_2	90 He	10 H_2	100	18.5	14.8	0.152	0.277	0.550
He-20%H_2	80 He	20 H_2	100	24.0	19.2	0.157	0.242	0.650
He-30%H_2	70 He	30 H_2	100	20.0[b]	16.0	0.155	0.314	0.495
Ar	25 Ar	–	25	9.0	7.2	0.054	0.253	0.213
Ar-10%N_2	22.5 Ar	2.5 N_2	25	10.0	8.0	0.066	0.277	0.238
Ar-20%N_2	20 Ar	5 N_2	25	10.5	8.4	0.075	0.259	0.290
Ar-30%N_2	17.5 Ar	7.5 N_2	25	12.5	10.0	0.084	0.292	0.288
He	50 He	–	50	13.5	10.8	0.120	0.253	0.475
He-10%N_2	45 He	5 N_2	50	12.5	10.0	0.111	0.265	0.420
He-20%N_2	40 He	10 N_2	50	13.0	10.4	0.111	0.271	0.410
He-50%N_2	25 He	25 N_2	50	14.0	11.2	0.100	0.278	0.359
He-0.02%Cl_2	49 He	1(He+1%Cl_2)	50	13.5	10.8	0.109	0.265	0.410
He-0.2%Cl_2	40 He	10(He+1%Cl_2)	50	13.0	10.4	0.127	0.229	0.555
He-0.8%Cl_2	10 He	40(He+1%Cl_2)	50	13.5	10.8	0.127	0.229	0.555

(a) Material: 1/4-in. type 304 stainless steel.
Welding Parameters:
Current 200 A
Arc length 0.080-in.
Travel 15 ipm
Electrode 3/16-in.-diameter, 2% thoriated tungsten tapered to 0.055-in. tip diameter.

(b) Erratic arc voltage, electrode contaminated.

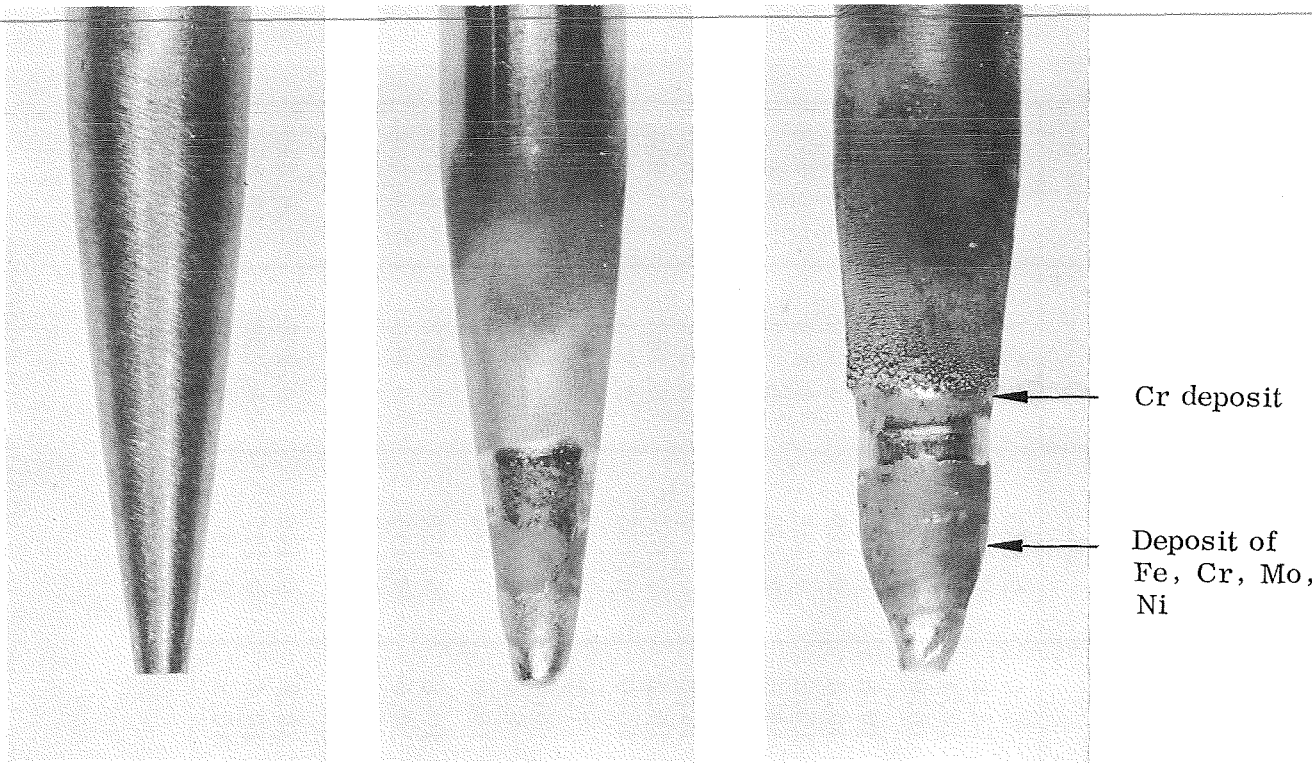

Electrode Contour Prior to Welding

After One Bead-on-Plate Weld Using He-5%H_2 Shielding

After One Bead on-Plate Weld Using He-10%H_2 Shielding

NOTE: A spectrographic analysis was made of the deposits on the electrode shown at the right with the results as indicated.

Fig. 4-8 Effect of Hydrogen Additions on Electrode Contour in GTA Welding Type-304 Stainless Steel Plate

Table 4-11

BEAD-ON-PLATE TESTS WITH VARIOUS SHIELDING ADDITIONS[a]

Shielding Gas Mixture (Vol %)	Gas Flow (cfh)		Total	Arc Voltage	Heat Input (kJ/in.)	Depth-of-Penetration (in.)	Bead Width at Top (in.)	Depth-to-Width Ratio
	Carrier	Additive						
He(Control)	100 He		100	14.0	11.2	0.136	0.300	0.454
He-5%H_2	95 He	5 H_2	100	15.0	12.0	0.183	0.325	0.563
He-20%H_2	80 He	20 H_2	100	17.0	13.6	0.223	0.330	0.677
He-0.02%Cl_2	49 He	1(He + 1%Cl_2)	50	14.0	11.2	0.147	0.297	0.500
He-0.20%Cl_2	40 He	10(He + 1%Cl_2)	50	14.25	11.4	0.145	0.283	0.510
He-0.40%Cl_2	30 He	20(He + 1%Cl_2)	50	14.0	11.2	0.147	0.276	0.530
He-0.01%SF_6	99 He	1(He + 1%SF_6)	100	14.0	11.1	0.145	0.300	0.476
He-0.10%SF_6	99 He	10(He + 1%SF_6)	100	14.0	11.1	0.143	0.277	0.518
He-0.50%SF_6	50 He	50(He + 1% SF_6)	100	13.25	10.6	0.136	0.269	0.505

(a) Material: 1/2-in. 2219-T87 aluminum plate.
Welding Parameters:
Current 200 A
Arc length 0.060-in.
Travel 15 ipm
Electrode 3/16-in. diameter, 2% thoriated tungsten, 10° taper to 0.055-in. tip diameter

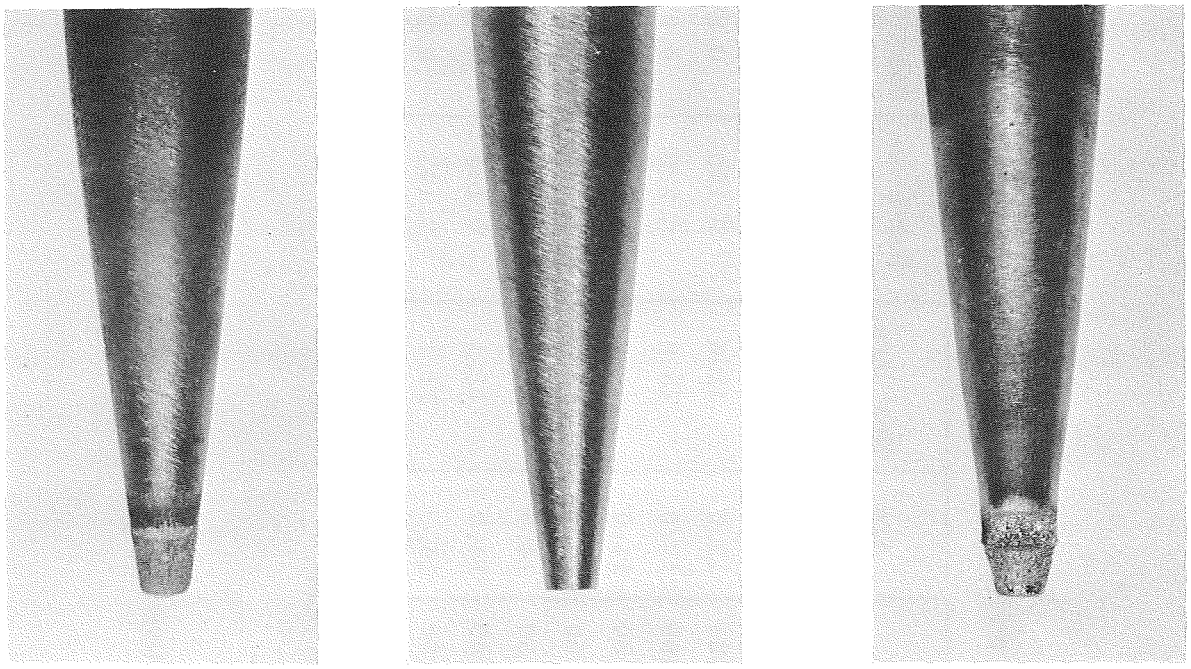

After One Bead-on-Plate Weld Using He-0.4%Cl_2 Shielding

Electrode Contour Prior to Welding

After One Bead-on-Plate Weld Using He-0.5%SF_6 Shielding

Fig. 4-9 Effect of Halogen Additions on Electrode Contour in GTA Welding 2219 Aluminum Plate

Table 4-12

BEAD-ON-PLATE TESTS WITH He + SF_6 ADDITIONS[a]

Shielding Gas Mixture[b] (Vol %)	Arc Voltage (V)	Arc Length (in.)	Current (A)	Heat Input (kJ/in.)	Depth of Penetration (in.)	Bead Width At Top (in.)	Depth-to-Width Ratio
He(Control)	12.0 (Set)	+0.010	250	22.5	0.224	0.314	0.712
He-0.01%SF_6	12.0 (Set)	+0.015	250	22.5	0.248	0.303	0.818
He-0.10%SF_6	12.0 (Set)	+0.040	250	22.5	0.245	0.319	0.768
He-0.50%SF_6	12.0 (Set)	+0.045	250	22.5	0.248	0.293	0.845
He-0.50%SF_6	12.0 (Set)	+0.045	250	22.5	0.238	0.278	0.855
He-0.50%SF_6	11.5 (Set)	+0.020	250	21.6	0.240	0.252	0.953
He-0.50%SF_6	11.0 (Set)	+0.020	250	20.6	0.270	0.245	1.10
He-0.50%SF_6	10.5 (Set)	+0.020	250	19.7	0.245	0.238	1.06
He-0.50%SF_6	10.0 (Set)	-0.010	250	18.8	0.238	0.210	1.14
He(Control)[c]	12.0 (Set)	—	300	27.0	0.302	0.354	0.854
He-0.50%SF_6[c]	12.0 (Set)	—	300	27.0	0.308	0.315	0.977

(a) Material: 1/2-in. 2219-T87 aluminum plate. Electrode: 3/16-in. diameter, 2% thoriated tungsten, 10° taper to 0.055 in. tip diameter, travel speed 8 ipm.
(b) Total gas flow 100 cfh except where noted.
(c) Total gas flow 50 cfh.

input maintained constant by presetting the current, travel, and arc voltage. Depth of penetration for these levels of addition did not change but the bead width decreased with increase of SF_6. In addition, there was a decided increase in the arc length for the two higher SF_6 additions. A second series of welds was made with the He-0.50%SF_6 mixture at preset arc voltages from 12.0 to 10.0 V. As the arc voltage was decreased, the arc length, heat input, and bead width decreased resulting in an increase in the depth-to-width ratio to greater than 1.0. Two additional bead-on-plate welds were made at 300 A, 12 V, and 8 ipm travel, one using the He-0.50%SF_6 mixture and the other a control weld made with helium. Data are given in Table 4-12.

4.3.4 Magnetic Field Effects

A series of experiments was conducted for determining the effectiveness of a longitudinal magnetic field for constricting the arc plasma in the region of the anode. Specifically, measurements were made of:

- Current distribution on the anode
- Continuum intensity distribution very close to the anode surface
- Plasma streaming pressure at the anode surface

each with the following conditions

- Helium shielding (45 and 110 cfh) and argon shielding (25 cfh)
- 2-mm and 4-mm arc length
- 100-A and 200-A total arc current
- Average magnetic field strengths from 0 to 300 G
- 3/16-in.-diameter W-2%ThO_2 cathode with a 10° taper to a 55-mil-diameter tip.

Bead-on-plate tests were made to evaluate the effect of the magnetic field on bead contour and weld penetration and to establish the extent of correlation between the power density inferred from the continuum and the welding characteristics.

The longitudinal magnetic field was produced by a coil wound on a water-cooled brass spool designed to replace the cup in the Linde HW 27 torch, as seen in Fig. 4-10.

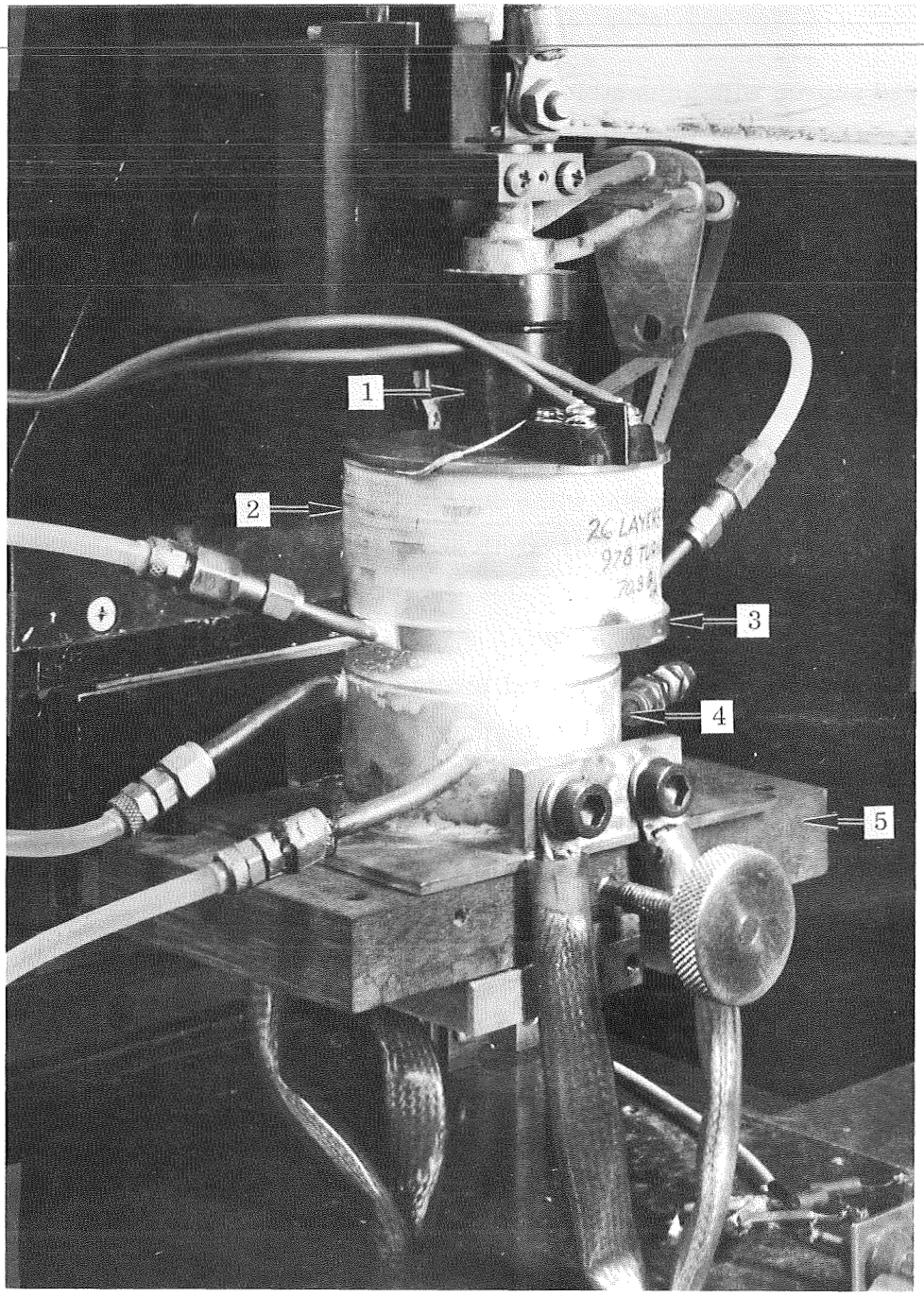

1. Torch Body
2. Electromagnet Coil
3. Water-Cooled Plate
4. Water-Cooled Copper Anode
5. Motor-Driven Anode Support

Fig. 4-10 Arc Apparatus With Longitudinal-Magnetic-Field Coil Surrounding the Electrode in Place of the Cup

A stabilized source with adjustable output provided the coil current. Spatial variation of the field strength was measured with a Hall-effect probe. The maximum field strength near the arc center was about 300 G. The field distribution is shown in Fig. 4-11.

The results of the experiments to determine the effect of a longitudinal magnetic field superimposed on the various arcs are presented below in tabular and graphical form. Table 4-13 shows a narrowing of the approximate current width when helium is the shielding gas. No consistent change is produced in the continuum half-width. For argon shielding gas, the current width decreases initially, then increases when the field is 200 G. The continuum half-width shows a similar pattern with indication of the arc being conical.

Figure 4-12 shows the effect of several levels of longitudinal magnetic field strength on the plasma-stream pressure on the anode surface for helium shielding. There is slight decrease in peak pressure and a narrowing of the distribution as the field strength is increased to 400 G. A further increase in field to 500 G depresses the peak pressure by nearly the same amount as the initial 400 G for a 250 A, 3-mm (0.120-in.) arc shielded with helium flowing at 110 cfh. A similar effect occurs if the current is reduced to 150 A and for fields to 200 G. This behavior correlates well with the current width and continuum half-width observations. The data at 400 G and 500 G were not recorded because of arc instability caused by the high fields.

Figure 4-13, the pressure distribution for the same conditions but with 18-cfh argon shielding, shows a much more dramatic influence of the longitudinal magnetic field on the plasma-stream pressure. The centrally peaked distribution occurring with a 50-G field is altered to a broader symmetrical two-peaked distribution with a field strength increase to 150 G, and the effect is more pronounced for a 200-G field for arc currents of 150 and 250 A. This behavior is similar to that observed with the continuum intensity technique and strongly suggests that the magnetic field causes the arc to operate in a conical mode, that is with the arc column in the form of a conical shell, at least in the case of argon shielding. No reason could be found to account for the difference in behavior caused bv the shielding gas (e.g., helium or argon).

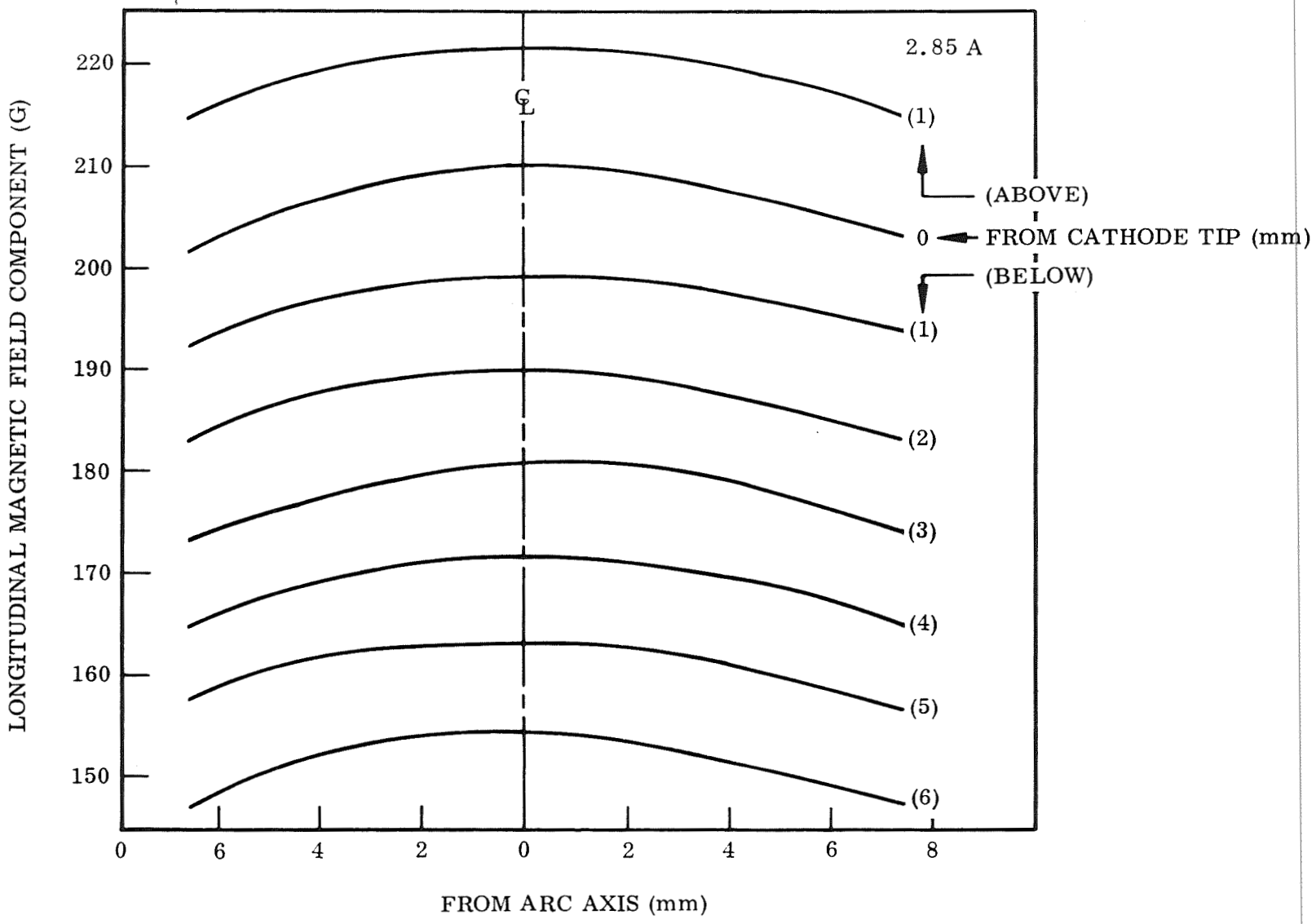

Fig. 4-11 Measured Applied Longitudinal Component of Magnetic Field in Vicinity of the Arc for 200-G Setting

Table 4-13

APPROXIMATE CURRENT PATH WIDTH AND CONTINUUM INTENSITY DISTRIBUTION HALF-WIDTH FOR GTA's(a) UNDER VARIOUS CONDITIONS OPERATING IN A LONGITUDINAL DC MAGNETIC FIELD OF STRENGTHS FROM 0 TO 300 G

Gas	Flow Rate (cfh)	Arc Length mm(in.)	Arc Current (A)	Arc Voltage (V)	Arc Power (kW)	Magnetic Field Strength (G)	Current Width (in.)	Continuum Half-Width (in.)*
He	45	2	100	16.7	1.67	0	0.14	0.11
He	45	2	100	16.8	1.68	100	0.13	0.11
He	45	2	100	16.8	1.68	150	0.14	0.09
He	45	2	100	17.0	1.70	200	0.09	0.10
He	45	2	100	17.2	1.72	250	0.13	0.11
He	45	2	100	17.6	1.76	300	0.09	0.09
He	45	4	100	20.1	2.01	0	0.25	0.12
He	45	4	100	20.1	2.01	100	0.17	0.15
He	45	4	100	21.2	2.12	150	0.16	0.17
He	45	4	100	21.3	2.13	200	0.17	0.14
He	45	4	100	21.6	2.16	250	0.16	0.13
He	45	4	100	21.6	2.16	300	0.16	0.12
He	110	2	200	15.5	3.10	0	0.13	0.11
He	110	2	200	15.7	3.14	100	0.12	0.11
He	110	2	200	16.0	3.20	150	0.16	0.10
He	110	2	200	16.2	3.24	200	—	—
He	110	2	200	16.3	3.26	250	—	—
He	110	2	200	16.6	3.32	300	—	—
He	110	4	200	17.4	3.88	0	0.29	0.11
He	110	4	200	19.4	3.88	100	0.26	0.15
He	110	4	200	19.7	3.94	150	0.23	0.14
He	110	4	200	20.0	4.00	200	0.21	0.14
He	110	4	200	20.2	4.04	250	0.20	0.14
Ar	25	4	100	10.3	1.03	0	0.26	0.12
Ar	25	4	100	10.7	1.07	100	0.23	0.10
Ar	25	4	100	11.0	1.10	150	0.24	0.14(b)
Ar	25	4	100	11.2	1.12	200	0.29	0.16(b)
Ar	25	4	100	16.7	1.17	250	—	—
Ar	25	4	100	12.0	1.20	300	—	—

(a) Cathode – 3/16-in. W-2ThO_2 with 10° taper to 55-mil tip. Anode, solid water-cooled copper.

(b) Continuum curve had broad flat top at 150 G and symmetrical double peaks at 200 G.

* Measured 0.50 mm (20 mils) above anode surface

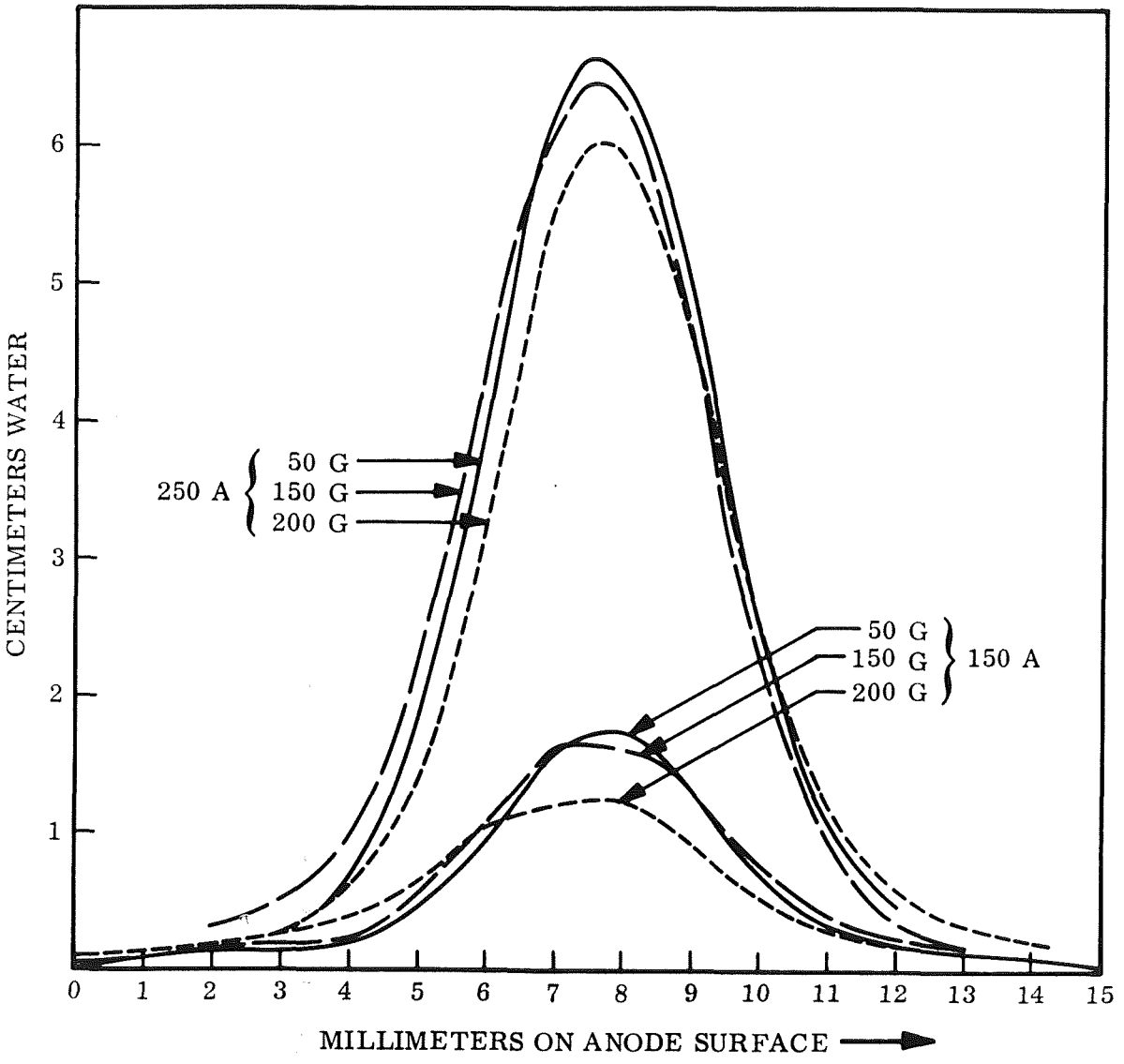

Fig. 4-12 Graph Showing the Effect of a Longitudinal Magnetic Field of Various Strengths on the Plasma-Stream Pressure of a 3-mm GTA Operating in Helium at 110 cfh Between a W-2ThO_2 Cathode 3/16 in. in Diameter With a 10° Taper to a 55-mil Tip and a Water-Cooled Copper Anode, at 150 and 250A

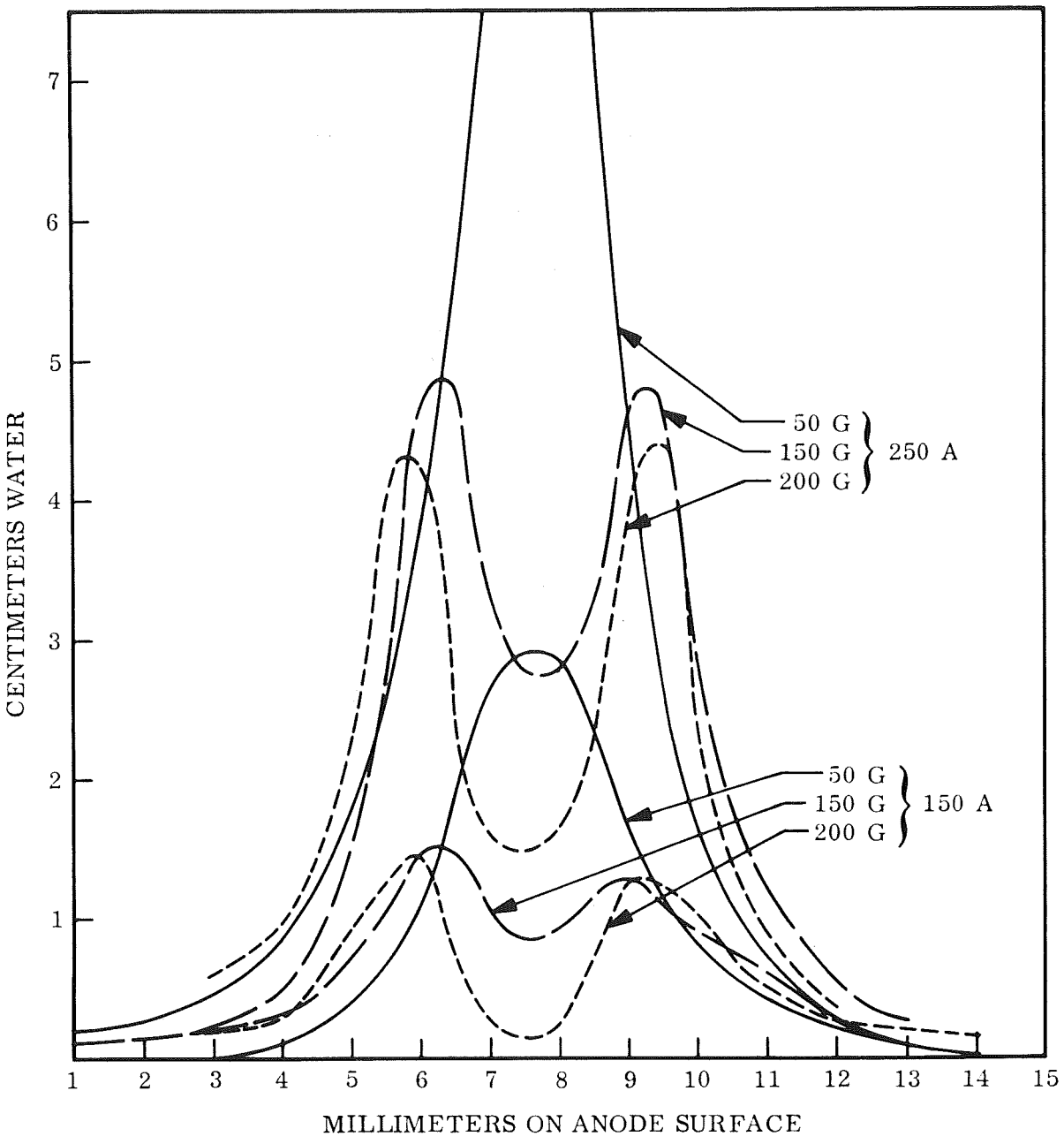

Fig. 4-13 Graph Showing the Effect of a Longitudinal Magnetic Field of Various Strengths on the Plasma-Stream Pressure of a 3-mm GTA Operating in Argon at 18 cfh Between a W-2ThO_2 Cathode 3/16 in. in Diameter With a 10° Taper to a 55-mil Tip and a Water-Cooled Copper Anode, at 150 and 250 A

Bead-on-plate welds were made on 1/2-in. 2219-T87 aluminum plate at 200-A current, 0.080-in. arc length, 14-ipm travel, 100-cfh helium shielding gas flow. Longitudinal magnetic fields of 0, 50, 150, and 250 G were applied. Undercutting on one side of the weld was noted at 50 G. At higher field strengths, the undercutting increased and at the same time weld metal was piled up on the opposite side of the bead. Penetration was decreased and the bead width increased. A similar effect was noted with argon shielding.

4.4 DISCUSSION OF EXPERIMENTAL RESULTS

Significant increases in arc power density, as measured by narrowing of the continuum, were noted for additions of 20 vol% hydrogen to helium or argon shielding gas. Nitrogen additions to helium also increased power density, particularly in concentrations of 40 vol% or greater. The greatest increase measured, however, was with the addition of 0.5 vol% SF_6 to helium.

The improvement in weld penetration and depth-to-width ratio obtained in the bead-on-plate tests is much smaller than suggested by the continuum data; e.g., an increase of about 30% compared to a tenfold increase in the continuum power density measured for the SF_6 addition. Moreover, nitrogen additions, actually resulted in lower depth-to-width ratios in stainless steel.

The use of materials with high thermionic emission for the electrode (cathode) shows some promise with up to a 60% increase in power density, as measured by the continuum, and about a 30% increase in depth-to-width ratios, for the tip configurations studied. Problems with thermal shock and melting of the lanthanum hexaboride tips could possibly be avoided by adding small quantities of the lanthanum to conventional thoriated tungsten electrodes. These tips would have the resistance to melting of the thoriated tungsten plus the high emissivity of the lanthanum.

The use of a longitudinal magnetic field resulted in a slight narrowing of the current width on the copper anode but caused severe distortion of the weld pool under practical welding conditions in the bead-on-plate tests.

No improvement in power density was observed in the experiments to modify the anode.

Surface melting of the water-cooled copper anode was observed in several of the continuum runs at high power density and are noted in the tables. Slight melting did not appear to interfere with the continuum measurement but in some instances small beads of copper were formed on the surface and tended to reflect light from the arc. This could result in erroneously high readings of power density. To avoid melting, all continuum runs were made at 150 A. In some cases, particularly with chlorine additions, a reaction with the copper surface was observed which could influence the measurement. The majority of the runs were made at 0.25 mm (~ 0.010 in.) above the copper anode surface but some runs were made at 0.50 mm (~ 0.020 in.) to avoid surface effects.

In general, the bead-on-plate tests were made under uniform conditions with little attempt made to optimize welding conditions for the specific arc modification under study. Therefore, the results should only be considered as showing possible trends.

Section 5

CONCLUSIONS AND DISCUSSION

Arcs of the type used for welding have been the topic of extensive basic and applied research during the past half-century. While many data on arc characteristics have been generated and a few theories have been proposed for various regions of the arc, there is yet no complete theory which predicts the power density to be expected for any given set of operating conditions. Also, there is no exact theory to account for the penetration and bead width a given power density will produce in specific workpiece materials. On this point it can only be said that the penetration produced by an arc is directly proportional to some function of the arc's power density.

Insight into the effect of very high power density can be had by examining a process which probably represents the highest available power density; i.e., electron-beam welding. The depth-to-width ratios attainable by this process are over 10 times greater than with the best GTA conditions. The total power for each of these processes is similar, say of the order of 5 kW. Yet because of the difference in the size of the heat source as it impinges on the work, the maximum electron-beam power density is of the order of 10^9 W/cm^2 whereas for GTA's the maximum power available is of the order of 10^5 W/cm^2 (Ref. 73). From these data it appears that a 10-fold increase in penetration (depth-to-width ratio) requires a power density increase of nearly 10^4-fold provided the energy transfer mechanism for GTA's is comparable to that for electron beams, a condition which remains unproved.

Laser beams also provide an extremely high power density but are disqualified for comparison with the GTA because of the drastically different energy transfer mechanism as well as the overall lower operating power levels.

Electron beam energy transfer is extremely simple because classical electron theory can be applied. The electrons emanating from a suitable cathode are focused and

accelerated and strike the workpiece (anode) with a well defined velocity over a well defined area. Most of the electron kinetic energy is converted to thermal energy at the work piece surface and, by rapid progressive melting and evaporation, penetration is achieved. Some scattering of the beam occurs upon collision of electrons with atoms of metal vapors in the "crater " but there is little divergence of the beam because of the low metal atom concentration resulting from the vacuum above the crater.

Near the cathode of a welding arc, where the plasma temperature is of the order of 20×10^3°K, the average thermal kinetic energy of electrons is about 2 eV as compared to 20 keV or more for electron-beams. Close to the anode of a 0.20-in. arc in argon at 200 A the temperature is about 10×10^3°K corresponding to an average kinetic energy of about 1 eV. Since the potential in an arc is only a few volts, the electrons reach the workpiece (or anode) with average energies of 10 eV, at the most (Ref. 11). The electron energy ratio between electron-beam welding and GTA agree well with El-Kareh's value of 10^4 given above. If all the energy available from each process were deposited uniformly over a circular area on an anode, the width of the deposition zones would be in the ratio of $(10^4)^{1/2}$ or 100; i.e., the GTA energy would be received over a circle of diameter 100 times that for the electron-beam case.

The generally accepted theories and general knowledge of GTA's and out-of-vacuum electron beams suggest that the increase in power density attainable by modifying the arc, short of mechanical constriction, will be significantly less than 10^4. This is evident upon considering the processes operating in an arc to transfer electron conduction from within the cathode to the anode, or workpiece, surface.

First of all, the arc is a self-regulating resistive element in a dc circuit. The plasma temperature and cross sectional area vary in proportion to the current. To pass a larger current, the plasma must become more conducting and this is possible by increasing the temperature (to 2×10^4°K, Ref. 11) and,when the peak conductivity is reached, by increasing the arc diameter.

Reducing the area on the cathode from which electrons are injected into the arc plasma by thermionic emission will not proportionally reduce the area on the anode over which the energy is deposited since each electron must undergo thousands of collisions with shielding gas atoms as it travels from the cathode. These collisions, in addition to ambipolar thermal diffusion, will produce a divergence of the plasma that is large compared to the cathode spot size. For example, Leonard (Ref. 74) shows that the ratio of unscattered-to-scattered electrons of 100 keV energy is about 0.4 for 1 cm of He at 1 atm, and for the same conditions in Ar the ratio is less than 0.05. For 150 keV electrons, the ratios are 0.7 and 0.07, respectively. It is clear that this ratio will approach zero when the initial energy is of the order of 1 to 10 eV.

Modifying the shielding gas properties may produce measurable changes in the anode power density by any of several processes. With diatomic gases, for example, the recombination of dissociated molecules at the anode surface will provide an additional source of energy, and this may be further enhanced by an increase in the plasma streaming the gas additives may cause. The theory of atmospheric pressure arc-plasmas is not sufficiently developed to permit an approximate calculation of the magnitude change to be expected. Heavier, less mobile, gaseous atoms might be expected to diffuse outward less rapidly and thus cause less plasma divergence. However, these atoms also present a larger collision cross section to electrons and this will produce more divergence. Much theoretical work and basic experimentation with arc plasmas is necessary before the mechanism of energy transfer to the anode is understood and accurate predictions of the feasibility of increasing the power density can be made.

Certain features of a GTA are of greatest importance for its characterization. The most basic "dimensions" of an arc are the shielding gas composition and pressure; the length, voltage,and current; the cathode (electrode) tip shape; the anode shape; and the materials of which the cathode and anode are constructed. All of these must be specified to produce a given power density distribution at the anode, although several different combinations of parameters may produce the same density distribution. Also, not all characteristics are independent. The voltage and current,

for example, cannot be adjusted separately – a change in current is always accompanied by a voltage change when all other parameters are fixed. The voltage is also a function of arc length, for constant current, and thus for a power source with a conventional drooping V-I characteristic, the current is also a function of arc length. These features have been studied extensively and an abundance of articles about them is available in the literature.

Power density distribution at the anode of a GTA has been studied much less. The present work is, in fact, the second study of this type that has ever been made. Furthermore, the correlation between the power density distribution at the anode and the weld penetration as experienced by the depth-to-width ratio was not studied prior to this work.

As a result of this investigation, a much better understanding of the GTA has been obtained particularly with regard to anode (or available) power density measurement and the factors involved in increasing GTA power density.

Peak power densities of the normal GTA at currents less than 300 A have been measured using a water-cooled copper anode and found to be of the order of 150 kW/in.^{2} (23 kW/cm^2). Power density has been found to increase with current and decrease with increased arc length. Increased average power densities of the order of 500 kW/in.^{2} (77 kW/cm^2) have been obtained with the use of high thermionic emissivity Ba-Ca-aluminate electrodes, and over 1000 kW/in.^{2} (150 kW/cm^2) by additions to the inert shielding gas of "active" gases such as H_2, N_2, or SF_6.

Measurement of the GTA power density at these high levels is limited by melting of the anode surface and by the influence of magnetic fields as the result of the current path in the anode.

In this study, a new method of estimating the power density distribution at the anode was tested. This method, though approximate, has advantages over that used previously

in that it is completely passive, in the sense that no perturbation of the arc is produced. It is based upon the fact that the continuum intensity from a very hot gas is theoretically proportional to the square of the electron concentration. Thus, a determination of the continuum intensity distribution in a plane just above the workpiece can be used as an estimate of the current distribution.

Measurement of power density under actual welding conditions, i.e., with a molten weld pool, is not possible by present techniques. The best approach is to use the above technique and measure the width of the continuum radiation produced in the arc "core" at a distance of 1 mm (~ 40 mil) or greater above the anode surface. The presence of the weld crater "lip" prevents any closer approach to the anode. Moreover, the presence of metal vapors in the vicinity of the crater can cause errors in measurement. However, this type of measurement does not indicate how the plasma shape is altered in the crater because of the crater shape.

Although a significant increase in GTA power density has been demonstrated in this program, the average power density obtained, circa, 10^6 W/in.^{2}, is still much lower than the 10^8 W/in.^{2} routinely achieved in electron beam welding.

It appears that there are limitations to increased GTA power density which may prevent attaining the power density levels of the EB process. To weld heavy sections by either process, an increase in total power is required. With the EB process, both the current and voltage may be increased to obtain the increased power whereas in the GTA process there is a practical limit on the arc voltage that may be used, and, therefore, only the current may be increased. Goldman (Ref. 75) has calculated the amount of anode heating due to electrons, the plasma jet (kinetic gas heating), and radiation for 4-mm gas-tungsten arcs in argon at several levels of current, as shown in Fig. 5-1. It can be seen that at low currents the major portion of anode heating is due to electrons, but, as the current increases, the plasma jet provides a greater portion of the heat. A similar result was observed in this work (Figs. 3-10, 3-14). The hot gases in the plasma-jet are not as concentrated in the GTA as is the electron stream and they are much less efficient in transfer of heat. Thus, the tendency will be for a broader, less concentrated arc at high currents.

Practical limitations to increased GTA power density include the problem of electrode contamination due to the greater volume of metal vapor produced, particularly with materials of high vapor pressure. To avoid this problem, it would be desirable to weld at greater arc lengths of the order of 1/2 in., instead of with the electrode submerged below the work surface. However, rapid divergence of the plasma precludes this approach. The best means of minimizing the plasma divergence would be to use a constricting nozzle, i.e., plasma arc welding. Three advantages of the plasma arc welding process would be:

(1) The much greater electrode-to-work distance would minimize electrode contamination.

(2) The higher arc voltage of this process as compared to the GTA would increase power at the same current level.

(3) Greater control could be exercised over the gas stream which is an increasingly important source of anode heating at high current levels (> 300 A).

In a general way, it may be assumed that the mechanisms responsible for penetration in the GTA process are similar to those proposed for electron beam welding (Refs. 61, 68, 73, 76) in that the major force on the surface of the weld pool is due to the reaction force of the evaporated material. However, since the GTA operates essentially at atmospheric pressure, the magnitude of the reaction force may be quite different with various materials. Other factors such as surface tension, convection currents in the weld pool, the effect of magnetic stirring, etc., could have great influence on penetration and be affected by additions to the shielding gas to increase power density or by the proximity and shape of the electrode. The increased quantity of metal vapor at high power density undoubtedly has an influence on heat transfer at the anode and on penetration. Despite the many studies of the mechanisms of penetration of the electron beam uncovered in the literature search, none were found which specifically treated GTA or plasma-arc welding. Another important factor which has received little study is the shape assumed by the molten weld pool under the influence of the arc. At short arc lengths, the shape of the weld pool, its distance from the electrode, and the shape

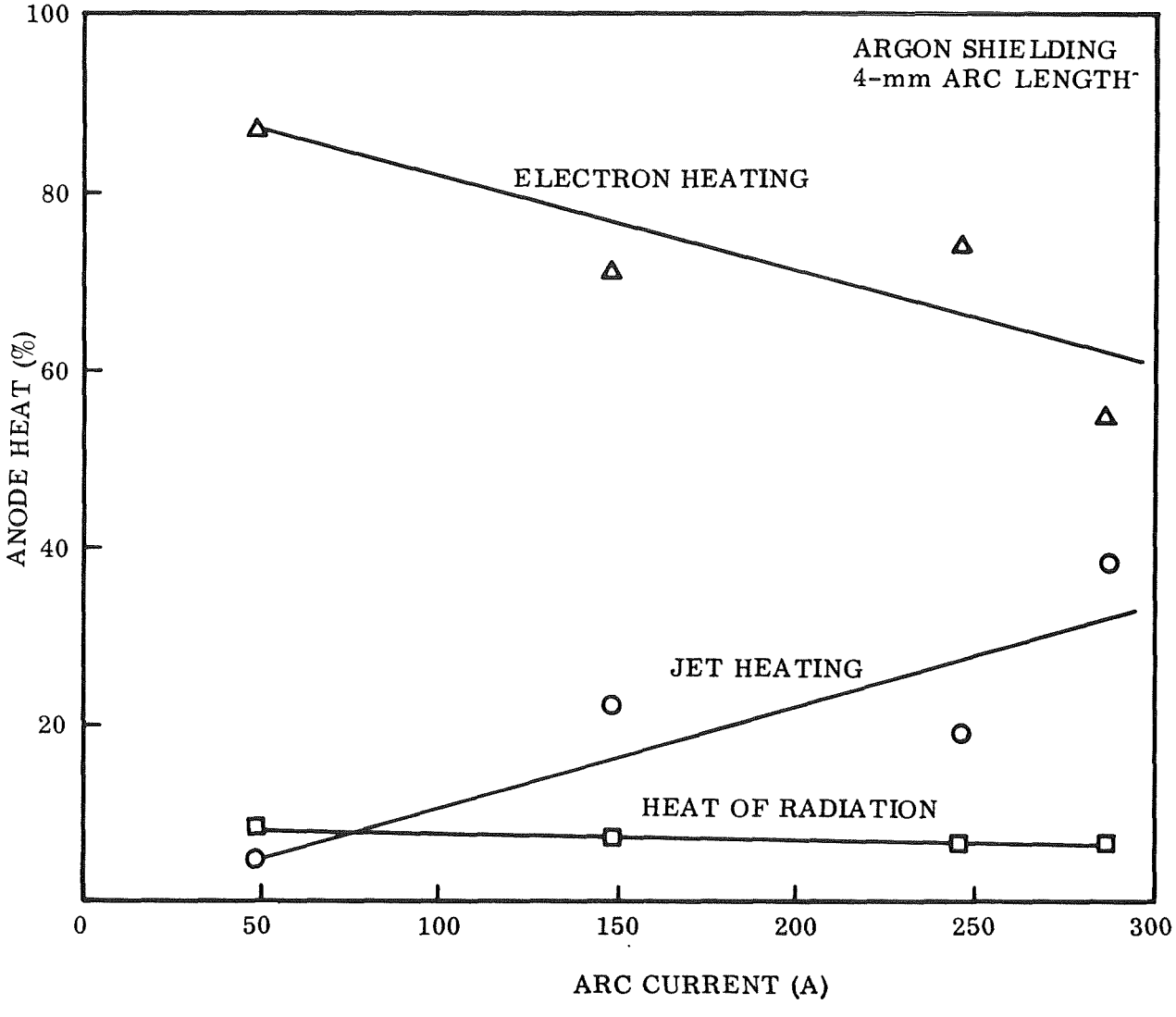

Fig. 5-1 Effect of Arc Current on Anode Heating for a 4-mm GTA in Argon (Ref. 75)

of the arc crater all have an influence on the arc and heat transfer to the anode. Therefore, increased GTA welding power density by itself may not result in increased penetration,as shown by the relatively small (~ 30%) increase in weld penetration obtained with SF_6 additions to the shielding gas compared to the large (~ 10-fold) increase in measured power density.

One factor which also may influence penetration and weld-bead dimensions is the pressure on the workpiece caused by the axially directed gas stream in an arc. Peak pressures of the order of 8 cm of water occur in argon arcs at 250 A. This pressure must depress the weld pool surface and thus contribute to penetration by allowing the electron and thermal energy to the arc to be deposited deeper in the workpiece. While pressure measurements were made for this program, insufficient data were obtained to permit any conclusions regarding the influence of plasma-streaming pressure on penetration.

The general conclusion to be made from this work and from the literature is that characterization of GTA's in terms of voltage, current, arc length,shielding gas, current density distribution at the anode, heat (power) intensity distribution at the anode, pressure on the anode, and continuum intensity distribution just above the anode, is not sufficient to clearly establish the penetration and weld bead contour produced in a given workpiece. The reason for this is that with the exception of current and arc length, there exist other factors particularly related to the workpiece metal characteristics which produce overriding effects that must be considered.

Most of the effort in arc research has been directed at understanding the mechanisms at and near the cathode, and in the plasma. The processes operating at the anode must be studied more extensively before the significance of power density in GTA's can be appreciated. In particular, the mechanisms of penetration must be defined.

Section 6

RECOMMENDATIONS

Further work to increase welding power density should concentrate on mechanical constriction of the arc (the plasma-arc process). This process has not been developed to its fullest potential, particularly with regard to the amount of constriction used. It may be possible, by forcing the plasma through a sufficiently small, specially designed orifice, with moderate streaming pressure, to arrive at power densities intermediate to those provided by GTA's in one case and electron beams in the other.

A detailed study should be made of the mechanisms of penetration in GTA and plasma-arc welding, and a comparison made with the mechanisms which have been proposed for electron beam penetration. The study should include further investigation of the "keyholing" phenomenon and metal motion in the weld pool. Results of this study would be of significant help in applying the GTA and plasma-arc processes to obtain maximum joint efficiency with minimum heat input.

Further research should be directed toward separation of the various heat transfer mechanisms at the anode of DCSP-GTA's operating under various conditions. The total local energy deposited in the anode is composed of four major components:

(1) Energy release due to the anode metal work function
(2) Thermal kinetic-energy of condensing electrons
(3) Energy gained by electrons passing through the anode-drop region
(4) Kinetic energy of the heat shielding gas impinging on the anode surface

Of these four, the first three are terms involving the product of the local current density and some energy factor such as a potential, and the last is independent of the current. Letting $Q(r)$ be the local heat-flux intensity, φ_e the anode work function, E_k the electron kinetic energy, V_a the anode-drop voltage, $q_k(r)$ the

kinetic gas-transfer term, and $j(r)$ the local current density, these are related as follows:

$$Q(r) = (\varphi_e + E_k + V_a)j(r) + q_k(r)$$

By using the split-anode surface probe to obtain $j(r)$ and $Q(r)$, and plotting $Q(r)$ as a function of $j(r)$, the resulting curve can be extrapolated to $j(r) = 0$ to obtain the kinetic gas transfer term (q_k) and the slope, which in this case is related to the sum of the electron potential and kinetic energies. From the slope, the electron kinetic energy can be estimated since φ_e is known and values of V_a have been calculated.

Applying the procedure just described to arcs operating in various gases and under other operating conditions will show if the partition of energy is invariant or upon which operating parameters it depends. Verification of the applicability of this method could be obtained by performing duplicate experiments in which only the anode material would be changed to alter the work function term (φ_e) resulting in a change in local heat-flux intensity equal to the local current density times the work function change.

Further extension of this work to include the effect of anode geometry on heat transfer mechanisms would provide valuable information more closely related to actual GTA welding conditions where the arc is operating primarily in the weld crater. The study by Tedeschi (Ref. 45) could be used as a starting point.

Section 7

SUMMARY

This report is an account of a study to theoretically and experimentally analyze the power density of direct current straight polarity (DCSP) gas-tungsten arcs (GTA's), and to determine if significant improvements could be made in the power density received at the workpiece (anode). The program was divided into three consecutive phases: (1) an exhaustive literature search, (2) experiments to characterize the arc, and (3) experiments to determine the possibility of increasing the power density at the anode. The main points of each phase are briefly described in the paragraphs that follow.

Phase I, the literature search, revealed a vast amount of information that can be separated into three main categories. First, there is a large number of items dealing with various specific arc phenomena in a rigorous theoretical manner. This category includes reports on basic arc experiments such as for determining arc plasma temperatures, electron and ion concentrations, electrical conductivity, electromagnetic reactions, etc.

The second category of reports and papers, was the most useful for this program, and consists of accounts of experiments to measure specific properties of GTA's by relatively simple techniques. Significant among these works are: experiments to measure the radial distribution of heat flux, current, and pressure on unmelted, water-cooled copper anodes; experiments to determine the thermionic efficiencies of various cathode materials; experiments to estimate the relative importance of the current and the plasma stream in heating the workpiece.

The third category of reports and papers consists of accounts of ad hoc experiments performed to determine the influence of various parameter changes on the characteristics

of the weld bead they produce. These were particularly useful as guides to indicate what modifications of the GTA, excluding mechanical constriction, might produce measurable increases in welding power density.

In total, the literature does not provide a sufficiently well integrated theory of the GTA to permit unequivocal conclusions from being made regarding the probability of producing significant welding power density increases.

In Phase II, techniques were developed for characterizing and measuring the power density of the normal DCSP gas-tungsten arc. The arcs studied were operated with argon or helium shielding at four currents (150, 200, 250, and 300A), arc lengths from 1 to 3 mm (and longer in certain cases) on both water-cooled copper and molten aluminum using 3/16-in.-diameter 2% thoriated tungsten cathodes (electrodes) tapered to either a 55-mil or 94-mil-diameter tip. The radial distributions of current density and heat-flux intensity were determined by means of a specially designed water-cooled copper split-anode. A determination of the radial distribution of the continuum intensity 0.25 and 0.50 mm (10 and 20 mils) above the anode were made simultaneously with the current and heat distribution determination. Measurements with the split-anode were limited to argon shielding because of arc instability and surface melting when helium was used. Pressure measurements were made with the same operating conditions but using a water-cooled copper anode with a small hole in the surface connected to a water manometer.

The experimental results from Phase II show a qualitative but not quantitative correlation between the current distribution and that for the continuum. The absence of a quantitative correlation appears to result from experimental complications which were not resolved. Specifically, the very design of the split anode introduces perturbations, in the arc shape, that are severely amplified during the numerical calculations required to convert experimental data to the desired radial distribution.

The distribution of arc pressure is very similar to the continuum intensity distribution demonstrating a relation between the distribution of plasma streaming velocity and the electron density.

Phase III experiments were designed to increase normal GTA power density through modifications of the electrode, the anode, the shielding gas, and the use of magnetic fields. Evaluation was made on the basis of bead-on-plate results, as well as measurement of the continuum intensity.

Significant increases in arc power density as measured by narrowing of the continuum intensity distribution were noted for hydrogen, nitrogen, and sulfur hexafluoride additions to the shielding gas, but the corresponding improvements in weld penetration and depth-to-width ratio in the bead-on-plate tests were much smaller. Electrodes made from materials with high thermionic emission (such as barium-calcium aluminate or lanthanum hexaboride) produced increased power density but some problems with thermal shock and melting of the LaB_6 were encountered. No improvement in power density was observed in the experiments to modify the anode. Longitudinal (axial) magnetic fields, used in an attempt to reduce plasma divergence, rendered the plasma conical and interacted with the weld pool to severely distort the weld bead.

Methods for producing measurable increases in GTA power density were demonstrated in this program. However, the average power density obtained, about 10^6 W/in.^{2}, is still much lower than the 10^8 W/in.^{2} routinely achieved in electron beam welding. It appears that the maximum available GTA power density is well below density levels of the EB process.

It is recommended that further work to increase welding power density should be concentrated on mechanical constriction of the arc, i.e., the plasma-arc process. In addition, it is recommended that a detailed study be made of the mechanisms of penetration in the GTA and plasma-arc processes, and further research also be done on heat transfer mechanisms at the anode of gas temperatures.

Section 8

REFERENCES

1. Hasemeyer, E. A., "Study of Porosity, Mismatch and Repair of Aluminum Weldments," Weld Imperfections, Addison-Wesley, 1968, pp. 209–220

2. Jackson, J. E., "Analysis of Time-Temperature Effects in 2219 Aluminum Welding," Welding J., Vol. 45, No. 4, Apr 1966, pp. 188s–192s

3. Burch, W. L., "The Effect of Welding Speed on Strength of 6061-T4 Aluminum Joints," Welding J., Vol. 37, No. 8, Aug 1958, pp. 361s–367s

4. Harris, W. J., High Speed TIG Welding, MRI 101.12, Lockheed Missiles & Space Company, 9 Oct 1964

5. Smith, C. O., Funk, E. R., and Udin, H., An Analytical Study of Aluminum Welding, Welding Research Council Bulletin No. 12, Jun 1952

6. Wood, F. W., and Beall, R. A., Studies of High-Current Metallic Arcs, Bulletin 625, Bureau of Mines, U.S. Department of the Interior, 1965

7. Spraragen, W., and Lengyel, B. A., "Physics of the Arc and the Transfer of Metal in Arc Welding," Welding J., Vol. 22, No. 1, Jan 1943, pp. 2s–42s

8. Jackson, C. E., "Science of Arc Welding – 1959 Adams Lecture," Welding J., Vol. 39, Nos. 4, 5, 6: Apr 1960, pp. 129s–140s; May, pp. 177s–190s; Jun, pp. 225s–230s

9. Finkelnburg, W., "The Physical Mechanisms of Low- and High-Current Arcs and Their Relation to the Welding Arc," Trans. AIEE, Vol. 70, pt 1, 1951, pp. 800–803

10. Maecker, H., "Plasmastromungen in Lichtoben infolge eigenmagnetischer Kompression" (Plasma Streaming in Electric Arcs as a Result of Self-Magnetic Compression), Z. Phys., Vol. 141, 1955, pp. 198–216

11. Olsen, H. N., "Thermal and Electrical Properties of an Argon Plasma," Phys. Fluid, Vol. 2, No. 6, Dec 1959, pp. 614–623

12. Nestor, O. H., "Heat Intensity and Current Distributions at the Anode of High Current, Inert Gas Arcs," J. Appl. Phys., Vol. 33, No. 5, May 1962, pp. 1638–1648

13. Goldman, K., "Electric Arcs in Argon – Volt-Amp and Volt-Arc Gap Characteristics," Physics of the Welding Arc: A Symposium, 29 Oct–2 Nov 1962, The Institute of Welding, London, 1966, pp. 17–22

14. Olsen, H. N., Bedjai, G., and Martindill, R. E., Determination of Departure From Local Thermodynamic Equilibrium in Arc Plasmas, USAF ARL 67-0060, [Contract AF 33(615)-5149], Plasma Sciences Laboratories, Van Nuys, Calif., Mar 1967

15. Reed, T. B., "Determination of Streaming Velocity and the Flow of Heat and Mass in High-Current Arcs," J. Appl. Phys., Vol. 31, No. 11, Nov 1960, pp. 2048–2052

16. Milner, D. R., Salter, G. R., and Wilkinson, J. B., "Arc Characteristics and Their Significance in Welding," Brit. Welding J., Vol. 7, No. 2, Feb 1960, pp. 73–88

17. Serdjuk, G. B., "Magnetic Forces in Arc Welding Metal Transfer," Physics of the Welding Arc: A Symposium, 29 Oct–2 Nov 1962, The Institute of Welding, London, 1966, pp. 175–180

18. Finkelnburg, W., Handbuch der Physik, XXII. Gasentladungen II, Springer-Verlag, Berlin, 1956

19. Maecker, H., and Peters, T., "Das Elektronenkontinuum in der Säule des Hochstromkohlebogens und in anderen Bogen," (The Electron-Continuum in the Column of High-Current Carbon Arcs and Other Arcs) Z. Phys., Vol. 139, 1954, pp. 448–463

20. Helmbrecht, W. H., and Oyler, G. W., "Shielding Gases for Inert-Gas-Welding," Welding J., Vol. 36, No. 10, Oct 1957, pp. 969–979

21. McElrath, T., and Gorman, E. F., "Argon-Hydrogen Shielding Gas Mixtures for Tungsten Arc Welding," Welding J., Vol. 36, No. 1, Jan 1957, pp. 28–35

22. Davis, E., and Terry, C. A., "Nitrogen-Arc Welding of Copper," Brit. Welding J., Vol. 1, No. 2, Feb 1954, pp. 53–64

23. Fedotov, L. E., and Varob'ev, V. V., "True Thermal Efficiency in Gas-Shielded Arc Welding of Copper," Welding Production (Svar. Proiz.), No. 9, Sep 1961

24. Wilkinson, J. B., and Milner, D. R., "Heat Transfer From Arcs," Brit. Welding J., Vol. 7, No. 2, Feb 1960, pp. 115–128

25. Uchida, A., "A Measurement of Arc Force in Argon Arc Welding," J. Jap. Welding Soc., Vol. 29, No. 6, Jun 1960, pp. 453–458

26. Ludwig, H. C., "Plasma-Energy Transfer in Gas-Shielded Welding Arcs," Welding J., Vol. 38, No. 7, Jul 1959, pp. 296s–300s

27. Kasen, M. B., and Pfluger, A. R., "Chlorine Additions for High-Quality Inert Gas-Metal-Arc Welding of Aluminum Alloys," Welding J., Vol. 37, No. 6, Jun 1958, pp. 269s–275s

28. Ludwig, H. C., "Arc Welding of Vacuum and Inert-Atmosphere Melted Zircaloy-2," Welding J., Vol. 36, No. 7, Jul 1957, pp. 335s–341s

29. Herring, C., and Nichols, M. H., "Thermionic Emission," Rev. Mod. Phys., Vol. 21, No. 2, Apr 1949, pp. 185–270

30. Wright, D. A., "Survey of Present Knowledge of Thermionic Emitters," Instn. Elec. Engrs. Proc., Vol. 100, Pt. 3 (Radio & Communication Engr.), No. 65, May 1963, pp. 125–142

31. Lee, T. H., and Greenwood, A., Space Charge and Ionization Regions Near the Arc Cathode, ARL-63-163, General Electric, Sep 1963 (AD-418 764)

32. Lee, T. H., Greenwood, A., Breingan, W. D., and Fullerton, H. P., Voltage Distribution, Ionization and Energy Balance in the Cathode Region of an Arc, USAF ARL 64-152 [Contract AF 33(657)-8206 S-1], General Electric Company, Philadelphia, Pa., Oct 1964

33. Langmuir, I., Phys. Rev., Vol. 22, 1923, p. 357

34. Neurath, P. W., and Gibbs, T. W., "Arc Cathode Emission Mechanisms at High Currents and Pressures," J. Appl. Phys., Vol. 34, No. 2, Feb 1963, pp. 277–283

35. Lafferty, J. M., "Boride Cathodes," J. Appl. Phys., Vol. 22, No. 3, Mar 1951, pp. 299–309

36. Gibbs, E. F., "Fundamental Study of Tungsten Arc," Metal Progress, Vol. 78, No. 1, Jul 1960, pp. 84–92

37. Savage, W. F., Strunck, S. S., and Ishikawa, Y., "Effect of Electrode Geometry in Gas Tungsten-Arc Welding," Welding J., Vol. 44, No. 11, Nov 1965, pp. 489s–496s

38. Chihoski, R. A., "The Effects of Varying Electrode Shape on Arc, Operations and Quality of Welds in 2014-T6 Aluminum," Welding J., Vol. 47, No. 5, May 1968, pp. 210s–222s

39. Kenyon, D. M., and Boyce, A. J., "Effect of Cathode Length and Diameter on Tungsten Arc Characteristics," Brit. Welding J., Vol. 13, No. 2, Feb 1966, pp. 103–108

40. Noesen, S. J., "Consumable Electrode Melting of Reactive Metals," J. Metals, Vol. 12, No. 11, Nov 1960, pp. 842–852

41. Lee, T. H., "Energy Distribution and Cooling Effect of Electrons Emitted From an Arc Cathode," J. Appl. Phys., Vol. 31, No. 5, May 1960, pp. 924–927

42. Goldman, K., and White, E. S., "Effect of Anode Material on Arc Mechanism," Brit. Welding J., Sep 1965, pp. 430–434

43. Rykalin, N. N., Kulagin, I. D., and Nikolaev, A. V., "Vaporized Electrode Material and Energy Balance in Welding Arcs," Physics of the Welding Arc: A Symposium, 29 Oct–2 Nov 1962, The Institute of Welding, London, 1966, pp. 46–49

44. Ludwig, H. C., "Current Density and Anode Spot Size in the Gas Tungsten Arc," Welding J., Vol. 47, No. 5, May 1968, pp. 234s–240s

45. Tedeschi, J. R., A Study of an Arc With a Variable Geometry Anode, Master's Thesis, GA/ME/62-7, Air Force Inst. of Tech., Wright-Patterson AFB, Ohio, Aug 1962, 92 pp. (AD-292 338)

46. Ginn, J. E., "Electrical and Metallurgical Factors Influencing Welding Arc Stability," Welding J., Vol. 40, No. 9, 1961, pp. 942–946

47. Hicken, G. K., and Jackson, C. E., "The Effects of Applied Magnetic Fields on Welding Arcs," Welding J., Vol. 45, No. 11, Nov 1966, pp. 515s–524s

48. Guile, A. E., "Magnetic Movement of Short Arcs With Reference to Arc Welding Problems," Brit. Welding J., Vol. 13, No. 6, Jun 1966, pp. 357–365

49. Kovalev, I. M., "Deflection of a Welding Arc in a Transverse Magnetic Field," Welding Production (Svar. Proiz.), No. 10, Oct 1965, pp. 5–9

50. Levakov, V. S., and Lyubavskii, K. V., "Influence of a Longitudinal Magnetic Field on an Electric Arc Using a Non-Consumable Tungsten Cathode," Welding Production (Svar. Proiz.), No. 10, Oct 1965, pp. 15–19

51. Gvozdetskii, V. S., and Mechev, V. S., "Displacement of the Electric Arc in a Magnetic Field," Automatic Welding (Avt. Svarka), No. 10, Oct 1963, pp. 49–55

52. Gruber, G. G., Pfender, E., and Eckert, E. R. G., Experimental Study of a Transpiration Cooled Constricted Arc, ARL Report 68-0023, Feb 1968

53. Dyatlov, V. I., "The Volt-Ampere Characteristic of the Constricted Arc," Automatic Welding (Avt. Svarka), No. 1, 1961, pp. 13–18

54. Kulagin, I. D., and Nikolaev, A. V., "The Arc Plasma Jet as a Heat Source in the Working of Materials," Welding Production (Svar. Proiz.), Vol. 5, No. 9, Sep 1959, pp. 1–11

55. Petrov, A. V., Slavin, G. A., and Verbitskii, V. G., "The Thermal Efficiency of Constricted Arc Welding on Thin Sheet Material," Welding Production (Svar. Proiz.), No. 2, Feb 1967, pp. 10–14

56. Stikhin, V. A., and Patskevich, I. R., "Determination of the Thermal Characteristics of a Constricted Arc," Welding Production (Svar. Proiz.), No. 8, Sep 1967, pp. 48–51

57. Okada, M., and Maruo, H., "Studies on the Plasma Jet," Physics of the Welding Arc: A Symposium, 29 Oct–2 Nov 1962, The Institute of Welding, London, 1966, pp. 23–34

58. Vilkas, E. P., "New Welding Current Pulsation Methods," Welding J., Vol. 47, No. 7, 1968, pp. 549–560

59. Vilkas, E. P., Reynolds, R. W., and Louden, J. T., Development of Manufacturing Methods for TIG Welding, Final Report, 1 Sep 1965–19 Apr 1966 [Contract AF 33(615)-3241], AFML TR-66-74, Apr 1966, 44 pp.

60. Needham, J. C., "Pulsed Current for Gas Shielded Arc Welding," Trans. IEEE, Industry & General Applications, Vol. IGA-2, No. 3, May–Jun 1966, pp. 225–233

61. Crawford, Charles K., "Electron Beam Machining," Introduction to Electron Beam Technology, Robert Bakish, ed., New York, John Wiley & Sons, Inc., 1962

62. Churchill, R. V., Modern Operational Mathematics in Engineering, New York, McGraw-Hill, 1944

63. Rosenthal, D. and Schmerber, R., Weld J., Vol. 17, 1938, pp. 2-5–8-5

64. Rosenthal, D., Weld J., Vol. 20, 1941, pp. 220s–234s

65. Christensen, N., et al., SINTEF, FTR-378, 15 Sep 1959

66. Christensen, N., et al., SINTEF, FTR-1530, 1 Jan 1962

67. Christensen, N., et al., Brit. Weld J., Feb 1965, pp. 54–75

68. Schwarz, H., "Mechanism of High-Power-Density Electron Beam Penetration in Metals," J. Appl. Phys., Vol. 35, No. 7, Jul 1964, pp. 2020–2029

69. Griem, Hans R., Plasma Spectroscopy, New York, McGraw-Hill, 1964, pp. 309–311

70. Finkelnburg, W. and Maecker, H., "Elektrische Bögen und Thermisches Plasma," (Electrical Arcs and Thermal Plasma) Handbuch der Physik, Vol. XXII, Gas Discharges II, S. Flugge, ed., Springer-Verlag, Berlin, 1956

71. Maecker, H., "Electron Density and Temperature in the Column of a High Current Carbon Arc," Z. für Phys., Vol. 136, 1953, pp. 119–136

72. Nestor, O. H. and Olsen, H. N., "Numerical Methods for Reducing Line and Surface Probe Data," SIAM Rev., Vol. 2, No. 3, Jul 1960, pp. 200–207

73. El-Kareh, A. B., "Design of a High Voltage, High Power Density Electron Beam," Proc., 5th Electron Beam Symposium, Alloyd Electronics Corp., Boston, Mass., Mar 1963, J. R. Morley, ed.,

74. Leonard, L. H., et al., Development of Non-Vacuum Electron-Beam Welding, ASD TR-63-7-926, Feb 1963

75. Goldman, K., "Electric Arcs in Argon: Heat Distribution," British Welding J., Vol. 10, No. 7, Jul 1963, pp. 343–347

76. Hashimoto, T. and Matsuda, F., "Penetration Mechanism of Weld Bead in Electron-Beam Welding," Trans. of National Research Inst. for Metals, Vol. 7, No. 5, Mar 1966

Appendix A

DERIVATION OF NUMERICAL FORMULAS FOR LINE PROBE AND SURFACE PROBE INVERSION TO RADIAL DISTRIBUTIONS*

Consider the cross section of an arc possessing cylindrical symmetry as indicated in Figs. A-1a and A-1b.

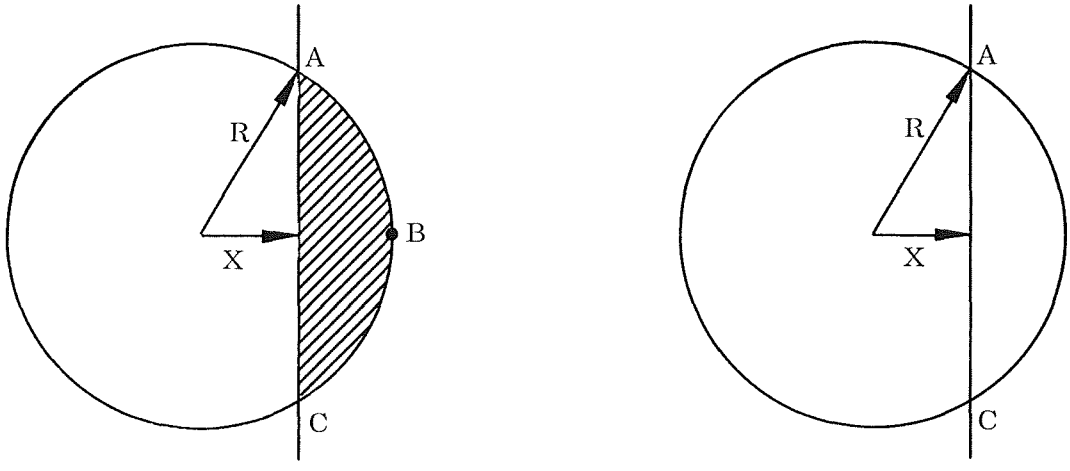

a. Surface Probe

b. Line Probe

Fig. A-1 Cross Section of an Arc Possessing Cylindrical Symmetry

For the surface probe

$$F(x) = 2 \int_{x}^{R} f(r) \cos^{-1} (x/r) r \, dr \qquad (A.1)$$

where f(r) is the radial distribution function. In the case of the line probe

*Ref. 14.

$$Q(x) = 2 \int_{x}^{R} \frac{f(r) r \, dr}{(r^2 - x^2)^{1/2}} \qquad (A.2)$$

Differentiation of $F(x)$ with respect to x reveals that

$$Q(x) = - F'(x) = dF(x)/dx \qquad (A.3)$$

This relationship is used to simplify the derivation of the numerical inversion formula for the surface probe.

Equation (A.2) is recognizable as the Abel integral which can be inverted to give

$$f(r) = - \frac{1}{\pi} \int_{r}^{R} \frac{Q'(x) \, dx}{(x^2 - r^2)^{1/2}} \qquad (A.4)$$

Numerical integration of (A.4) can be performed once the transformation $r^2 = v$ and $x^2 = u$ are introduced, i.e.,

$$f[r(v)] = - \frac{1}{\pi} \int_{v}^{R^2} \frac{Q'(u) \, du}{(u - v)^{1/2}} \qquad (A.5)$$

By dividing the interval $x = 0$ to $x = R$ into N equal subintervals of length $x = a$, (A.6) can be expressed as a series of subintegrals of the form

$$f_k \equiv f(ak) = - \frac{1}{\pi} \sum_{n=k}^{N-1} Q'_n(u) \int_{(an)^2}^{[a(n+1)]^2} \frac{du}{[u - (ak)^2]^{1/2}} \qquad (A.6)$$

where

$$Q'_n(u) = \frac{Q_{n+1}(u) - Q_n(u)}{a^2[(n+1)^2 - n^2]} \tag{A.7}$$

Solving the integral in (A.6), combining with (A.7) and simplifying, gives

$$f_k = -\frac{2}{\pi a} \sum_{n=k}^{N-1} A_{k,n}[Q_{n+1}(x) - Q_n(x)] \tag{A.8}$$

where

$$A_{k,n} = \frac{[(n+1)^2 - k^2]^{1/2} - [n^2 - k^2]^{1/2}}{2n+1} \tag{A.9}$$

Equation (A.8) can be further simplified to permit the use of direct experimental data; as follows

$$f_k = -\frac{2}{\pi a} \sum_{n=k}^{N} B_{k,n} Q_n \tag{A.10}$$

where

$B_{k,n} = -A_{k,k}$ for $n = k$

$B_{k,n} = A_{k,n-1} - A_{k,n}$ for $n \geq k+1$ for the $A_{k,n}$ defined by (A.9).

The equivalent of (A.10) for the surface-probe can be obtained by substituting the relationship $Q(x) = -F'(x)$ over two subintervale, i.e.,

$$F'_n = \frac{1}{2a}(F_{n+1} - F_{n-1}) \tag{A.11}$$

into (A.10) to give

$$f_k = \frac{1}{\pi a^2} \sum_{n=k}^{N} B_{k,n}(F_{n+1} - F_{n-1}) \qquad (A.12)$$

which can be further simplified to the same form as (A.10), that is

$$f_k = \frac{1}{\pi a^2} \sum_{n=k-1}^{N-1} C_{k,n} F_n \qquad (A.13)$$

where

$$C_{k,n} = B_{k,n-1} - B_{k,n+1}$$

$$B_{k,n-1} \equiv 0 \qquad \text{for} \quad n - 1 \leq k$$

Appendix B

EXTRAPOLATION OF THE HEAT-FLUX DENSITY CURVES

Consider the data curves in the following figure where the experimental heat-flux data curve, $W[n(x)]$ represented by the solid line attains a zero value at a very large

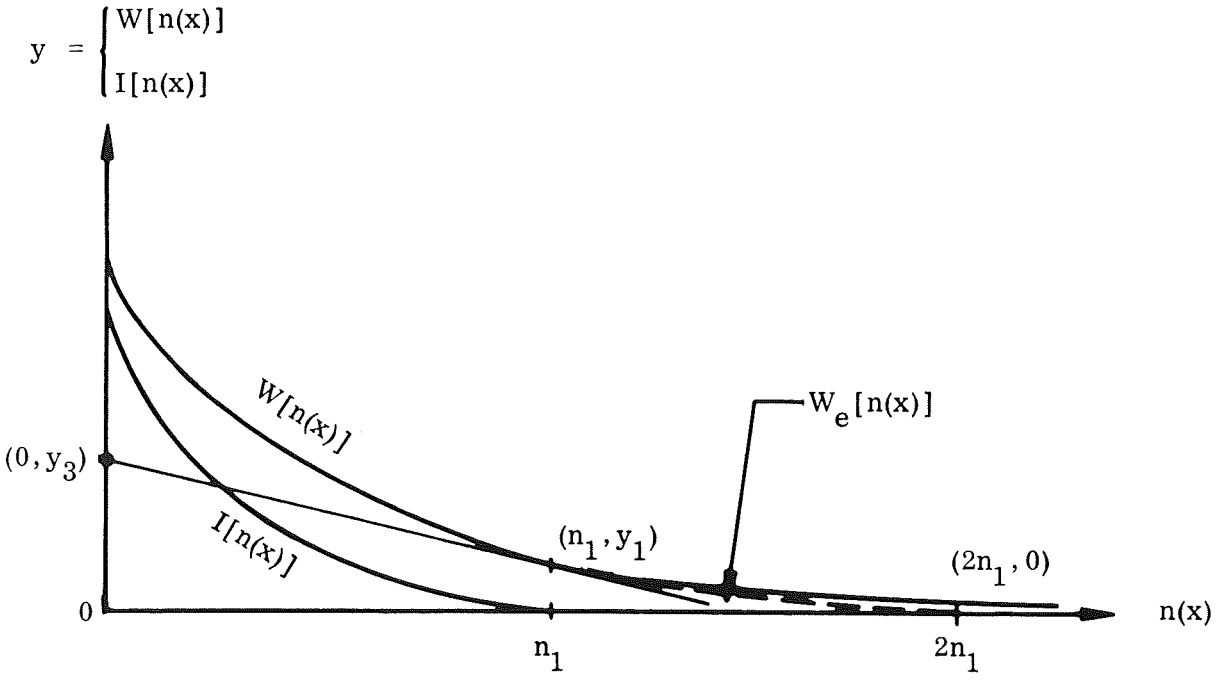

distance from the arc axis $(n = 0)$ and the experimental current data curve becomes zero at n_1. The n are integral subinterval values for the inversion scheme. An approximation to the heat-flux curve for $n_1 \leq n \leq 2n_1$ is required to satisfy the following conditions:

$$\left.\begin{aligned}
&(1) \quad W[n_1(x)] = W_e[n_1(x)] \\
&(2) \quad W_e[2n_1(x)] = 0 \\
&(3) \quad \frac{d}{d[n(x)]} W[n_1(x)] = \frac{d}{d[n(x)]} W_e[n_1(x)] \\
&(4) \quad \frac{d}{d[n(x)]} W_e[2n_1(x)] = 0
\end{aligned}\right\} \qquad (B.1)$$

where $W[n(x)]$ is the experimental data curve and $W_e[n(x)]$ is the extrapolate curve satisfying the four conditions above. The extrapolated curve will be a third-degree polynomial because of the four conditions it must satisfy, i.e.,

$$W_e[n(x)] = a_o + a_1 n + a_2 n^2 + a_3 n^3 \tag{B.2}$$

Applying the boundary conditions to (B.2) results in four simultaneous equations from which the coefficients can be determined:

$$\left.\begin{aligned} W[n_1(x)] &= y_1 = a_o + a_1 n_1 + a_2 n_1^2 + a_3 n_1^3 \\ W_e[2n_1(x)] &= 0 = a_o + a_1(2n_1) + a_2(2n_1)^2 + a_3(2n_1)^3 \\ \frac{d}{d[n(x)]} W[n_1(x)] &= y_1' = 0 + a_1 + 2a_2 n_1 + 3a_3 n_1^2 \\ \frac{d}{d[n(x)]} W_e[2n_1(x)] &= 0 = 0 + a_1 + 2a_2(2n_1) + 3a_3(2n_1)^2 \end{aligned}\right\} \tag{B.3}$$

Solving Eq. (B.3) for the coefficients results in

$$\left.\begin{aligned} a_o &= -4(2y_1 - y_3) \\ a_1 &= -\frac{4}{n_1}(5y_1 - 2y_3) \\ a_2 &= \frac{1}{n_1^2}(14y_1 - 5y_3) \\ a_3 &= \frac{1}{n_1^3}(3y_1 - y_3) \end{aligned}\right\} \tag{B.4}$$

where y_3 is the ordinal intercept of a tangent to the data curve extended from the cutoff point (n_1, y_1).